Title

LONGITUDINAL DISPERSION IN SOLVENT-EXTRACTION COLUMNS: PECLET NUMBERS FOR ORDERED AND RANDOM PACKINGS

Authors

Jacques, Gabriel L.
Vermeulen, Theodore.

Publication Date

1957-11-01

UCRL 8029

UNIVERSITY OF
CALIFORNIA

Radiation

LONGITUDINAL DISPERSION IN SOLVENT-EXTRACTION COLUMNS: PECLET NUMBERS FOR ORDERED AND RANDOM PACKINGS

BERKELEY, CALIFORNIA

DISCLAIMER

UCRL-8029

UNIVERSITY OF CALIFORNIA

Radiation Laboratory
Berkeley, California

Contract No. W-7405-eng-48

LONGITUDINAL DISPERSION IN SOLVENT-EXTRACTION COLUMNS: PECLET NUMBERS FOR ORDERED AND RANDOM PACKINGS

Gabriel L. Jacques and Theodore Vermeulen

November 1957

Printed for the U. S. Atomic Energy Commission

LONGITUDINAL DISPERSION IN SOLVENT-EXTRACTION COLUMNS: PECLET NUMBERS FOR ORDERED AND RANDOM PACKINGS

Contents

LONGITUDINAL DISPERSION IN SOLVENT-EXTRACTION COLUMNS: PECLET NUMBERS FOR ORDERED AND RANDOM PACKINGS

Gabriel L. Jacques and Theodore Vermeulen

Radiation Laboratory and Department of Chemical Engineering
University of California, Berkeley, California

November 1957

ABSTRACT

Dispersion phenomena in packed beds in both axial and radial directions were studied to provide basic data for extraction-tower design. Nine different beds were used, involving regular and random arrangments of spheres, and random arrangements of Raschig rings and Intalox saddles.

For one-phase flow a wide range of Reynolds numbers was used (5 to 2000), covering regions of laminar, transition, and turbulent flow. For the axial Peclet number, different constant values were found in the turbulent range and in the laminar range. The existence of a fairly sharp transition region was observed. Radial-dispersion results showed similar behavior. The axial Peclet number was found to vary inversely with bed porosity, while the radial Peclet number was almost proportional to porosity.

For two-phase flow, measurements were made up to the flooding point, which occurred at Reynolds numbers near 100. The axial Peclet number for both continuous and discontinuous phases is a function of the Reynolds numbers for the two individual phases. For each phase, the laminar value of the axial Peclet number obtained for one-phase flow is an upper limit. Values as low as one-fifth of this limiting value were found at relatively large flow rates of the second phase. The radial Peclet number was measured only for the continuous phase of two-phase systems; it was found to decrease in the same direction, but by a smaller percentage.

LONGITUDINAL DISPERSION IN SOLVENT-EXTRACTION COLUMNS: PECLET NUMBERS FOR ORDERED AND RANDOM PACKINGS

Part I. SINGLE-PHASE FLOW

Introduction

In a packed bed containing a single fluid phase, heat transfer and material transfer take place through the combined effect of molecular diffusion and of mixing. The mixing is produced by eddies behind, and adjacent to, the packing units, and also by nonuniformity of the velocity of the various fluid elements, which brings together various portions of fluid having dissimilar temperatures and concentrations. The effects of such mixing can be expressed in terms of an empirical parameter, E, the dispersion coefficient.

This dispersivity is not isotropic, but has two components in cylindrical symmetrical beds: a radial component and an exial component. In turbulent flow, both components are proportional to the linear velocity through the bed, and to some extent a function of the particle diameter. An exact knowledge of the dispersivity is useful in the design of reactors and extractors. Longitudinal dispersion affects the residence time and the concentration gradient within the bed; radial dispersion plays an important part in temperature control.

By use of dimensional analysis a dimensionless number, the Peclet group, can be defined,

$$N_{Pe} = Ud_p/E,$$

where N_{Pe} is the Peclet number; U, the interstitial mean velocity; E, the dispersion coefficient; and d_p, the particle diameter.

The Peclet number, either radial or axial, is widely used to characterize dispersion in packed beds. It is a function of the Reynolds number on the porosity of the bed. For a packing of 40% porosity, in turbulent flow, the radial Peclet number[4,19,31] has a value of about 10 and the axial Peclet number has a value of 2.[17,28,40] It is found in this study that both values may decrease markedly, for the continuous fluid phase, when a second fluid is present.

In the design of packed extraction towers, it has always been difficult to scale up bench experiments. This difficulty can be explained by two factors: channeling (or variation in velocities at any given cross section) and longitudinal eddy dispersion. The combined effect of these two factors can be expressed as a longitudinal dispersion. In this project longitudinal-dispersion coefficients have been measured in two-phase countercurrent flow for both the continuous and the discontinuous phase.

The effects of this dispersion can be expressed mathematically,

$$H_{oxP} = H_{ox} + H_{oxD},$$

where H_{oxP} is the height per transfer unit observed; H_{ox} is the true height per transfer unit based on the mass-transfer rate; and H_{oxD} is a correction for dispersion.[23] The H_{ox} term is dependent upon flow conditions; H_{oxD} is independent of flow conditions, but is a function of the packing porosity, size, and arrangement. As this dispersion term can be substantial, it explains the failure of certain attempts reported in the literature to correlate HTU's for liquid extraction.

For chromatography, Klinkenbert et al. have introduced a similar consideration,[38] so that $(HETP)_P = HETP + HETP_D$, where the subscripts P and D have the same significance as above.

Probably the most important application of axial diffusion is in reactor design. With fast reaction rates, the unevenness of residence time can greatly modify the products of the reaction; especially in two-phase flow and in fluidized beds, where low values of the Peclet are obtained. Longitudinal dispersion considerations are also extremely important in the design of pulse columns, rotating-disc and other agitated contactors, and spray columns.

HISTORICAL REVIEW

1. Eddy Dispersion

The first eddy-diffusion studies were reported by Towle and Sherwood for an unpacked conduit in turbulent flow.[37] Since the turbulence in the central part of a pipe is known to be nearly isotropic and uniform, these authors applied the Wilson equation[42] to derive an eddy diffusivity that was assumed to be the turbulent diffusion of water in a rectangular duct, using the mixing-length theory of Prandtl and Von Karman. This paper related the eddy diffusivity (assumed to be isotropic) to the average velocity, the half-width of the conduit, and the friction factor.

Kalinske and Pien described eddy-diffusion measurements in open channels.[12] In 1955 Taylor et al. studied longitudinal diffusion in a 9,000-foot pipeline, and found that the coefficient of dispersion was proportional to the diameter of the duct, the flow velocity, and the square root of the friction factor.[34] This expression was observed to be independent of the Schmidt number, a confirmation of the work of Taylor in 1954 for water in an open pipe.[35] A similar study for turbulent gases was made recently by Sage et al.[30]

In the first paper reporting results for turbulent flow through a fixed packing, Bernard and Wilhelm measured radial eddy diffusion; their mathematical analysis is not complete because they neglected the effect of nonisotropic diffusion.[4] Singer and Wilhelm confirmed that that for sufficiently high Reynolds numbers and sufficiently high tube-to-particle-diameter ratios, the radial Peclet number must be about 11.[31] Then Baron, from a random-walk analogy, estimated a radial Peclet number between 5 and 13;[1] and Ranz, by a detailed analysis of the splitting of the streams in a packed rhombohedral arrangement of spheres, showed that this number is around 11.2.[26]

For some time it was thought that packed-bed diffusion was isotropic; however, Klinkenberg, Krajenbrik, and Lauwerier, in a comprehensive theoretical treatment of concentration distributions caused by diffusion in a fluid moving in a packed bed at uniform velocity, noted

that it could be a mistake to neglect longitudinal with regard to radial dispersion, since the longitudinal dispersion might be much larger than the radial.[15] These authors have given equations and charts for the steady-rate solute concentration as a dimensionless function of downstream distance and radial position, for central injection of a tracer solute. Their derivation involves both axial and radial Peclet numbers and provides the most complete numerical solution available on the problem of radial dispersion.

There are some apparent disagreements in the literature between the different experimental values obtained for axial Peclet number. The values of longitudinal Peclet number corresponding to experimental measurements range from 0.294 to 1.88, as summarized in Table 1.

Table 1

Experimental Peclet number for longitudinal dispersion

Investigators	Reference number	Type of packing	N_{Re} range	$(N_{Pe})_\ell$
Klinkenberg et al.	38	Sand = 0.388 d_p = 125 to 210μ	Re < 1	0.294 to 0.400
Kramers and Alberta	17	Raschig rings	Turbulent flow (liquid)	0.900
Danckwerts	6	Raschig rings	Laminar flow (liquid)	0.55
Wilhelm and coworkers	9,22	Random-packed spheres	Turbulent flow (gas)	1.88
Rifai	27	Sand	Laminar flow (liquid)	0.30 to 0.55

It will be shown later that these differences can be explained by variations in porosity of the bed, and by a state of laminar, transition, or turbulent flow.

Hydraulic engineers for a long time have studied flow in porous media; they first considered these media as ordered bundles of capillaries, applied the law of viscous flow, and attempted to deduce

relationships between flow variables and the physical properties of the fluid.[7,32] Many investigators have shown recently that the relationships thus derived are quite inaccurate, presumably because the flow through porous media is completely disordered.[29] On this basis Oplatke and Cyrillus used an equation similar to Fick's second law of molecular diffusion,[25] while others started directly from a probability distribution.[29] In 1953 Scheidegger deduced from the ergodic hypothesis that the microscopic variations of the celocities of the fluid particles tend to follow a normal probability distribution;[29] twenty years earlier this same distribution was found experimentally by Kitagawa.[13,14] On the basis of Newton's laws of motion, Scheidegger deduced a theoretical relationship between the coefficient of dispersion and such parameters as velocity and porosity, which Danckwerts[6] and others[18] had indicated earlier were involved.

Also in 1953, Taylor described a kind of longitudinal dispersion, in flow through pipes, due to the combined effect of a parabolic velocity distribution and molecular diffusion.[33] In 1955 Beran discussed the work of Taylor, and showed on a statistical basis that Taylor's results were a consequence of the central-limit theorem which states that any sufficient number of random variables will be approximately randomly distributed, regardless of the distribution of the individual variables;[3] consequently in flow through porous media, after a long time, the concentration will be normally distributed.

Early in 1956, Day, at the University of California, applied Scheidegger's approach on the analysis of longitudinal dispersion of sodium chloride in a column of sand, and noted that the coefficient of normal dispersion exceeded the corresponding molecular diffusion coefficient.[8] Also in 1956 Rifai, Kaufmann, and Todd experimentally found a value of 0.55 for the longitudinal Peclet number in a column of Monterey sand.[27]

Only lately has enough consideration been given to dispersion phenomena in such operations as chromatography, extraction, and catalytic reactor design. In studying the hydrogenation of ethylene in a catalyst

bed with an isothermal wall, Ogburn found experimentally that temperature profiles showed a severe departure from those calculated when all other major effects except axial dispersion were taken into consideration.[24]

Similarly, of the many factors involved in the dynamic behavior of an adsorption column, the longitudinal-diffusion effect received little attention before Wicke partially studied the problem in 1939,[40,41] his work has been reviewed by Thiele.[36] Further attention was given to this effect by Lapidus and Amundson in 1952.[18] Klinkenberg et al. also used the Amundson-Lapidus approach, but with considerable simplification. A combination of these two lines of thought leads to a simple relation between the HETP (or HTU) and the various parameters of the rate theory.[38]

Recent studies at the University of California by Vermeulen, Lane, Lehman, and Rubin[39] and by Miyauchi[23] have provided data on the effect of axial diffusion on extraction-column performance in agitated, packed, and pulsed columns.

2. Previous Studies of Ordered Packings

Many investigations have been conducted on the flow of fluid through porous media. These investigations have led to a variety of correlations involving the density, the viscosity, and the velocity of the fluid; the diameter, shape, and roughness of the particles; and the porosity or void fraction of the packed bed. Since packed beds usually are formed by random dumping, the possible effects of orientation have been more or less neglected. J. J. Martin, W. L. McCabe, and C. C. Monrad studied the effect of orientation upon pressure drop through stacked spheres, and found a definite effect of packing arrangement.[21] They based their project on the thorough investigation made in 1935 by Graton and Fraser on the stacking of spheres.

According to Graton and Fraser, among the infinite number of ways to arrange spheres on an horizontal plate there are two simple arrangements.[11] One of these has all the spheres lying at the corners of squares, while the other one has the sphere centers at the apexes of

equilateral triangles. The first arrangement is called a square layer, the second a rhombic layer. Then there are only three possible choices for the second layer on top of this one: the spheres can be centered at the centers of the triangles (or squares), at the apexes (or corners), or in the middles of the sides. This gives us six (3 x 2) possible combinations for packing spheres, as listed in Table 2. Here S_1, S_2, S_3 are square-based packings, and R_4, R_5, R_6 are rhombic packings.

Table 2

Ordered packing arrangements for uniform spheres

Designation	Name	Distance between layers	Porosity	Number of nearest neighbors
S_1	Cubic	d_p	0.475	6
S_2	Orthorhombic-1	$0.866d_p$	0.3954	8
S_3	Rombohedral-1	$0.707d_p$	0.2595	12
R_4	Orthorhombic-2	d_p	0.3954	8
R_5	Tetragonal	$0.866d_p$	0.3019	10
R_6	Rombohedral-2	$0.816d_p$	0.2595	12

In Table 2, although it first appears that there are several arrangements of the same porosity, it turns out that some arrangements with different names are really identical; what is different is the major axis of observation. Orthorhombic-1 with blocked passages, observed along the proper axis, will prove to be the same as orthorhombic-2 with clear passages. The same observation applies for rhombohedral-1 and -2.

Martin's and co-workers' results, when compared with Carman's,[5] showed that for the same porosity a regular packing gives generally a lower friction factor than the corresponding random packing. The results, however, are slightly higher for a tetragonal than for a random arrangement, and considerably higher for the orthorhombic-2 arrangement. It is

interesting to note that the orthorhombic-2 arrangement, having the same porosity as orthorhombic-1, gives a friction factor nearly five times as high. This can be explained by the smaller orifices or row openings in the parallel channels of the orthorhombic-2 arrangement.

THEORETICAL ANALYSIS

1. Longitudinal Dispersion

In a stream of material that flows steadily through a vessel, usually neither piston flow nor perfect mixing is realized. Instead, a distribution of residence times is obtained which is a function of the geometry of the vessel and of the flow conditions. The distribution is best visualized if one suddenly changes a property (e.g., concentration of the incoming stream) from one steady value to another. If the residence time is the same for all elements, the response curve also is exactly a step function which is delayed (with respect to the original disturbance) by the time of residence. If there is complete mixing in the system, the curve response for a stepwise disturbance is an exponential function. In between these two extremes we find the response curves observed in practice.

Instead of a stepwise disturbance, any kind of initial disturbance can be introduced, and the same information can be obtained by analyzing the resulting response curve. As special cases, the stepwise disturbance and the delta or pulse function are convenient because for these the mathematical relation to the distribution of residence times can be established. However, it is difficult to produce a sharp step, especially in relation to short residence times.

This difficulty could be partly overcome by applying a sinusoidal disturbance to the incoming stream. The frequency-response diagram can be transformed into a distribution curve by using the method of

Fourier analysis. The main advantages of such harmonic analysis are that no discontinuities have to be introduced into the fluid stream and that one thus avoids the mathematical complexities of the step-function method. For liquid flow, to produce a good sinusoidal disturbance is not easy, either.

In the study described here, longitudinal dispersion has been measured by the breakthrough curves resulting from step-function inputs. Several known mathematical approaches can be used to derive the breakthrough behavior as a function of the dispersion coefficient. These approaches, which also could be used to describe the output from a pulsed or a periodic input, are:

(a) the random-walk or statistical model;

(b) perfectly mixed regions of equal volume, in series;

(c) the continuous differentially varying concentration gradient.

In each of these treatments, the system is considered as one-dimensional; that is, concentrations are taken as uniform in the cross section perpendicular to the direction of flow.

a. Random-Walk Model

Einstein has developed equations for the stream transport of suspended solid particles.[10] His derivation can be applied to this problem. A tracer molecule in a packed bed may be considered as advancing from point to point in a somewhat erratic way, with its general direction of displacement always in the direction of the flow. The path followed by the molecule is made up of a succession of random steps involving different distances and occurring at different times.

By analogy with the kinetic theory of gases, we may define an average length of steps H, which is likely to be of the same order of magnitude as the characteristic packing length; and a corresponding time $\theta = H/u$, where u is a velocity that is characteristic of the molecules (but not necessarily of the main stream).

Thus it is possible to define a dimensionless time and a dimensionless length,

$$N = h/H, \tag{1}$$

$$T = \tau/\theta = u\tau/H, \tag{2}$$

where h is the length of the bed, N the number of dispersion units available in the corresponding length h, τ the actual elapsed time, and u a characteristic velocity.

We now examine the probable position of a molecule after n + 1 steps, corresponding to

$0 < N_1 < N_2 < \cdots < N_{n+1}$ dispersion units and

$0 < T_1 < T_2 < \cdots < T_{n+1}$ units of time.

Galton's probability distributions, involving exponential decay with length and time, can be used:

$$p(N)\, dN = e^{-N}\, dN, \tag{3}$$

$$p(T)\, dT = e^{-T}\, dT. \tag{4}$$

It is necessary to consider all molecules starting from point zero at time T = 0. The probability that a molecule will travel a distance N is e^{-N}. Since this is the first step, the probability density for particles that have as yet taken only one step is $e^{-N\ -T}$. This can be written

$$p_1 = p(N_1, T_1)\, dN_1\, dT_1 = e^{-N_1\ -T_1}\, dN_1\, dT_1. \tag{5}$$

For step 2, starting at any point N_1, at a time T_1, the probability density for particles that have as yet taken only their second step is $e^{-(N_2-N_1)\ -\ (T_2-T_1)}$. Combination of this with Equation 5 gives

$$P_2 = e^{-N_1-T_1}\ dN_1\, dT_1\ \ e^{-\ (N_2-N_1)-(T_2-T_1)}\, dN_2\, dT_2. \tag{6}$$

Similarly, the result for the (n+1)th step is

$$P_{n+1} = e^{-\ N_{n+1}\ -\ T_{n+1}}\, dN_1 dN_2 \cdots dN_{n+1}\ dT_1 dT_2\ \cdots\ dT_{n+1}. \tag{7}$$

To take into consideration all the possible combinations of time and distance intervals that may lead the molecule into the element $dN_{n+1}\, dT_{n+1}$, Equation 7 requires integration with respect to $T_1 \cdots T_n$ and $N_1 \cdots N_n$. As utilized by Einstein, the successive integrals take the form

$$\int_0^{N_n} (N_{n-1})^{n-2}/(n-2)!\ dN_{n-1} = N_n/(n-1)!.$$

For the time variable in the nth step, the upper integration limit is not T_{n+1}, but instead the instant of measurement T.

For (n+1) steps, then, the integrated result is

$$P'(N_{n+1},T_{n+1})\, dN_{n+1} dT_{n+1} = [\exp(-N_{n+1}-T_{n+1})](N_{n+1}^n/n!)(T_{n+1}^n/n!) \qquad (8)$$

As T is less than all possible values of T_{n+1} the values of T_{n+1}, range from T to ∞. Integration of dT_{n+1} over these limits gives the total probability of encountering molecules at time T.

We note

$$\int_T^{\infty} \exp(-T_{n+1})\, dT_{n+1} = \exp(-T) \qquad (9)$$

The foregoing results can be used, with the multiplier dN_{n+1} dropped and N_{n+1} set equal to N, to give

$$p_T(N) = \exp(-N-T)\ (N^n/N!)\ (T^n/n!) \qquad (10)$$

But the point (N,T) has been reached after (n+1) steps. To obtain a complete description of the phenomenon it is necessary to sum n over all values from 0 to infinity, to give the expression

$$p_T(N) = \sum_{n=0}^{n=\infty} [\exp(-N-T)].\ (N^n/n!)\ (T^n/n!) \qquad (11)$$

or

$$p_T(N)\, dT = \exp(-N-T)\ I_o\ (2\sqrt{NT})\, dT. \qquad (12)$$

Expression (12) is normalized; i.e.,

$$\int_0^{\infty} \exp(-N-T)\ I_o\ (2\sqrt{NT})\, dT = 1.$$

This can be proved by writing

$$\sum_{n=0}^{n=\infty} e^{-N} \, (N^n/n!) \qquad \int_0^{\infty} e^{-T} \cdot (T^n/n!)$$

and using $\int_0^{\infty} e^{-T} \, T^n \, dT = n!$, as given in standard tables.

Then one has

$$e^{-N} \sum_{n=0}^{n=\infty} (N^n/n!) \, (n!/n!),$$

hence

$$e^{-N} \cdot e^{+N} = 1.$$

If a tracer is fed continuously at the plane N = 0, starting at time T = 0, the equation of the concentration at the plane N = N is obtained by integration with respect to the time T. The result is

$$c/c_0 = \int_0^T \exp(-N-T) \cdot I_0 (2\sqrt{NT}) \, dT. \qquad (13)$$

This expression meets the boundary conditions $c/c_0 = 0$ for T = 0 and $c/c_0 = 1$ for $T = \infty$. It follows from the derivation that it can be applied even to short beds in which the number of dispersion units is low.

Equation 13 includes the normal distribution as a special case for large values of N. An approximation for this expression, given by Klinkenberg,[16] is

$$\frac{c}{c_0} = \frac{1}{2} \left[1 + \operatorname{erf} \left(\sqrt{T} - \sqrt{N} - \frac{1}{8\sqrt{N}} - \frac{1}{8\sqrt{T}} \right) \right] \qquad (14)$$

and for large values of N and T this reduces to

$$c/c_0 = 1/2 \left[1 + \operatorname{erf} \left(\sqrt{T} - \sqrt{N} \right) \right]. \qquad (15)$$

With the use of Equation s 1 and 2 this can be written

$$\frac{c}{c_0} = \frac{1}{2} \left[1 + \text{erf} \frac{h - u\tau}{2\sqrt{E\tau}} \right], \tag{16}$$

where $E = H\ u.$ (17)

Equation 17 gives a definition of the dispersion coefficient E as a function of the characteristic length of the bed and the characteristic velocity, which will be discussed later.

b. Poisson Distribution

In the words of Bennett and Franklin,[2] "the Poisson distribution arises when we have discrete events occurring randomly over a long period of time, and when we consider as a random variable the frequency with which these events will occur in any small amount of time chosen at random. The numbers of possible events should be large, but the probability of occurrence of any individual event in the time interval should be small."

If the input of tracer molecules and their probability of reaching the plane N is again considered, the residence time of a tracer molecule can be regarded as a random variable having an expected value N. From the definition of the Poisson distribution, the probability of appearance of a tracer molecule after time T is

$$p(T)\ dT = (e^{-T}\ T^N/N!)\ dT \tag{18}$$

Consequently it is possible to apply the Poisson distribution to the dispersion problem in the hypothetical case of a bed made of independent mixing units. If in the derivation of Equation 13 the number of steps n is such that $n + 1 = N$, and if the interaction of the various mixing cells is neglected, Equation 7 becomes

$$P_{n+1} = e^{-T_n}\ dT_1 \cdot\cdot\cdot\cdot\cdot dT_N, \tag{19}$$

and integration as in Equation 8 leads to the expression

$$p_T(N)\ dT = T^N e^{-T}/N!\ dT,$$

which is identically the Poisson distribution given by Equation 18.

As a consequence of this derivation Equation 13 reduces to a Poisson distribution at large values of N.

c. Apparent Diffusion Method

Another approach to the dispersion problem is given by the differential equation for convestive diffusion,

$$E \frac{\partial^2 c}{\partial h^2} - U \frac{\partial c}{\partial h} = \frac{\partial c}{\partial c} . \tag{20}$$

For the assumptions $E = Hu$, and $u = U$, where U is the interstitial velocity in the bed, this reduces to the dimensionless form

$$\frac{\partial^2 c}{\partial N^2} - \frac{\partial c}{\partial N} = \frac{\partial c}{\partial T} \tag{21}$$

The solution to the equation depends on the boundary conditions.

(a) The bed is assumed to be finite in length, and the plane of measurement is at finite distance.

The boundary conditions are, at the inlet,

$$N = 0 \; ; \; c - c' = \partial c/\partial T. \tag{22}$$

The concentration of the tracer in the entering stream is c'. Owing to dispersion, the concentration just inside the entrance of the reactor, at N = 0, is less than c'. The boundary condition expresses the fact that the rate at which the tracer is fed to the bed is equal to the rate at which it crosses the plane N = 0 by the combined effect of flow and dispersion.

A similar boundary can be written for the outlet ($N = N_D$):

$$c - c'' = \partial c/\partial T \tag{23}$$

where c'' is the concentration of the exit stream. If $\frac{\partial c}{\partial T}$ were negative, the concentration in the exit stream would be greater than that at the end of the packing. If $\frac{\partial c}{\partial T}$ were positive, the concentration inside the column would pass through a minimum and then rise towards the downstream end. Neither of these alternatives is possible, so that the boundary

condition will be, at $N = N_D$,

$$\partial c / \partial T = 0. \tag{24}$$

A useful transformation is given by a change of coordinates,

$$c = \psi \exp (N/2 - T/4), \tag{25}$$

which provides the new equation

$$\frac{\partial^2 \psi}{\partial N^2} = \frac{\partial \psi}{\partial T}. \tag{26}$$

By separation of variables, Miyauchi[23] has obtained the expression

$$\frac{c}{c_0} = \sum_{n=0}^{n=\infty} \exp \left[\frac{Nb}{2} \left\{1-\frac{T}{2} \left(1+\left[\frac{2\mu_n}{N}\right]^2\right)\right\}\right] \cdot \frac{N \mu_n \left[N \sin \mu_n b + 2 \mu_n \cos \mu_n b\right]}{\left[(N/2)^2 + N + \mu_n^2\right] \left[(N/2)^2 + \mu_n^2\right]}, \tag{27}$$

where b = (measured length)/(total length), (28)

$$\mu_n = \cot^{-1} \mu_n/N - N/4 \mu_n, \tag{29}$$

and N now represents N_D.

The solution of this equation has been plotted on Figures 1 and 2 for b = 0.2 with Nb = 2 and Nb = 10, for comparison with other solutions of the dispersion problem.

(b) The bed is assumed to be infinite in length. The boundary conditions are, in this case,

$$\text{at } T > 0 \text{ and } N > 0, \quad c - c' = \partial c/\partial T; \tag{30}$$

$$\text{at } T < 0, \quad c = 0; \tag{31}$$

the solution is

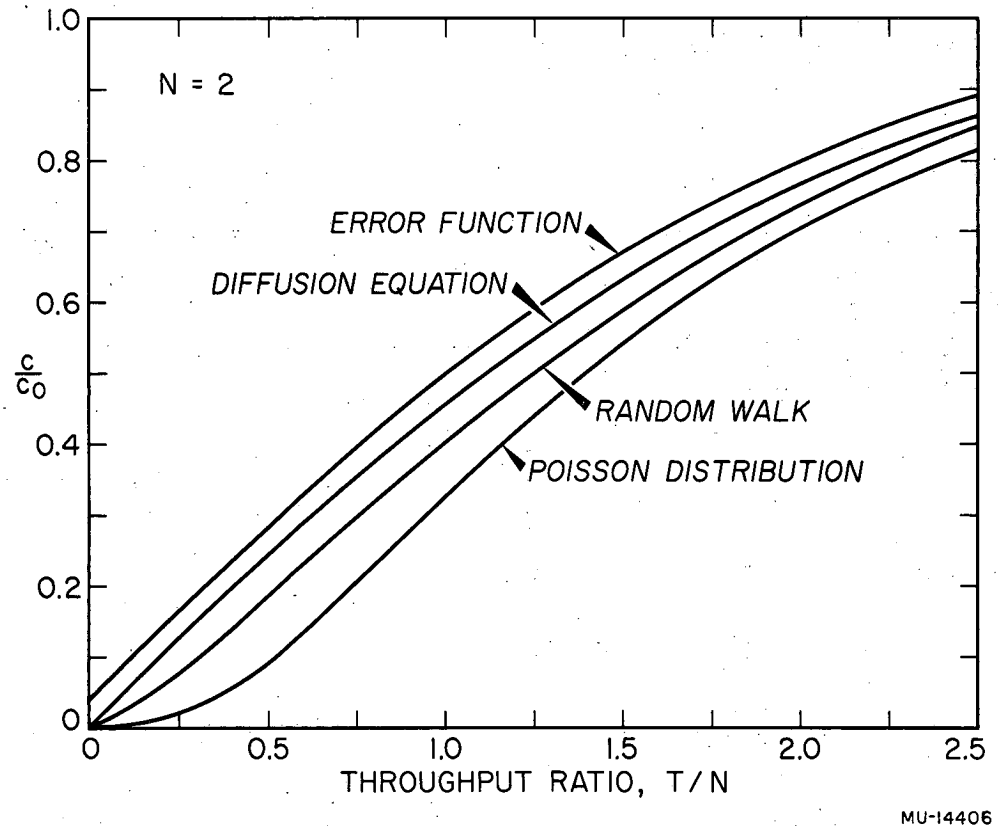

Fig. 1 Breakthrough curves given by various derivations (N=2).

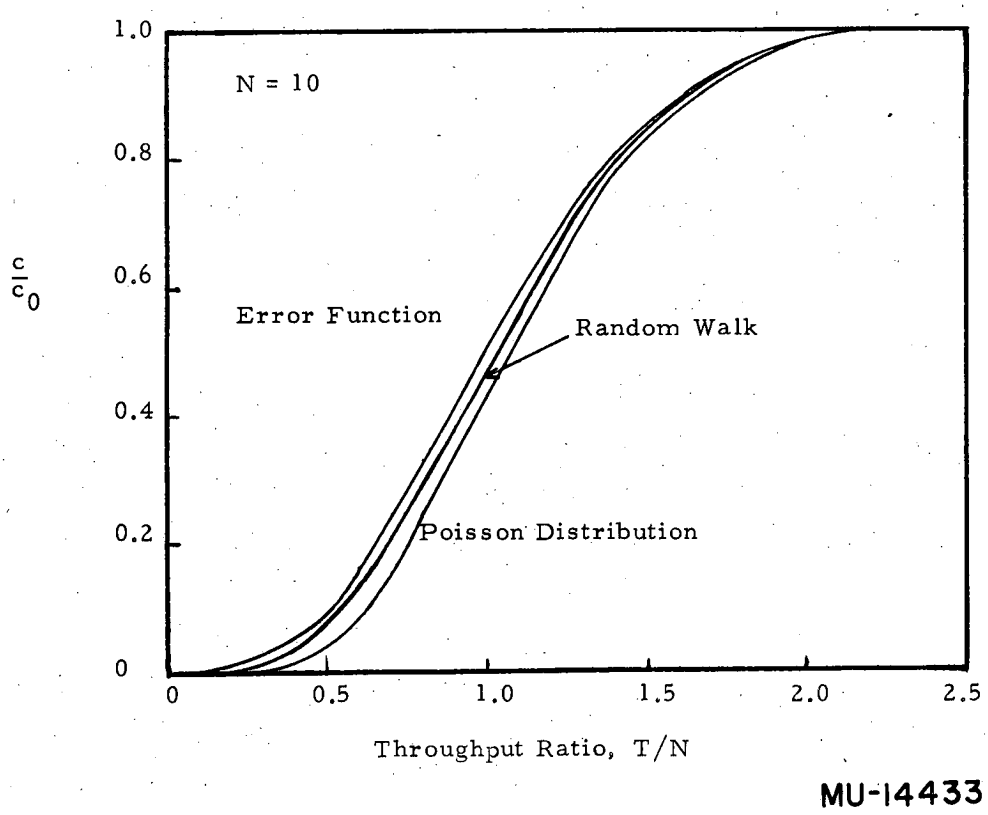

Fig. 2 Breakthrough curves given by various derivations (N=10).

$$c/c_0 = 1/2 \left[1 + \operatorname{erf} \left(\frac{T - N}{2\sqrt{T}} \right) - \exp N \cdot \operatorname{erfc} \left(\frac{T + N}{2\sqrt{T}} \right) \right]$$

$$+ \int_0^T \exp - \left(\frac{(N - T)^2}{4T} \right) \cdot 1/2 \sqrt{\pi \tau} \left[1 - \frac{2T}{N + T} \cdot \left(1 - \frac{2T}{(N + T)^2} \right) + \frac{12 T^2}{(N + T)^4} \cdots \right] d T. \qquad (32)$$

The last term of Equation 32 is a corrective term that is negligible for large values of N and T; similarly the term erfc drops for (N+T) large, the first two terms of the equation predominate, and we again find Equation 16 as the limiting normal distribution. This is a consequence of the central-limit theorem that states that an accumulation of any kind tends towards a normal distribution.[13,14,29] Numerical evaluation of Equation 32 at N = 2 confirms the results of Equation 27 at Nb = 2 (with N large).

Comparison of the random-walk results with those from the dispersion equation shows that the dispersion coefficient can be written E = H U, where H is the average length of the mixing path and U is the interstitial velocity (assumed equal to the characteristic mixing velocity u).

d. Discussion of Theoretical Derivation

Figure 1 shows the results of Equations 13, 18, 16, and 27 for N = 2; Figure 2 those for N = 10. Note that Equation 27 falls between Equations 13 and 18. Above N = 10 the results for all practical purposes are equivalent. Consequently the various solutions of the problem have an interest for short beds only; for medium-sized beds the solution is already close to the error-function curve.

In short-bed derivations, Equation 13 fits the data reasonably well, with better accuracy than the other solutions, and it is therefore the preferred result. Figure 3 gives the numerical concentration values calculated for the random-walk approach (actually using Equation 14).

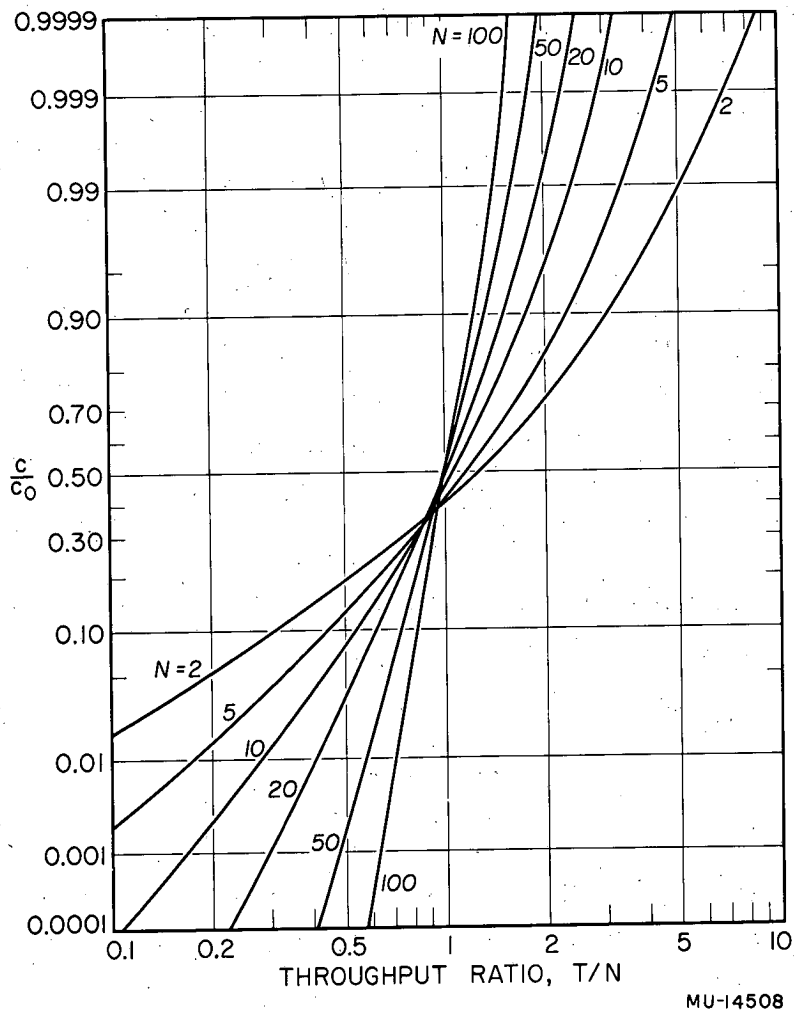

Fig. 3 Random-walk breakthrough concentration.

e. Application to Experimental Results

(i) Longitudinal diffusion.

If Equation 13 is differentiated with respect to the throughput parameter T/N_D, we get

$$s = \partial(c/c_0)/\partial(T/N_D) = \partial(c/c_0/\partial T)\cdot(\partial T/\partial(T/N_D) , \qquad (33)$$

which can be written

$$s = [\exp(\sqrt{N_D} - \sqrt{T})^2/\exp(2\sqrt{N_D T})]$$

$$\cdot [I_0(2\sqrt{N_D T})] N_D, \qquad (34)$$

where s is the dimensionless slope.

Let

$$\frac{I_0(2\sqrt{N_D T})}{\exp(2\sqrt{N_D T})} \cdot 2\sqrt{\pi}\sqrt[4]{N_D T} = \gamma. \qquad (35)$$

Since this is based on the asymptotic form of the I_0 function, γ approaches unity at large values of $N_D T$.

At $N_D = T$, Equation 34 thus gives

$$s = \gamma\sqrt{N_D}/2\sqrt{\pi} . \qquad (36).$$

Consequently the expression of N $(= N_D)$ is $N = 4\pi s^2/\gamma^2$, and as N is a function of the eddy diffusivity E,

$$N = h/H = h\,U/E , \qquad (37)$$

we see that the determination of the slope gives us the eddy diffusivity E, the mixing length H, and the Peclet number N_{Pe}. The correction factor γ is plotted on Figure 4.

Another correction factor should be applied to the calculation of the Peclet number, through the determination of the slope. We have to write N = T in the expression of the derivative to obtain N. This point would correspond to 50% concentration for an error function,

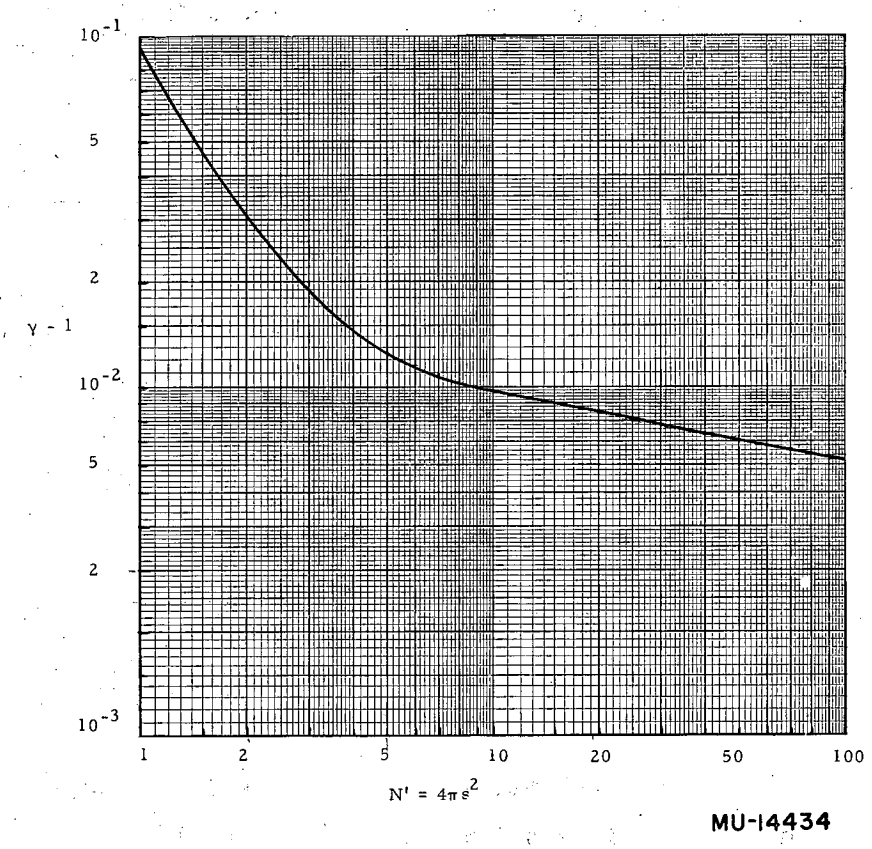

Fig. 4 Midpoint slope-correction function.

but not exactly to 50% in the actual case. For experimental determination it is convenient to take the slope at the 50% point, and to apply a correction on the time scale. In calculating this correction Equation 14 was used.

The computation of the second correction factor is given in Table 3,

Table 3

Midpoint intercept correction for calculating N_D from slope

N_D	$50 - 100(c/c_0)_{N_D=T}$ (%)	Slope	$1 - T/N_D$ [for c/c_0 = 50%]	δ	δ^2
2	10.0	0.400	.25	1.25	1.56
5	5.90	0.63	.0936	1.1	1.21
10	4.40	0.892	.0490	1.05	1.106
20	3.15	1.26	.0249	1.025	1.052
30	2.575	1.54	.0167	1.017	1.035
40	2.22	1.78	.0124	1.012	1.024
50	1.99	1.995	.0099	1.099	1.0198
60	1.82	2.185	.0083	1.0091	1.0182

and the final expression of N is obtained by the expression

$$N_D = 4 \pi s^2/(r\delta)^2 = 4 \pi s^2 \beta , \qquad (38)$$

where s is obtained by plotting the concentration in percents versus the ratio of the actual elapsed time to the time at the 50% point and taking the slope for T = 1. The correction factor δ^2 is plotted in Figure 5. In using these curves, the slope is first used for calculating the approximate value N_D':

$$N_D' = 4 \pi s^2. \qquad (39).$$

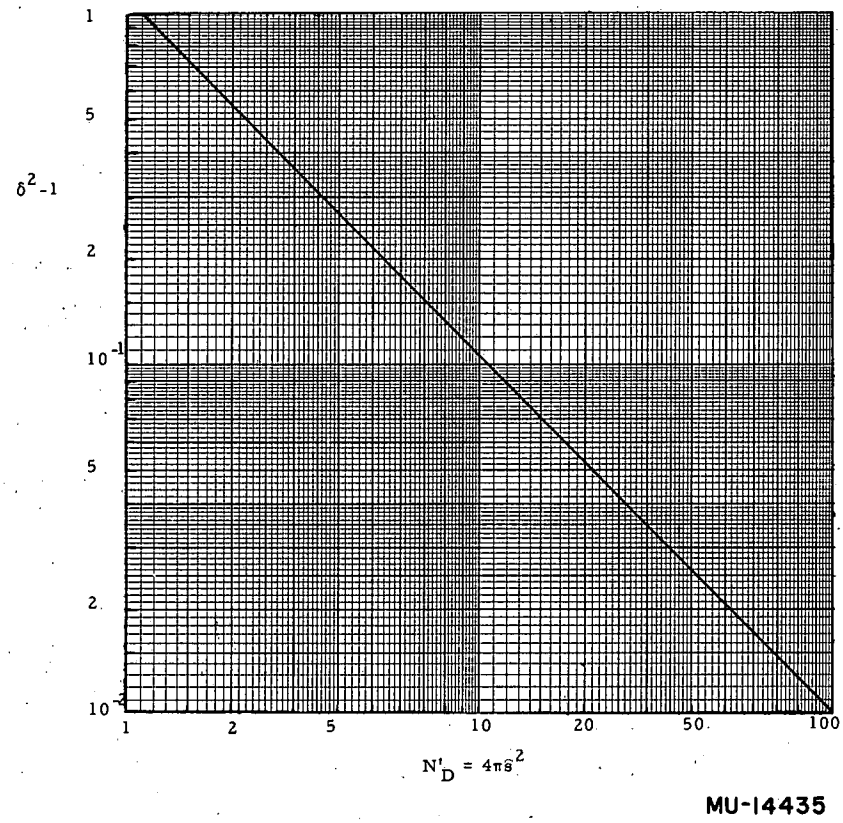

Fig. 5 Midpoint intercept-correction function.

2. Radial Dispersion

If a solute emerges from a continuous source in a point on the axis of the tube, a concentration gradient is established in the column. This is caused by subdividion and recombination of the stream around the particle, and -- at high flow rate -- also by eddy formation. The measurement involves steady-state conditions, and the analysis of experimental results is fairly straightforward as long as we are operating in an infinite space and far enough from the point source. But in most practical cases the effects of the wall cannot be neglected and the mathematical derivation becomes more complex. This problem has been solved exactly by Klinkenberg,[15] and the results of the derivation can be plotted conveniently, as in Figure 6.

If we consider the dispersion of a solute from a continuous source in a point on the axis of a tube, the general equation is

$$E_r \frac{1}{r} \frac{\partial}{\partial r} \left(r \frac{\partial c}{\partial r} \right) + E_\ell \frac{\partial^2 c}{\partial z^2} = U \frac{\partial c}{\partial z} , \qquad (40)$$

where E_r and E_ℓ are the radial and longitudinal dispersion coefficients respectively, with the boundary conditions

$$z = -\infty, \quad c = 0, \quad r = R, \quad \partial c/\partial z = 0. \qquad (41)$$

$$r/R = \rho , \qquad (42)$$

$$\sqrt{E_r} \cdot z / \sqrt{E_\ell} \cdot R = \zeta , \qquad (43)$$

$$UR/(\sqrt{E_\ell} \cdot \sqrt{E_r}) = \psi , \qquad (44)$$

$$c/c_\infty = X, \qquad (45)$$

Equation 40 transforms to

$$\frac{1}{\rho} \frac{\partial}{\partial \rho} \left(\rho \frac{\partial X}{\partial \psi} \right) + \frac{\partial^2 X}{\partial \psi^2} = 2 \psi \frac{\partial X}{\partial \zeta} , \qquad (46)$$

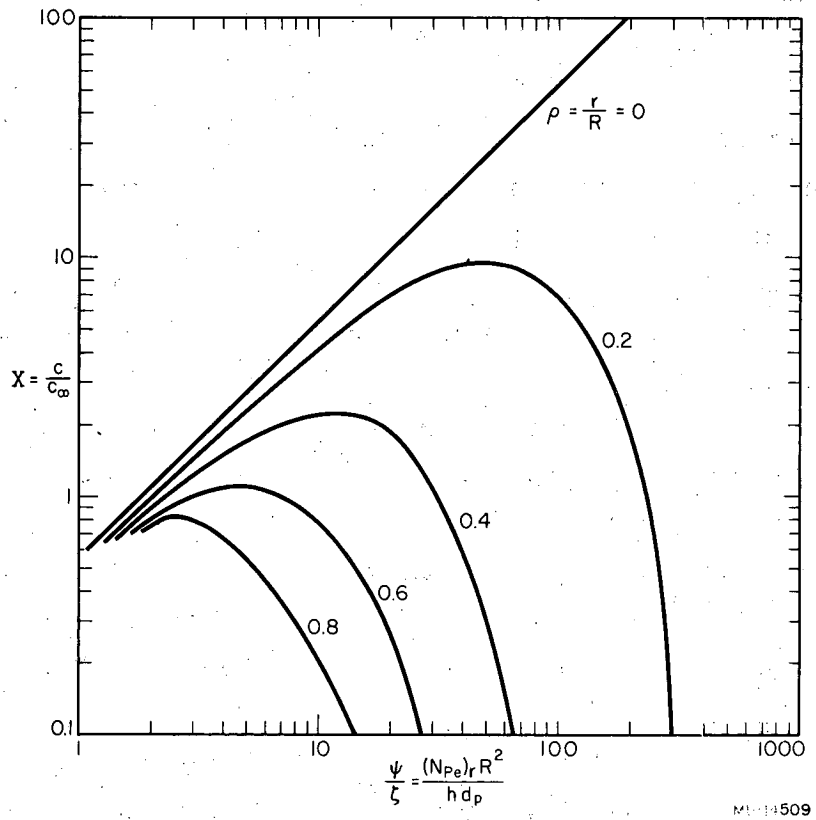

Fig. 6 Radial-dispersion function.

and for $\rho = 0$ we may express X as a function of ψ/ζ , which is a modified Peclet number.

$$\psi/\zeta = UR^2/2\, E_r\, h. \tag{47}$$

This equation can be rewritten as

$$(N_{Pe})_r = (\psi/\zeta)\, h\, d_p/R^2. \tag{48}$$

Figure 6 is a plot of X against ψ/ζ for $\rho = 0$; this chart was used for the determination of the radial Peclet in all runs.

This result was used to compute the efficiency of the nine injectors used in the octagonal columns. Concentration variations of less than 10% were calculated for a plane five particle diameters downstream from the injection level. This indicates that, for the step-function measurements, the observed ratio c/c_{max} would be close numerically to the theoretical ratio c/c_∞ (where c_∞ is the limiting concentration reached in perfect mixing).

It will be noted that the molecular diffusion has been neglected in these calculations, as the order of magnitude is much smaller than that of the eddy diffusion. According to Beran [3] the effect of the molecular diffusion is negligible for $Udp/D_m > 1$, where D_m is the molecular diffusion. As $D_m = 1.2 \cdot 10^{-5}$ cm^2/sec for dilute $NaNO_3$ solutions, only at extremely low velocity would there be need to consider molecular diffusion in the dispersion calculations.

3. Angle of Dispersion

On the basis of the discussion in Section 1.d above, the Peclet number can be written

$$(N_{Pe})_\ell = Ud_p/E = d_p/H\ , \tag{49}$$

where H is a function of the packing porosity, and of flow characteristics. Any knowledge of the mixing length specifies the Peclet number, and conversely any knowledge of the Peclet number fixes the mixing length. The determination of either H or N_{Pe} can only be experimental, as far as the

absolute value is concerned. However, it is possible to predict qualitative behavior of the parameters involved.

Coming back to H, let us consider that it is possible to assume the existence of a path vector H' parallel to the average direction of the displacement, and parallel to an eddy diffusion vector E'. This eddy diffusion vector has two components, E_ℓ and E_r (one parallel to the flow, the other one perpendicular to the flow); similarly, the path vector has two components, H and H_r.

Consequently expression 49 can be written

$$(N_{Pe})_\ell = d_p/H \,, \tag{50}$$

and similarly

$$(N_{Pe})_r = d_p/H_r \,, \tag{51}$$

by using the definitions

$$H = H' \cos \alpha \,, \tag{52}$$

$$H_r = H' \sin \alpha \,, \tag{53}$$

where α is a small angle between a path vector and the direction of flow. Two new expressions result:

$$(N_{Pe})_\ell = d_p/H' \cos \alpha \,, \tag{54}$$

$$(N_{Pe})_r = d_p/H' \sin \alpha \,. \tag{55}$$

As this dispersion angle α is small, it follows that:

(a) The value of (N_{Pe}) does not differ greatly from the value given by Equation 49.

(b) The expression of the radial diffusion is smaller by a factor of $\sin \alpha / \cos \alpha = \tan \alpha$; conversely the determination of the ratio of the two components, radial and axial, gives the value of $\tan \alpha$. The value of this angle is a function of the geometry of the packing, and of the flow conditions. Consequently:

(i) The value of α is smaller for loose packing. The longitudinal diffusion increases and the radial diffusion decreases with increasing porosity.

(ii) For equal packing porosity, the value of the angle is affected by the state of flow -- turbulent, laminar, or transition. The value of α is smaller in laminar flow, and the lengths of the mixing steps are longer. These two effects tend to increase the value of the axial Peclet number; the value of the radial Peclet number tends to increase owing to the decrease of the dispersion angle but to decrease owing to the increase of the mixing length. The net effect is therefore uncertain, but in any case smaller than the corresponding effect on the axial Peclet number.

EXPERIMENTAL OBJECTIVES

In this portion of the over-all project, the effective dispersion coefficient was measured in single-phase flow through packed beds, with the following objectives:

1. To develop methods of measurement that would be satisfactory in liquid-phase systems, including the case in which a second liquid phase is present. Both conductimetric and colorimetric methods were selected for use.

2. To establish a frame of reference for subsequent studies of two-phase flow that would simulate extraction conditions. The variables to be considered were: packing-unit, shape, arrangement, porosity, and wettability; fluid properties; and flow rates and regimes. The effect of packing orientation on the effective dispersion coefficient was investigated in beds with ordered geometrical arrangements of spherical particles.

3. To measure, in addition, the radial-dispersion coefficient. Although this study was intended primarily to provide numerical values of the axial-dispersion coefficient that could ultimately be used in the correlation and design of packed extraction columns, the availability of the apparatus provided the opportunity to make this additional measurement. The radial-dispersion coefficient is of theoretical interest for a fuller description of flow phenomena in packed columns, and is of practical interest in connection with nonisothermal flow.

APPARATUS AND PROCEDURE

1. General Specifications

The equipment was designed for the combined study of a wide range of flow rates with various sizes and types of packing arrangements, and this leads to the following specifications.

(a) Owing to the labor involved in the packing and installation of the conductivity probes and injection head of a chosen arrangement, a column once packed was kept intact for repeated experiments. Consequently different columns were designed and built corresponding to the different packings chosen for the investigation. Table 4 lists the columns and their corresponding specifications.

(b) In order to avoid an expensive duplication of the accessories, everything except the packing section was a single installation. Packed sections were locked between retaining grids of suitable design and were interchangeable. The upper and lower column heads with their accessories (level control, pressure taps, nozzles, and photocell probe) were mounted permanently on the frame in a manner that permitted rapid exchange of the packed sections. A hand-wheel-operated sling supported the head for lifting or lowering, in order to substitute any of the nine different packing sections. Metallic flexible hoses were connected to the inlet and outlet manifolds for both the top and bottom of the column, the upper hoses providing the height adjustment required for the different sections. The packed sections (weighing approximately 100 lb.) were transported between the column frame and the storage bench by a hoist supported by an overhead rail.

(c) In order to meet the flow-rate requirements (for one-phase flow with tracer injection, and for two-phase flow with tracer injection), a complex set of valves, pumps, and rotameters had to be used.

(d) The same flexibility was required of the measuring instruments, and a set of switches on the main control panel connected the two recorders for either continuous recording of a chosen conductivity cell or a photoconductivity unit, or simultaneous recording of six conductivity cells.

Table 4. Dimensions and Packing of Experimental Columns

Column number	Packing*	Diameter (in.)	Arrangement	Distance between layers(in.)	Porosity %	Column height (in.)	Injection height above grid (in.)	Useful height(in.)	Figure number
1	Spheres	0.75	Rhombohedral	0.530	25.95	26.88	2.54	23.60	6,10,13
2	Spheres	0.75	Orthorhombic-1	0.649	39.54	25.80	1.725	22.95	7,10,13
3	Raschig rings	0.22**	Random	0.293	73.00	26.38	0	26.00	11,14
4	Pellets (Tenite polyethylene)	0.232	Random	0.210	35.00	26.38	0	26.00	11,14
5	Spheres	0.75	Random	0.715	40.00	26.00	2.00	24.00	11,14
6	Spheres	0.75	Orthorhombic-2	0.75	39.54	26.25	1.125	24.00	12,15
7	Raschig rings	0.65**	Random	0.880	73.00	26.38	0	26.00	11,14
8	Intalox saddles	0.72**	Random	0.96	74.00	26.38	0	26.00	11,14
9	Sand	0.017 (av.)	Random	0.016	39.50	26.38	0	26.00	11,14

*U.S. Stoneware, except for columns 4 and 9.

**Equivalent diameter calculated according to a table by Leva.[20]

2. Columns

a. Column Bodies

The selection of regular packings implies the solution of many problems. First of all, the triangular and square arrangements chosen required flat-sided columns; thus hexagonal and octagonal columns of calculated cross section were built, in order to simulate as closely as possible a cylindrical symmetry. Such an operation requires an involved welding operation, and furthermore a corrosion-resistant material had to be chosen. Considerations of minimum weight, cost, and deformation during the welding operation necessitated the choice of aluminum rather than stainless steel for the project. Consequently each column was made of corrosion-resistant 3/16-inch 61ST aluminum sheet (alloyed with 0.25% copper, 0.6% silicon, 1% magnesium, and 0.25% chromium). Cylindrical columns of the same material were retained for the random packings. Fins were welded on the sides of each column for strengthening and handling purposes. Further, the design of each of the grids that locked the packing inside the column had to be selected according to the packing geometry.

The photograph in Figure 7 shows Column 1 (see Table 5), before packing and before drilling for the introduction of conductivity leads and sampling tubes. The bottom grid is attached to the body; the top grid and the corresponding spacer plate are removed. (It is possible to see the O-ring seal and the sample holes of the spacer plate.) There are two rings of bolts at each end; the inside rings are used for locking the grid to the body and the outside rings to attach the column to the permanent head and bottom; the four slots in the grid were cut out for the bolts attaching the bottom to the frame. Finally, 3/16-inch reinforcing plates were welded on to provide needed thickness for installation of the sampling outlets. These outlets were placed at nominal distances of 0, 3, 6, 12, and 18 inches from plane zero (the spacer plate corresponding to 24 inches), where plane zero is the level of the injection manifold. The holes in the fins are for the insertion of the lifting hoist.

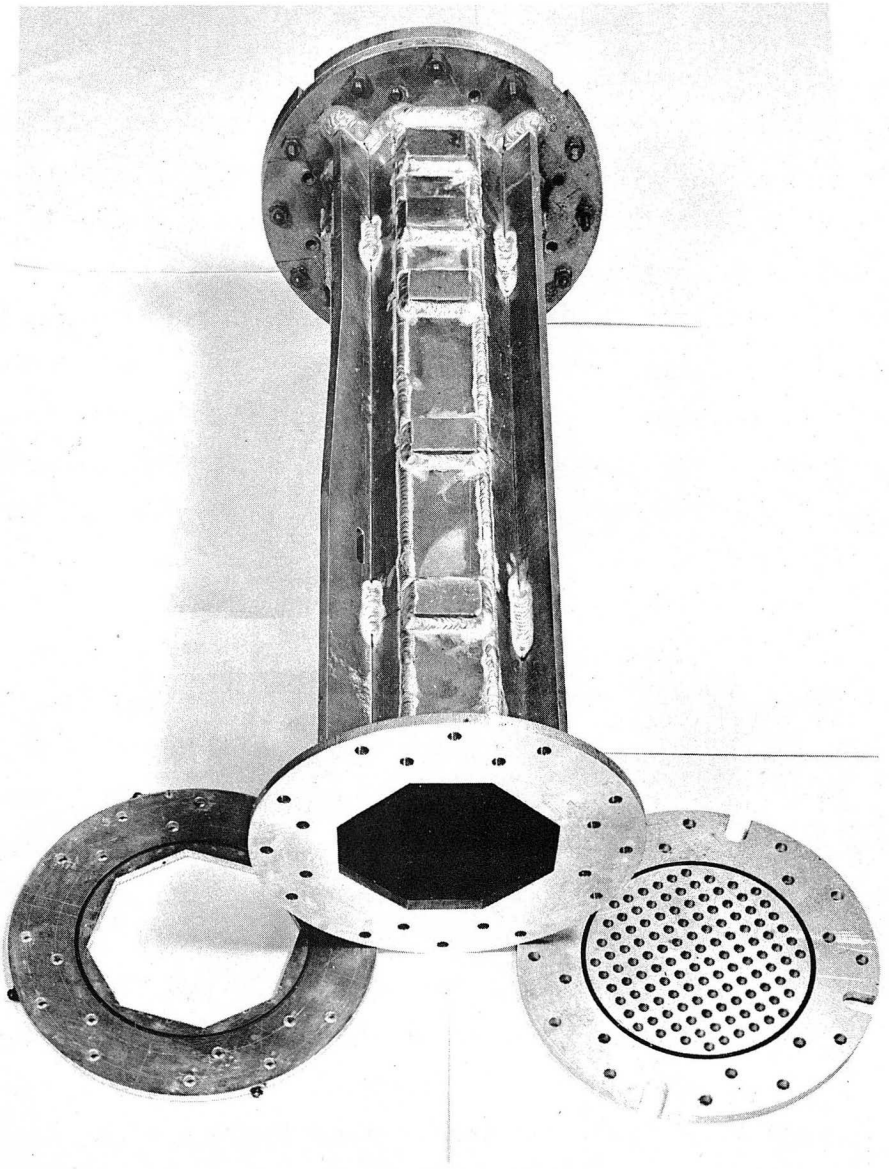

ZN-1818

Fig. 7 Octagonal column before assembly.

Table 5
Conductivity Cell Arrangement in Experimental Columns

Column No.	Nominal height above the injection plane (inches) 0		3		6		12		18		24	
	No. of layers	Cells	No. of layers	Cells	No. of layers	Cells	No. of layers	Cells	No. of layers	Cells	No. of layers	Cells
1	5	$1,3_a,3_b$	11	$1,3_c,3_d$	17	$1,3_a,3_b,4_c$	27	$1,3_c,3_d,4_a,4_b,2$	39	$1,3_a,3_b,4_c$	49	$1,3_c,3_d,4_a,4_d,2$
2	3	$1,3_a,3_b$	7	$1,3_c,3_d,4_c$	11	$1,3_a,3_b,4_a$	21	$1,3_c,3_d,4_a,4_b,2$	37	$1,3_a,3_b,4_d$	37	$1,3_c,3_d,4_a,3_a,3_b$
3, 4, 7, 8, 9*	(0)	1	(5)	$1,4_c$	(8)	$1,4_c$	(14)	$1,4_c$	(20)	$1,4_a$	(26)	$1,4_b$
5*	(0)	$1,3_a,3_b$	(3)	$1,3_c,3_d,4_c$	(6)	$1,3_a,3_b,4_d$	(12)	$1,3_c,3_d,4_a,4_b,2$	(18)	$1,3_a,3_b,4_d$	(24)	$1,3_a,3_b,3_c,3_d,4_a$
6	2	$1,3_a,3_b$	7	$1,3_c,3_d,4_c$	11	$1,3_a,3_b,4_c$	19	$1,3_c,3_d,4_a,4_b,2$	27	$1,3_a,3_b,4_c$	34	$1,3_a,3_b,3_c,3_d,4_d$

*For the random columns, the numbers in parentheses indicate the distance in inches from the injection plane.

b. Packing

Table 4 and Figure 8 give details on the nine different types and arrangements of packing used for the investigation. The 0.75-inch spherical balls were obtained as oversized balls with rough surfaces. They were wet-ground in a ball mill with granular alundum, and classified between 0.740 and 0.760 inch. Because of the geometry of the ordered packing, a boundary problem arose: as the design called for the spheres in one layer to be tangent to the wall, some of the spheres in the next layer would have to be either omitted or cut. This difficulty was avoided by insertion, in alternate layers, of spacers between the walls and the balls. Wall spacers for the second layer for columns 1 and 2 are shown in Figures 9 and 10 (the second layer is drawn in light lines; the first layer in heavy lines). Figure 11 shows the top of Column 2 before the spacer plate and the grid plate were attached.

c. Conductivity Cells

On Figure 11, in order to show the arrangement of conductivity cells in the uppermost measuring layer, the covering layer has been partly removed and the leads of the conductivity cells (that would be set inside the spacer-plate sampling holes) can be seen dangling. (The covering layer, which lay beyond the region of the measurements, was not staggered relative to the top measuring layer because of the impracticability of fitting wall-spacers inside the spacer plate.) These conductivity cells were of a special design to avoid disturbing the packing arrangement; they were made of two spherical sectors of 3/4-inch Bakelite balls connected by two rhodium-plated pins, as shown on Figure 12. On the average, twenty-five conductivity cells were installed permanently in each bed, distributed among the sampling planes at 0, 3, 6, 12, 18, and 24 inches (nominal), as indicated in Table 5 and Figures 13, 14, and 15.

d. Injection and Sampling Tubes

The injection device was installed at the 0-inch nominal level. It consisted of several injection tubes connected to an injection manifold, the arrangement and number of tubes being dependent on the packing (see Figures 16, 17, and 18). There was only one sampling tube for each sampling

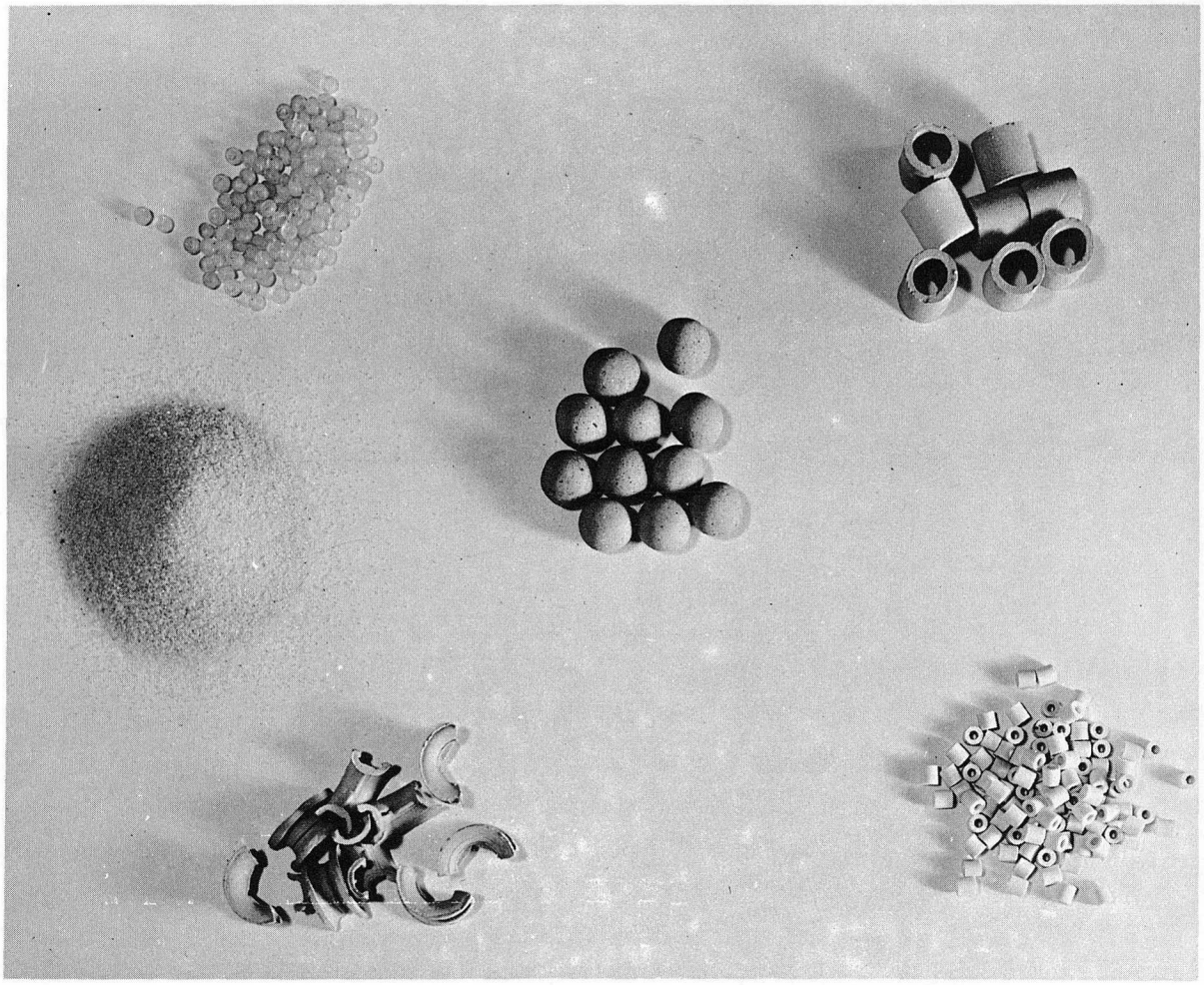

ZN-1819

Fig. 8 Column packings used.

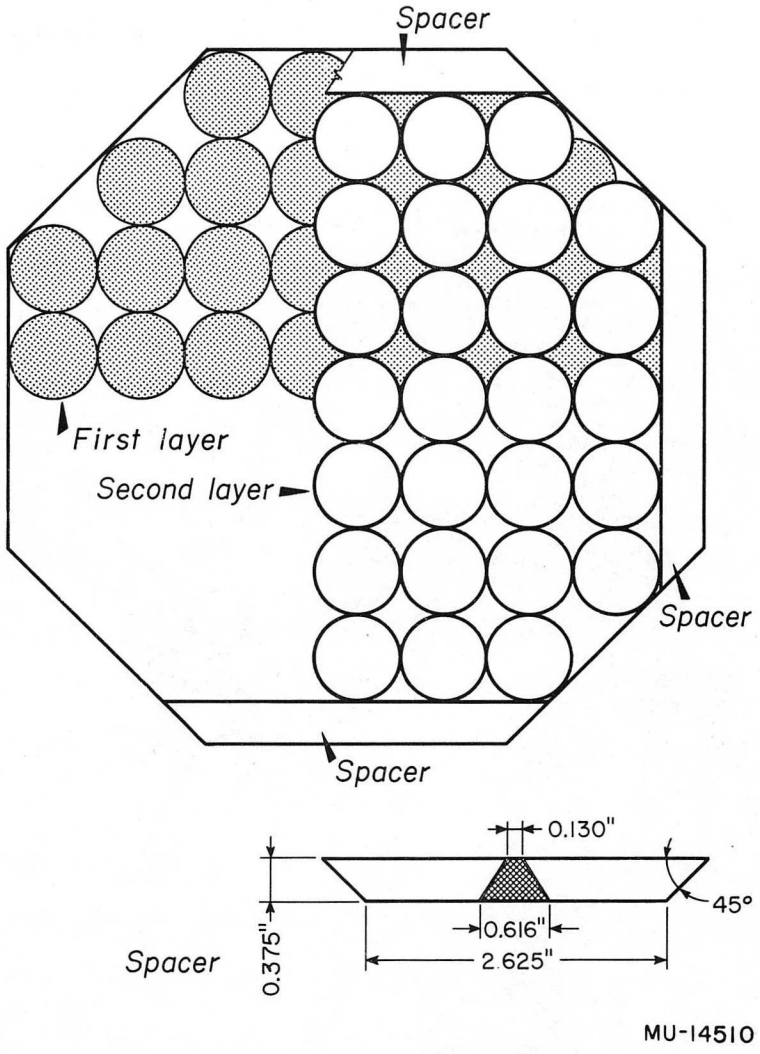

Fig. 9 Arrangement of packing and spacers, Column 1 (Rhombohedral).

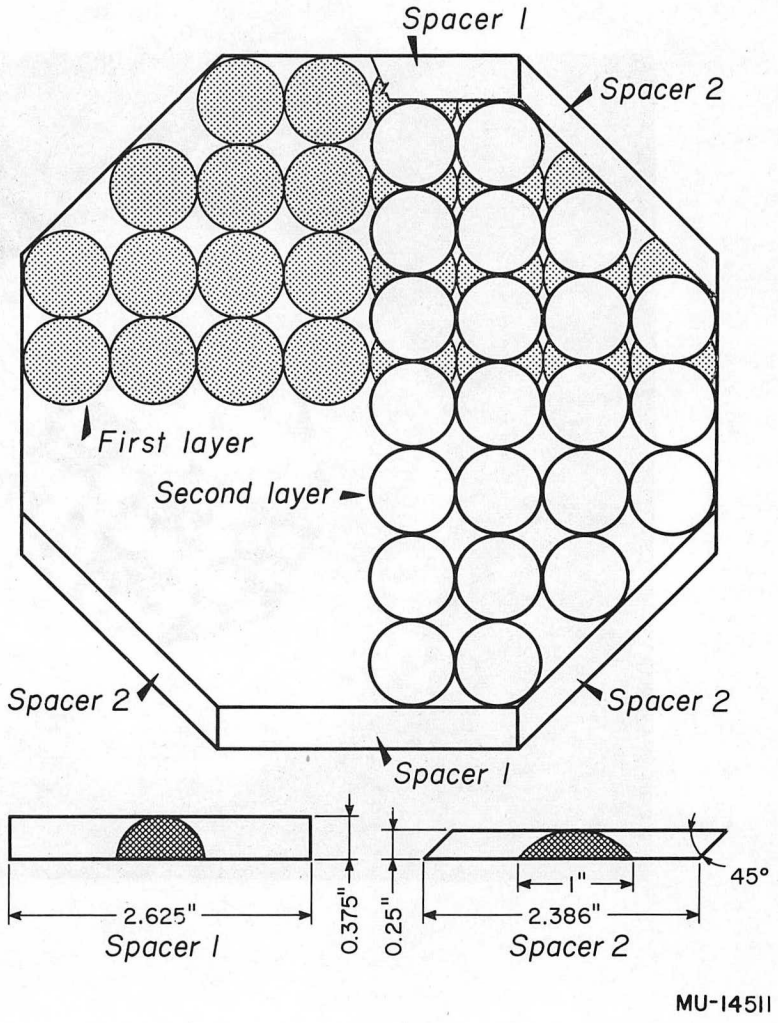

Fig. 10 Arrangement of packing and spacers, Column 2 (orthorhombic-1, octagonal).

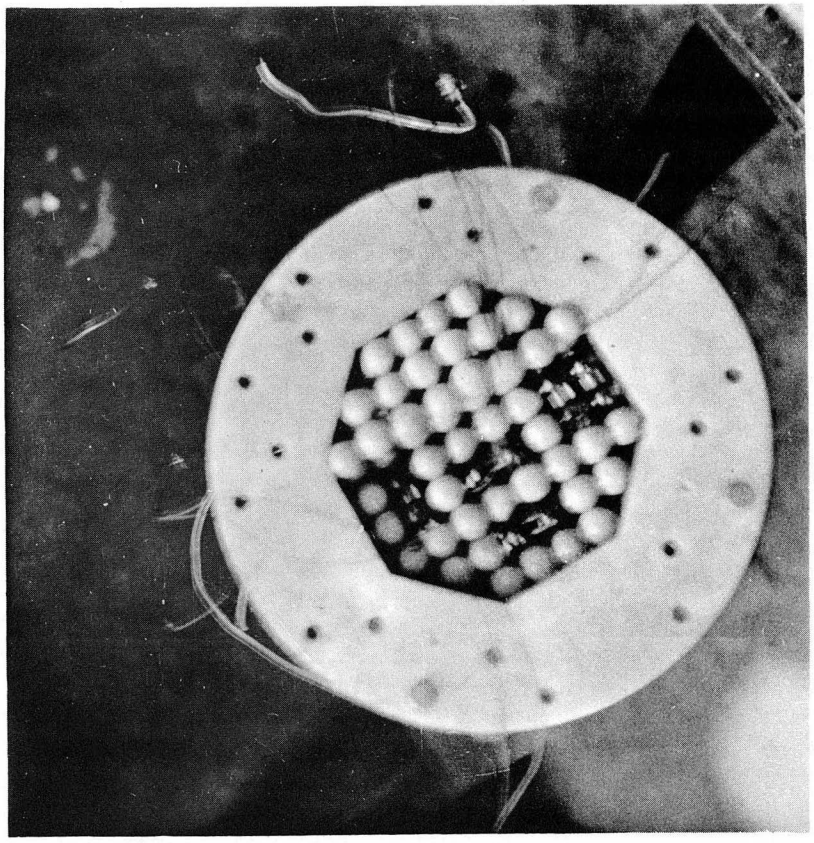

ZN-1813

Fig. 11 Packing in place in Column 1.

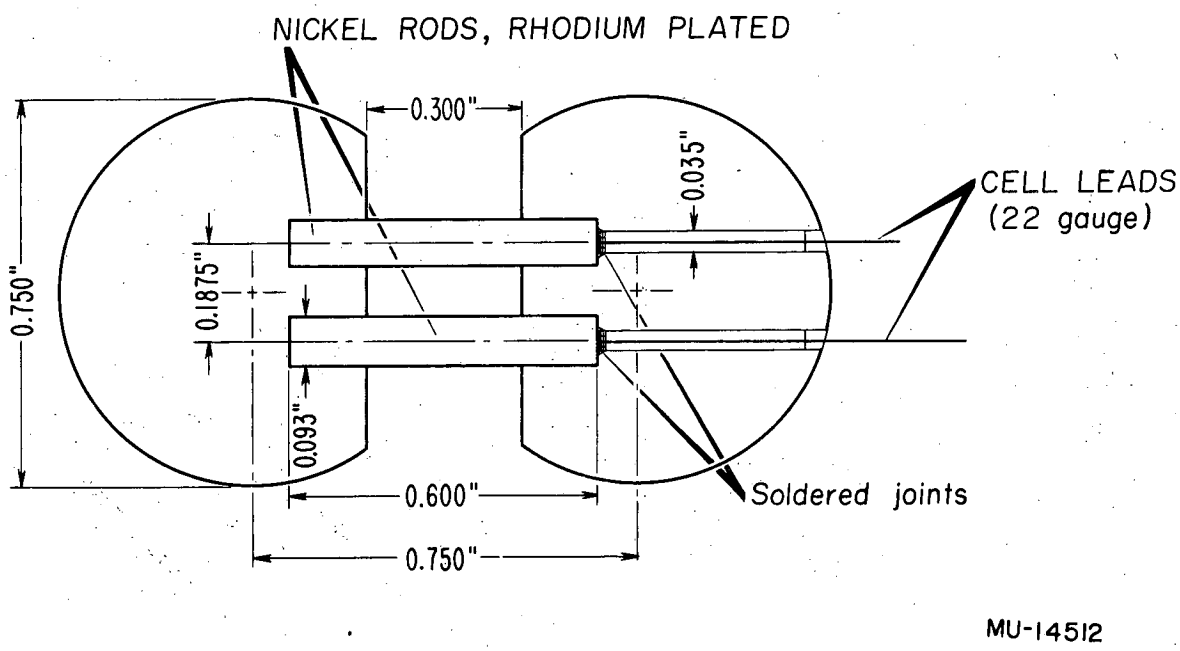

Fig. 12 Construction of conductivity cell.

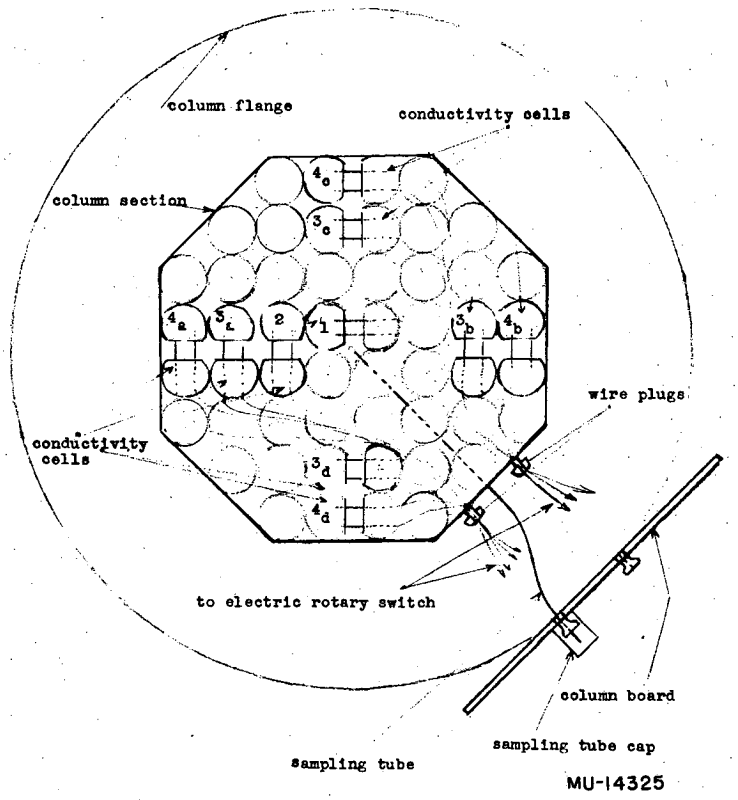

Fig. 13 Location of conductivity cells--Columns 1 and 2 (octagonal). The cells at each level were identified by the reference numbers shown.

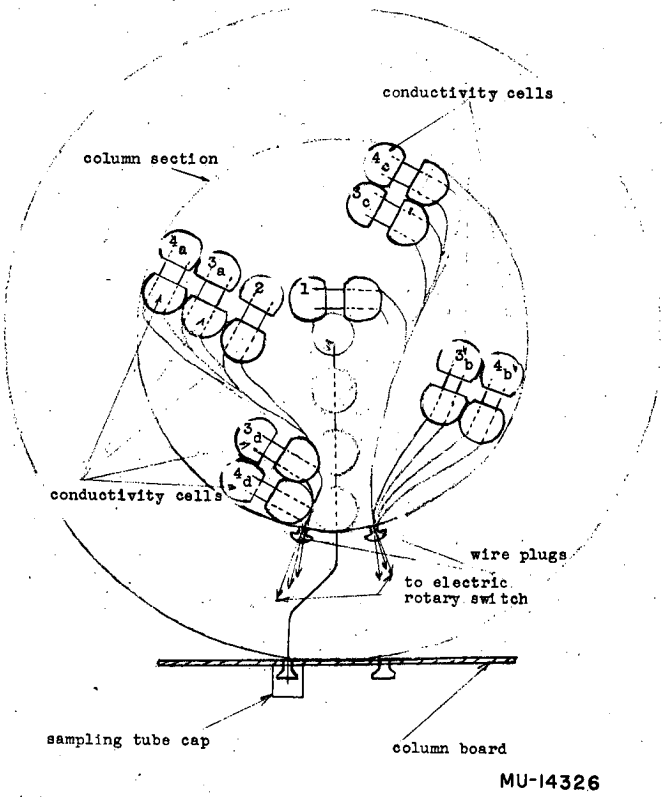

Fig. 14 Location of conductivity cells--Column 5 (cylindrical).

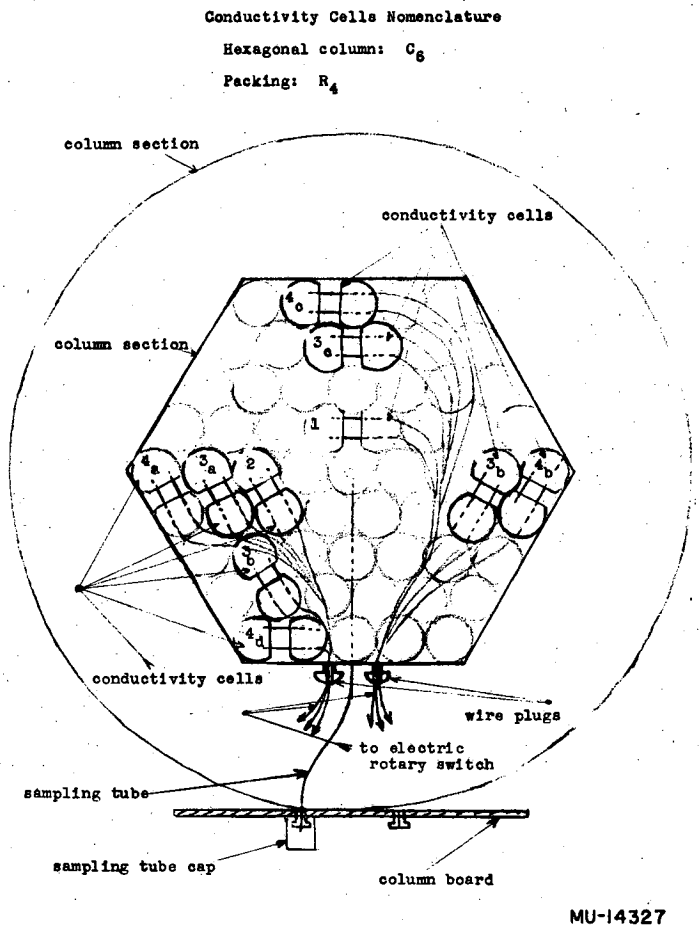

Fig. 15 Location of conductivity cells--Column 6 (hexagonal).

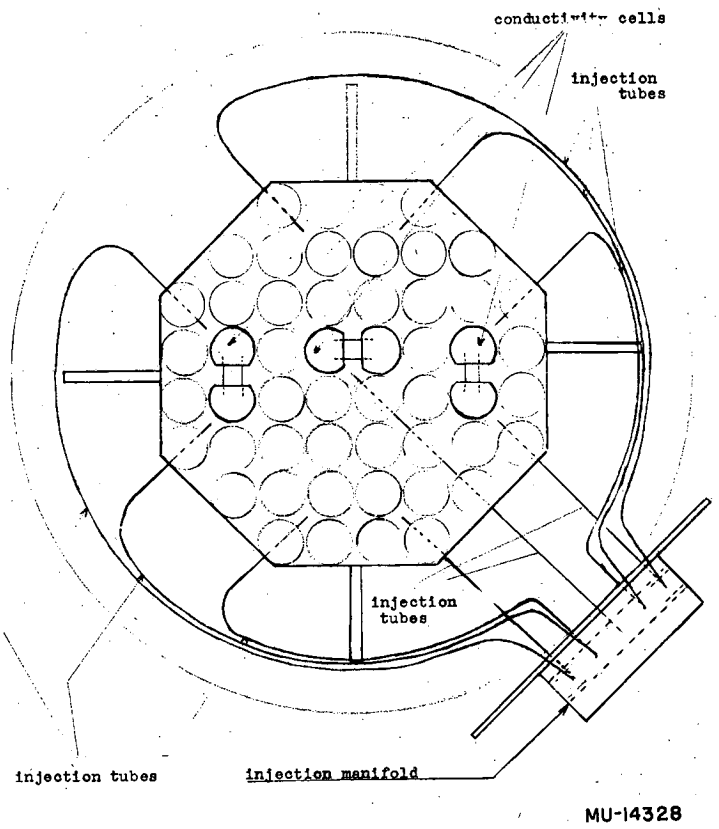

Fig. 16 Location of injection outlets--Column 1 and 2 (octagonal).

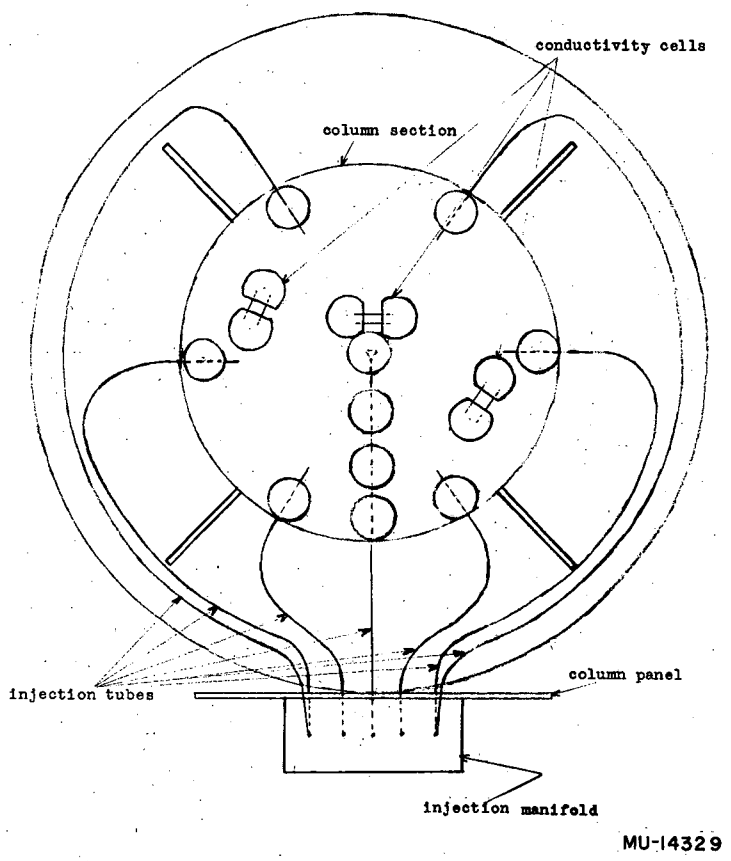

Fig. 17 Location of injection outlets--Column 5 (cylindrical).

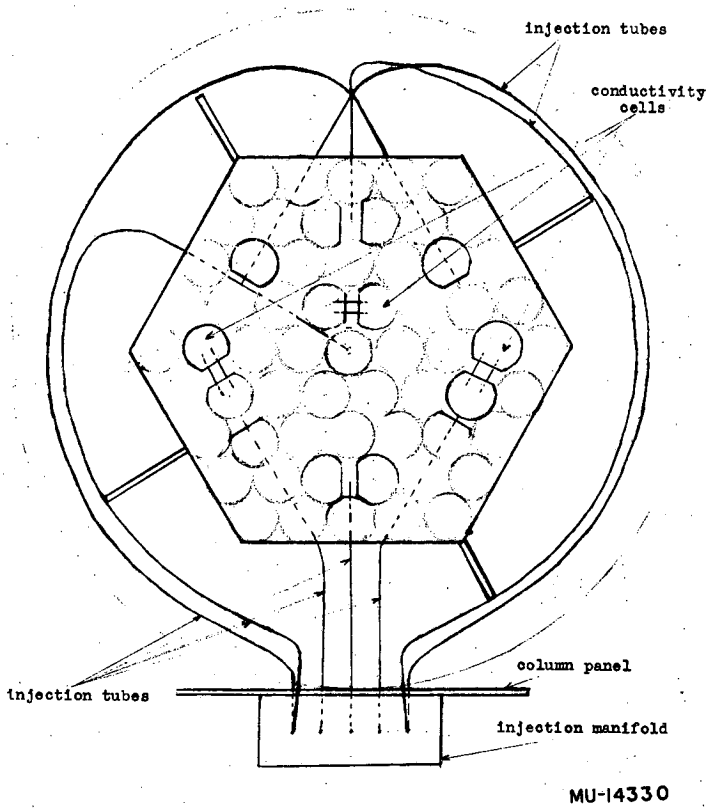

Fig. 18 Location of injection outlets--Column 6 (hexagonal).

plane at 3, 6, 12, 18, and 24 inches nominal distance as shown on Figures 13, 14, and 15. Each injection (or sampling) tube was made of annealed 302 stainless-steel tubing (0.0625-inch o.d., 0.031-inch i.d.) and ran inside the packing through drilled balls in order to minimize the disturbance of the arrangement.

e. Column Heads

Expanded end sections, identical in construction, were connected above and below the particular packed section in use. As the columns were designed to operate in upward as well as in downward flow (see Figures 19 and 20), the same accessories were adapted for both upper and lower end sections: two windows for visual observation and introduction of a photoelectric probe, an inlet nozzle designed to give a velocity profile as flat as possible (see Figure 21), two outlets in symmetrical positions with respect to the center, a liquid-level control probe, and four pressure taps.

3. Instrumentation

a. Electronics

So that available recording and switching units could be used, it was determined to measure conductances with current as the variable parameter, in a calibrated-source amplifier system. A constant-current source at 1000 cycles was impressed across the conductance to be measured, and was followed by sufficient amplification so that the resulting output when rectified would be displayed on a dc recorder. The system was found to be easy to calibrate and was capable of plotting rapid changes and of sampling a series of conductances at a high rate of switching (see Figure 22).

The electronic measurement system thus had four parts: an amplitude-stable oscillator, a constant-current generator, an output amplifier, and an ac to dc converter to feed the strip chart recorder.

The 1000-cycle oscillator circuit employed (V_1, V_2 of Figure 23) was of the bridge "T" type with thermal nonlinear element stabilization.

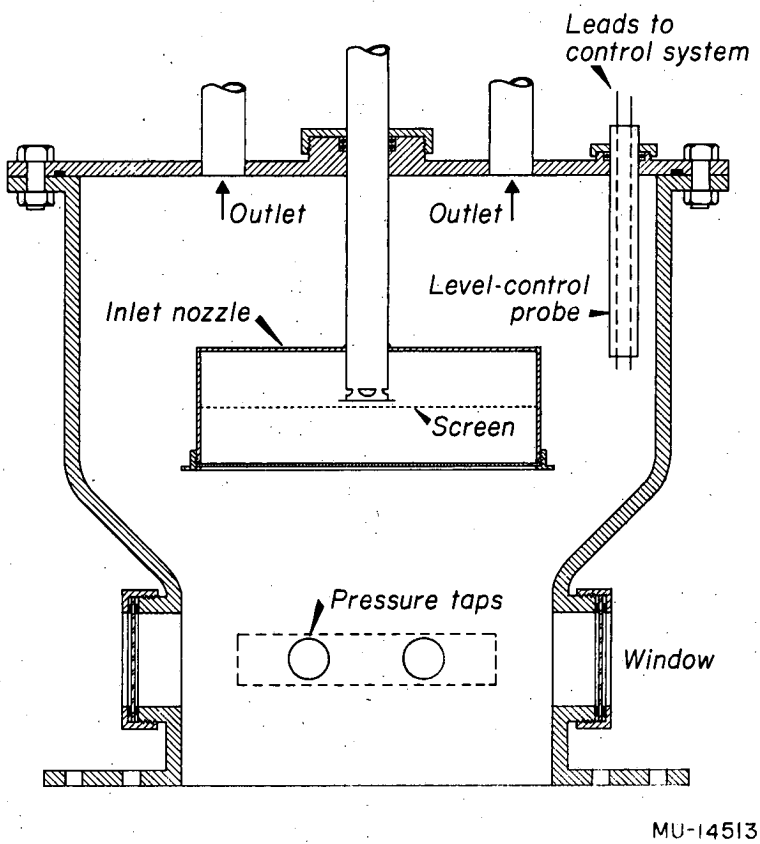

Fig. 19 Diagram of column head.

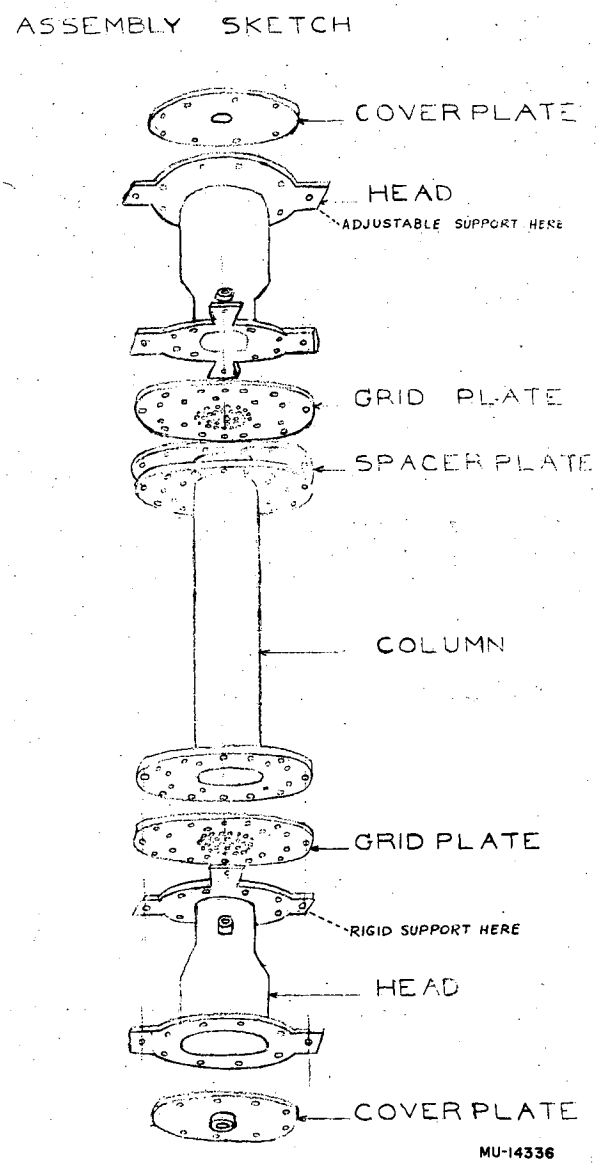

Fig. 20 Exploded assembly diagram of entire column.

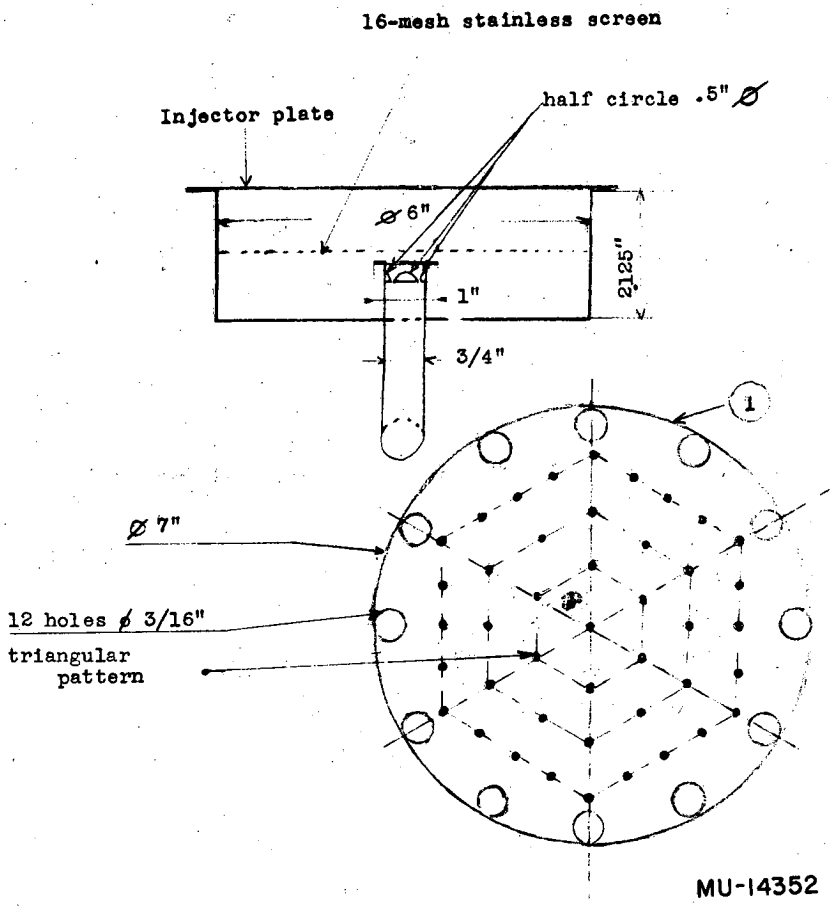

Fig. 21 Detail of nozzle construction.

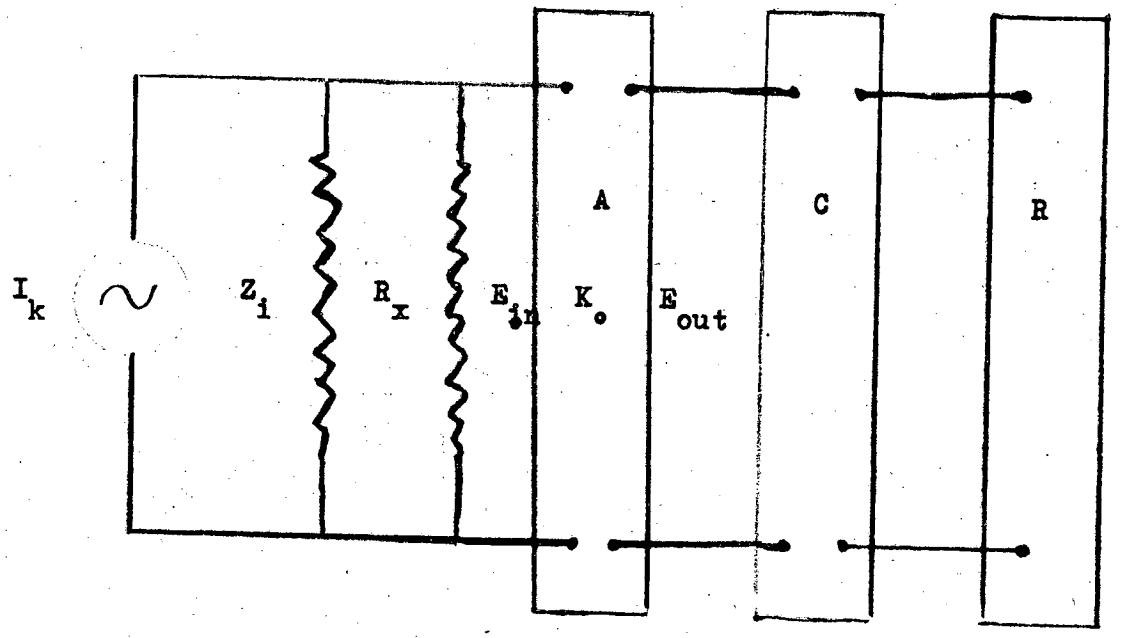

Fig. 22 Circuit for constant-current system.

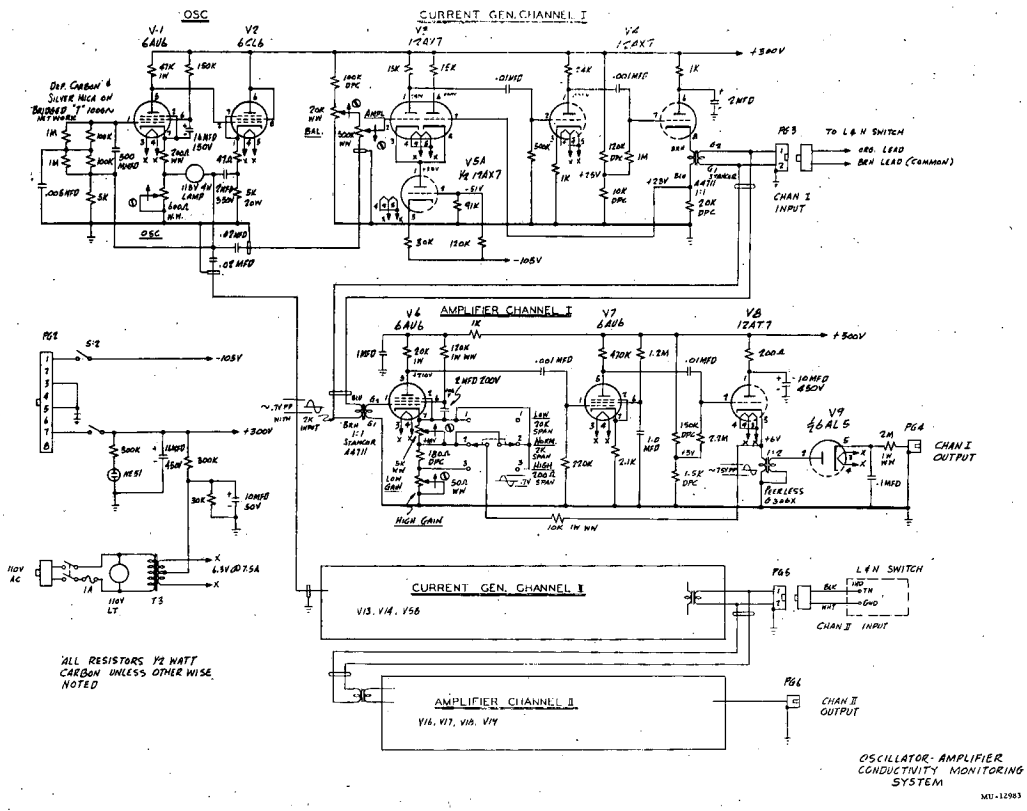

Fig. 23 Oscillator circuit.

Negative feedback was supplied from the output to the grid of V_1 through the frequency-determining network. The lamp and 600-ohm cathode resistor of V_1 formed a variable positive-feedback path.

To establish a linear relationship within 0.1% for a resistivity range from 20 ohms to 2000 ohms an output amplifier gain of 10 was selected to cover the range, and a current generator of 5 ma output and a source impedance of 2 megohms were used. The first stage of the generator was a differential amplifier with a cathode constant-current tube provided for application of the feedback potential at the second grid. The second stage, V_4, had a gain of 25 to make the over-all internal gain approximately 250. The last stage was designated to provide a low internal impedance, less than 2000 ohms. Output impedance as seen by the conductivity cell, however, was on the order of 4 megohms. The potential drop across the cell, which was amplified by circuit stages V_6, V_7, and V_8 varied from 10 mv to 1 volt over the desired range. The voltage amplifier had a gain of 100 in the normal position, and an output from 1 volt to 100 volts peak.

The system was stable against drift within 0.1% in 8 hours and covered a range from 20 ohms to 2000 ohms with equivalent linearity. Provision for monitoring the regions to either side of the primary range were made to include resistance ranges of 2 to 200 ohms and 200 to 2000 ohms, although linearity and stability are not critical for this range.

b. Circuitry

To meet the flexibility requirements of the system, two channels were needed: one for the continuous monitoring of a single cell connected to a Leeds and Northrup Speedomax (Channel 1), and a second one automatically switching six different cells (through a Beckman automatic switch) to a Honeywell-Brown six-point recorder (Channel 2). As noted in the specifications, a photoelectric system was also connected through the control panel to the Speedomax recorder (see Part II of this report); details on the control-panel connection and on the general electronic arrangement are given in Figures 24 and 25.

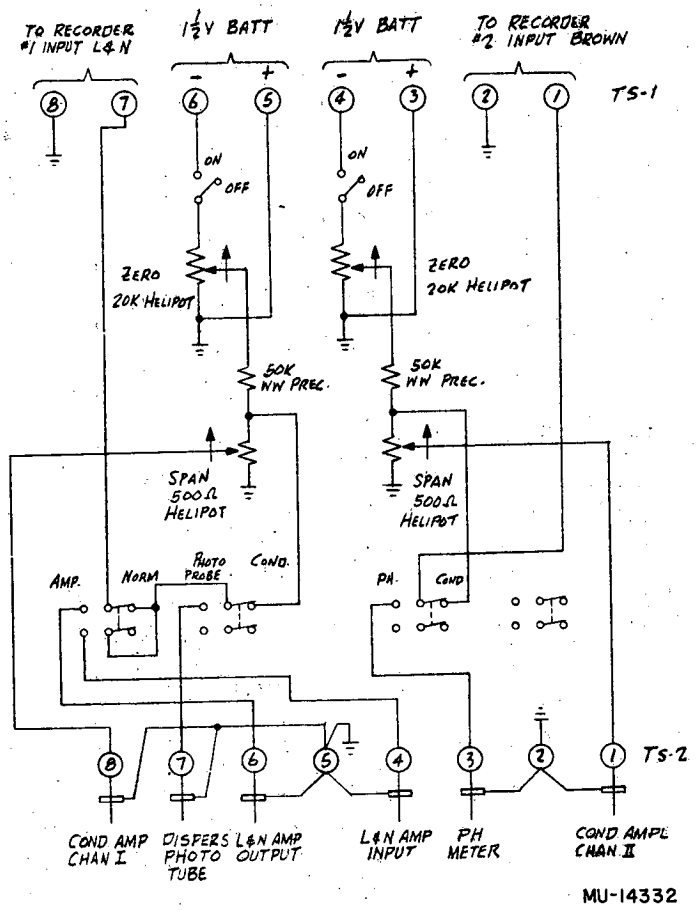

Fig. 24 Switching arrangement for conductivity recorders.

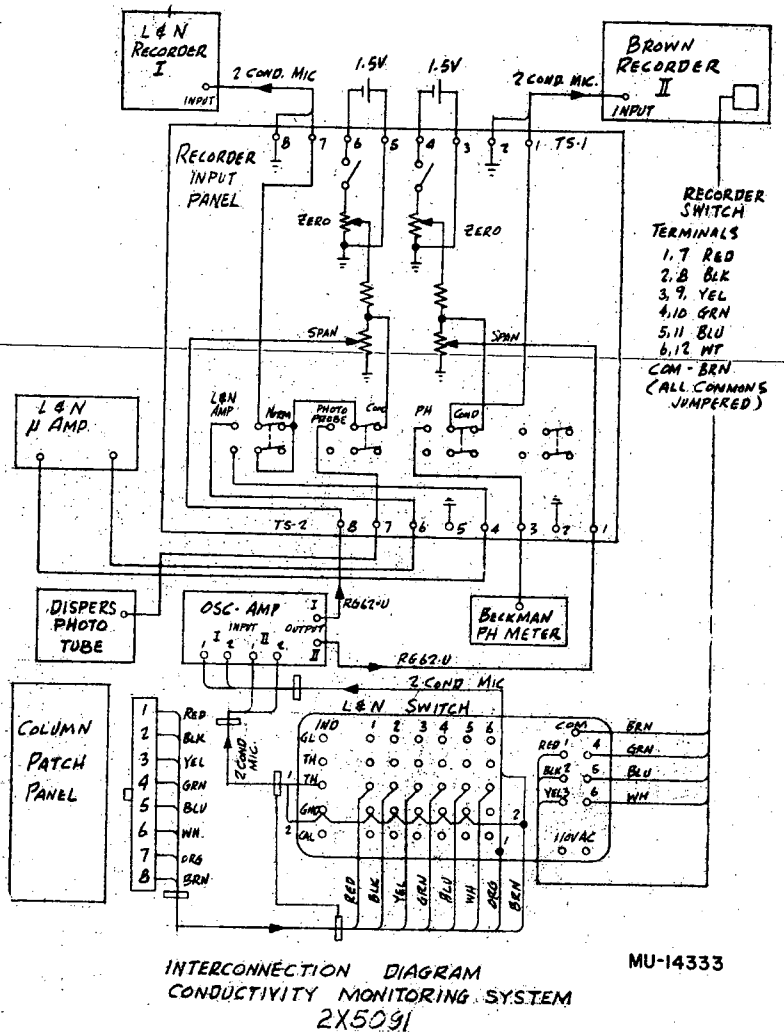

Fig. 25 Switching arrangement for conductivity recorders.

Each column body had its own panel board. All the conductivity leads of the column were connected to a rotary switch on the individual panel corresponding to five possible combinations of six electrodes. All the injection tubes were also connected to a manifold, as were the sampling tubes to protective caps installed on the panel, as shown on Figures 26 and 27. Six double-pole double-throw switches on the column panel allowed the selection of any cell for Channel 1 or Channel 2. Finally, an eight-wire plug on the column panel allowed connection to the electronic measurement and recording system.

4. Accessories

As noted in the specifications, the design and construction of a complete pilot-plant unit with extensive manifolding was needed. The flow arrangement is shown in Figure 28, and the completed assembly in Figures 29 and 30. A set of five pumps, five tanks, and six rotameters made it possible to feed and meter three different types of liquids at the same time for a range of 0.005 gpm to 40 gpm.

Water for the experiments was provided from a 150-gallon constant-head tank mounted on the roof of the building, about 25 feet above the column.

The rotameters were each calibrated by weight-flow of water. Flow rates for kerosene were corrected by assuming that equal-weight flow rates gave equal readings, and by using standard correction charts supplied by the Fischer-Porter Company. The working ranges of water flow through the six rotameters were 0 - 40 gpm, 0 - 6 gpm, 0 - 6 gpm, 0 - 0.8 gpm, 0 - 0.3 gpm, and 0 - 0.55 gpm.

5. Electrical Calibrations

a. Recording Potentiometers

The resistivity of a cell could be measured in nine different ranges on both recorders. These ranges, corresponding nominally to a

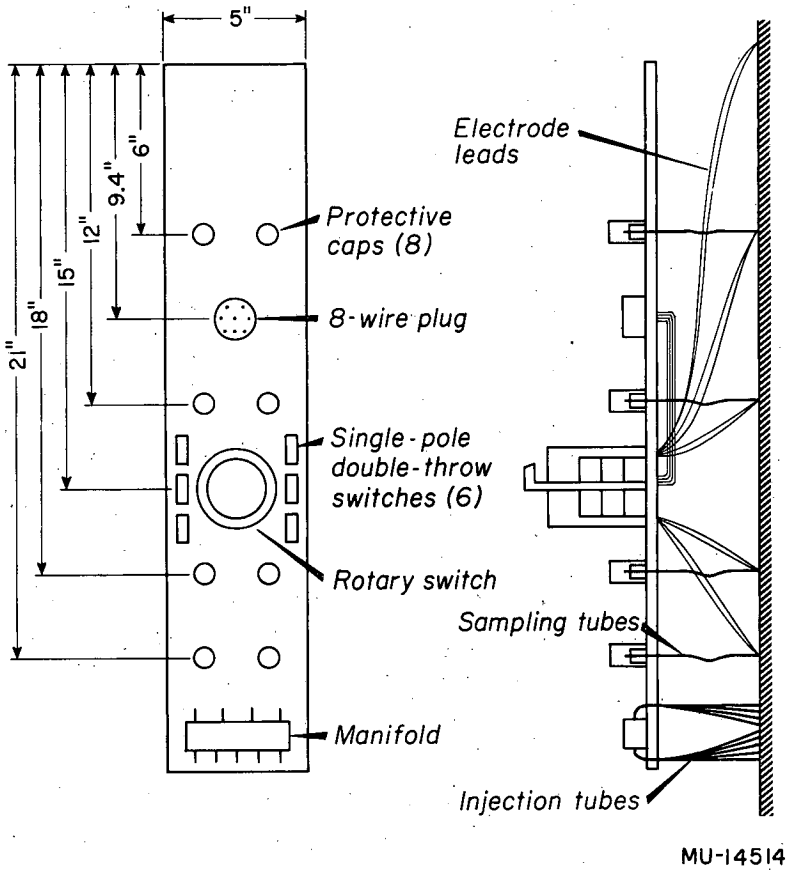

Fig. 26 Design of metering panel for column sections.

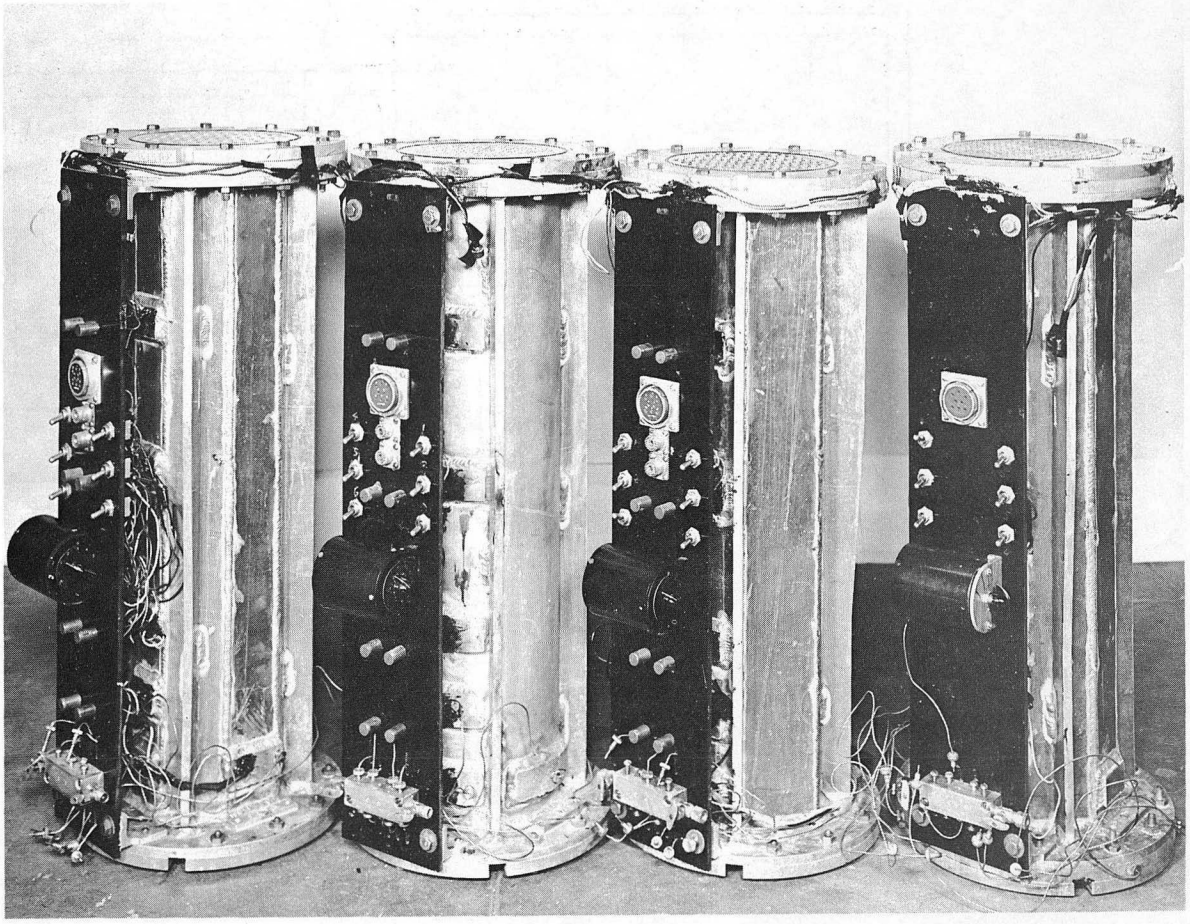

ZN-1817

Fig. 27 Assembled columns, showing metering sections.

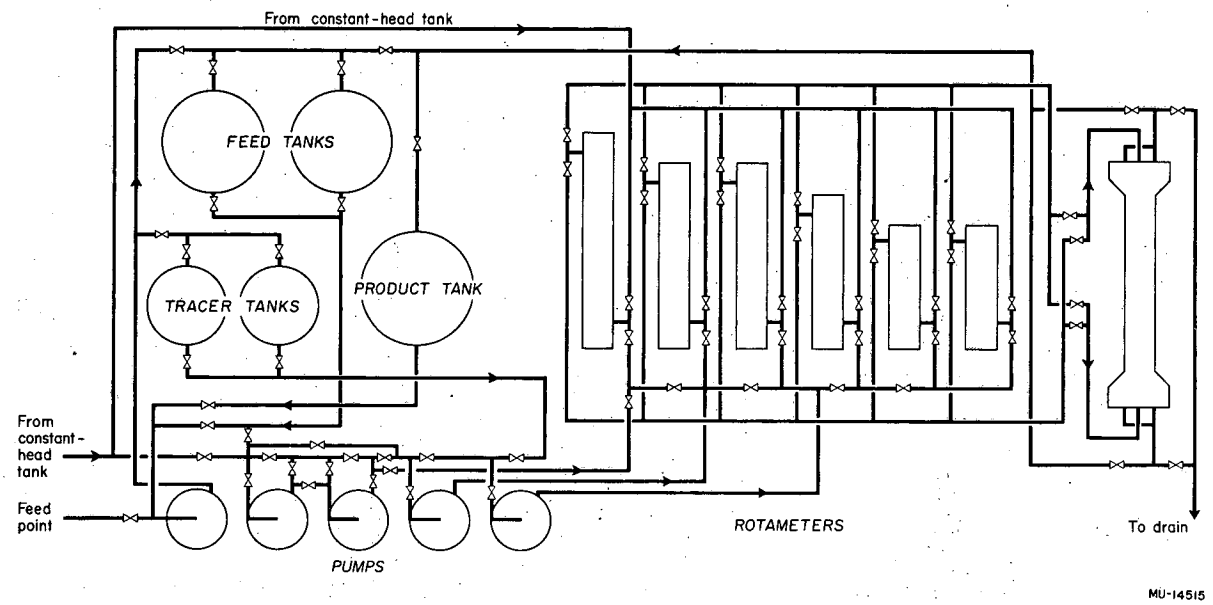

Fig. 28 Layout of flow system.

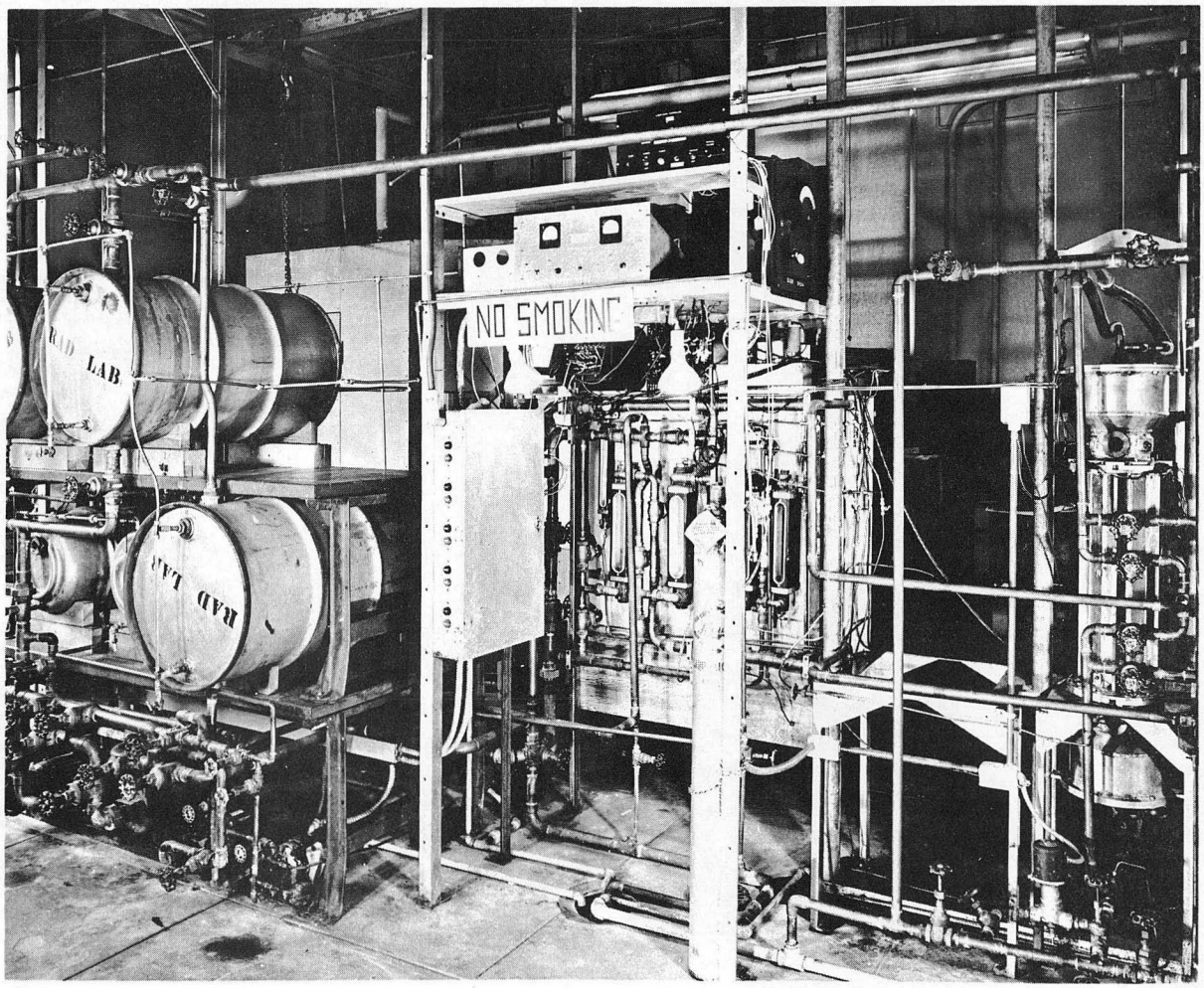

ZN-1814

Fig. 29 Apparatus assembly, showing storage and piping.

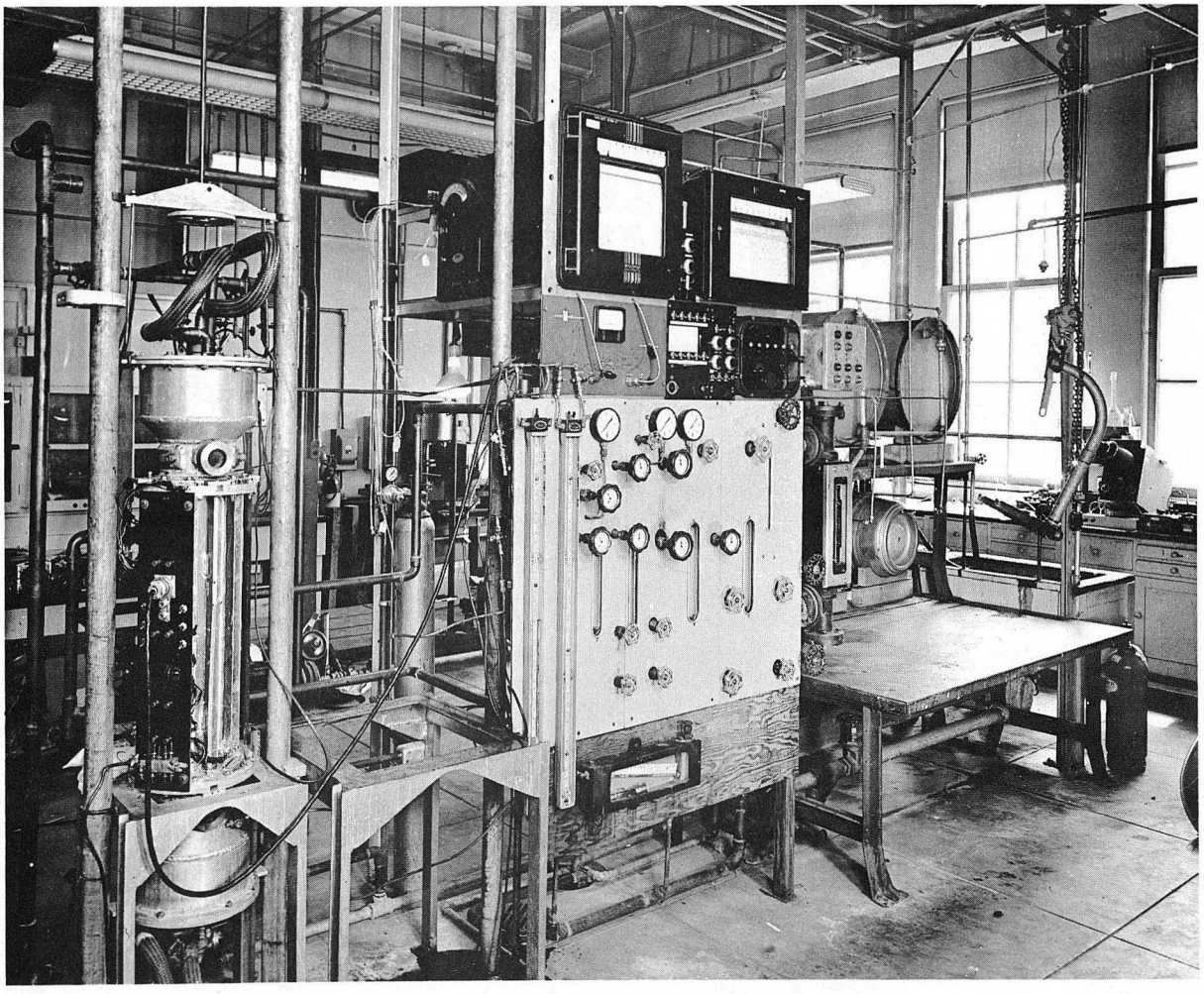

ZN-1816

Fig. 30 Apparatus assembly, showing control valves and instruments.

full-scale reading of 10 on the recorders, were:

0 to 30,000 ohms;	0 to 3,000 ohms;	0 to 300 ohms;
0 to 15,000 ohms;	0 to 1,500 ohms;	0 to 150 ohms;
0 to 7,500 ohms;	0 to 750 ohms;	0 to 75 ohms.

Calibrations accurate to 0.5% were made for each range on each recorder, with a Beckmann Helipot resistor as a reference resistance.

b. Cell Constants

All cell constants were determined by running a 7.4789-g./liter KCl solution (resistivity 0.012856 ohm cm) through the bed. The cell constant is defined as $1/\omega = a/\Omega$, with ω, the resistivity of the solution, ohm-cm; Ω, the resistance measured, ohm; and a the cell constant, cm^{-1}.

In order to minimize interference of the metallic wall with the conductivity readings, a floating ground was adopted; that is, an isolation transformer was installed between the ground of the frame and the ground of the measuring circuit.

The cell constants for Column 5 are given in Table 6, as a representative set, and show that there is little effect on the cell constant due to the proximity of the metal wall of the column. Arrangement D, corresponding to cells near the wall, gives an average value very close to arrangement A, near the center.

c. Resistivity of Sodium Nitrate Solution

In order to check the cell constants and also to develop a curve for concentration as a function of resistivity, a series of $NaNO_3$ solutions of known concentration was fed into the column. At each concentration level, the resistivities measured by the different cells all agreed within 0.5%. Figure 31 gives the concentration-resistivity curve thus obtained.

Table 6
Sample Cell Constants (Column 5)

Lead No.	1		2		3		4		5		6			Radial
Circuit	h in.	a^{-1} cm	h in.	a^{-1} cm	h in.	a^{-1} cm	h in.	a^{-1} cm	h in.	a^{-1} cm	h in.	a^{-1} cm	Average	position[a]
A	0	6.72	3	5.33	6	5.16	12	4.99	18	5.50	24	6.82	(5.75)	1
B	0	7.15	3	6.26	6	6.20	12	7.36	18	6.47	24	6.39	(6.63)	3
C	24	6.39	18	6.20	12	6.52	6	6.53	3	6.75	0	6.73	(6.51)	3
D	24	5.54	18	4.35	12	6.43	12	6.43	6	6.43	3	4.86	(5.67)	4
E	24	7.67[b]	24	7.36[b]	24	6.79[b]	24	7.28[b]	24	6.35[c]	12	5.33[d]	(7.09)[e]	Various

a. see Fig. 11

b. position 3

c. position 4

d. position 2

e. 24-inch level only.

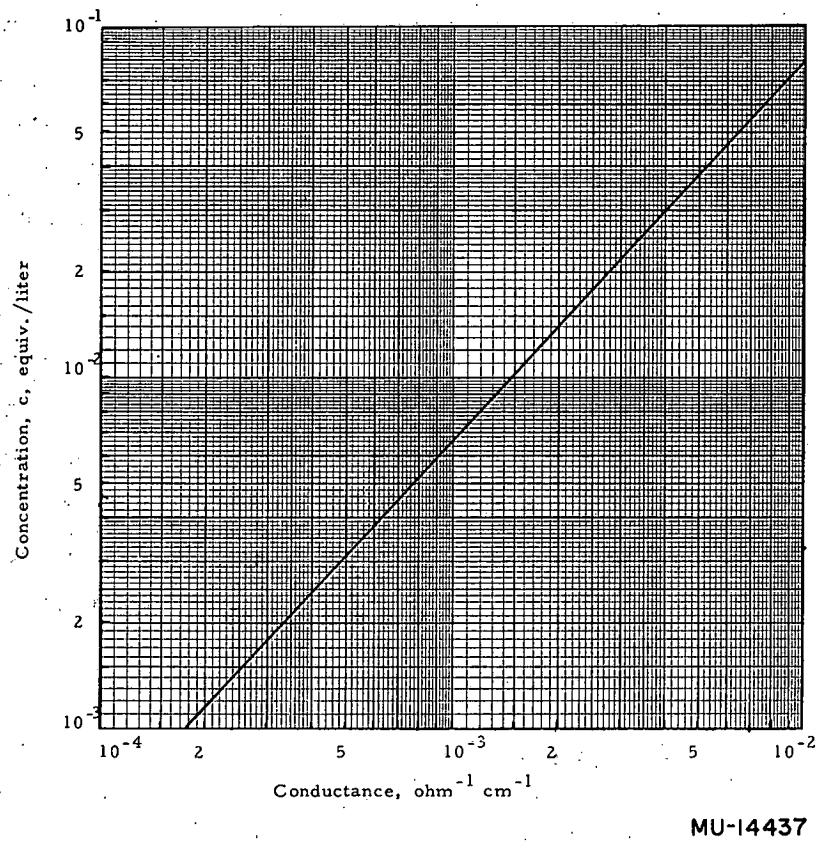

Fig. 31 Specific conductance of sodium nitrate solutions.

6. Experimental Procedure

a. Longitudinal Dispersion

A solution of sodium nitrate was used as tracer, and was injected through the nine injection points at level 0, in an amount from 0.25 to 2.0 volume % of the water stream. Water from a constant-head tank was allowed to flow through the bed at a chosen flow rate. After selection of the conductivity cell to be recorded and switching on of the recorder, the tracer was injected into the column, starting at a time that was marked electrically on the recorder chart. Tracer injection was stopped after a constant reading was reached on the recorder chart, and the conductivity was again followed as a function of time. The results were analyzed as explained below.

A reverse step function, involving discontinuance of salt injection, should be an exact mirror image of the saturation function, and might therefore be used interchangeably for determining the breakthrough behavior. Because resistivity (rather than conductivity) was measured in the present apparatus, the direct step function was more accurate ahead of the midpoint; and the reverse step function more accurate beyond the midpoint. Hence only a few trial runs were made with the latter.

b. Radial Dispersion

A sodium nitrate solution was injected continuously through the tube at the center of the injection plane. Concentrations downstream from this point could be read through Channel 2 (six cells at a time) on the Brown-Honeywell recorder, or through Channel 1 (one cell at a time) on the Leeds and Northrup Speedomax, and were read for a period of time sufficient to insure that steady state had been reached.

c. Temperature for the Measurements

All runs were made at ambient temperature, 68 ± 2°F.

RESULTS

1. Data

a. Longitudinal Dispersion

The calculation method used will be demonstrated with the data from Run 217-1. The recorder chart is shown in Figure 32. The chosen range in Channel 1 corresponds to a full-span reading on the recorder of 16,000 ohms; the cell constant was 6.82 cm^{-1} as indicated in Table 7, and the chart speed was 12 inches per minute. Table 7 indicates the results of the calculations for the breakthrough curve. The results are plotted on Figure 33 and give a slope of 1.89. Corresponding to this, $N' = 44.68$ from Equation 39.

In this way a plot of the concentration (in percent) versus the ratio of the elapsed time to the time at the 50% concentration point was prepared for each run. (Compare Figure 33.) The slope at $T = 1$ was taken, and the Peclet number was calculated according to

$$(N_{Pe})_\ell = 4 \pi s^2 (D_p/h) \beta ,$$

where β is a correction factor defined in Equation 38, s is the slope at $T = 1$, and h is the height of the bed (distance between the injection plane and the plane of measurement). For run 217-1, with $N'_D = 44.86$, Figure 4 gives $\gamma = 1.0072$ and Figure 5 gives $\delta^2 = 1.026$, hence $\beta = 0.963$; then $N_D = N'_D \beta = 43.20$; and $N_{Pe} = (0.75/24) N_D = 1.350$.

The results obtained are tabulated in Appendix I. A separate table is given for each column; the subdivisions within each table correspond to the five different flow rates used. The data included in the tables are run number, cell position, slope of the break-through curve, the number of mixing units N_D, and the Peclet number. Generally several runs were made for each experimental condition.

Figures 34 and 35 correspond to the plotted average for each group of runs. Figure 34 is a plot of the Peclet number (based on particle size) versus the Reynolds number expressed as

$$N_{Re} = U_0 d_p/\nu , \qquad (56)$$

where ν is the kinematic viscosity of the fluid. The factor $\epsilon^{1/2}$ has been introduced in order to align the transition ranges for the

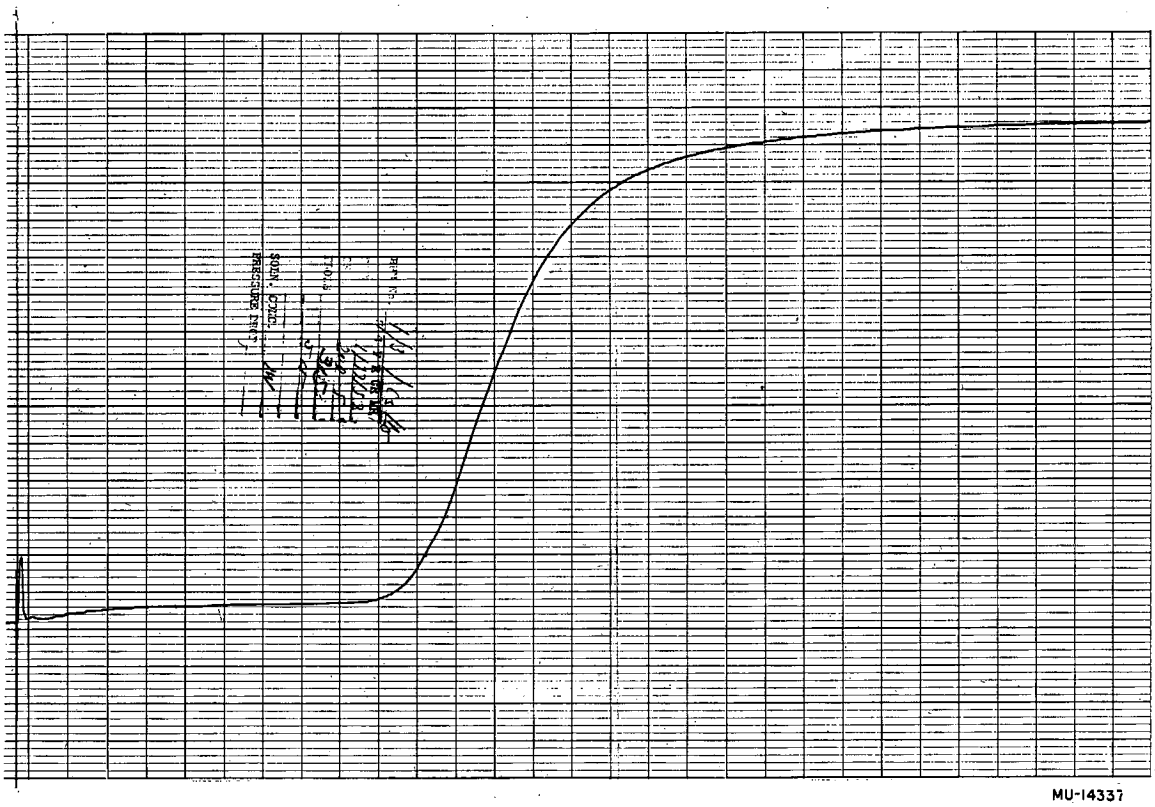

Fig. 32 Recorder chart for step-function breakthrough (Run 217-1) (Chart speed, 24 time-scale units per minute)

Table 7

Details for the calculation of a breakthrough curve (Run 217-1)

Reading from the recorder		Breakthrough curve	
Time (sec)	Concentration ($\times 10^3$)	c/c_0, %	$t/t_{50\%}$
0	3.40	0	0
27.1	3.60	0.9	0.67
29.2	4.50	4.97	0.72
30.8	5.5	6.20	0.76
32.8	6.8	15.38	0.81
35.2	9.4	27.14	0.87
40.4	14.5	50.22	1.005
48.30	20.00	75.10	1.19
60	23.50	90.90	1.48
∞	25.5	100	∞

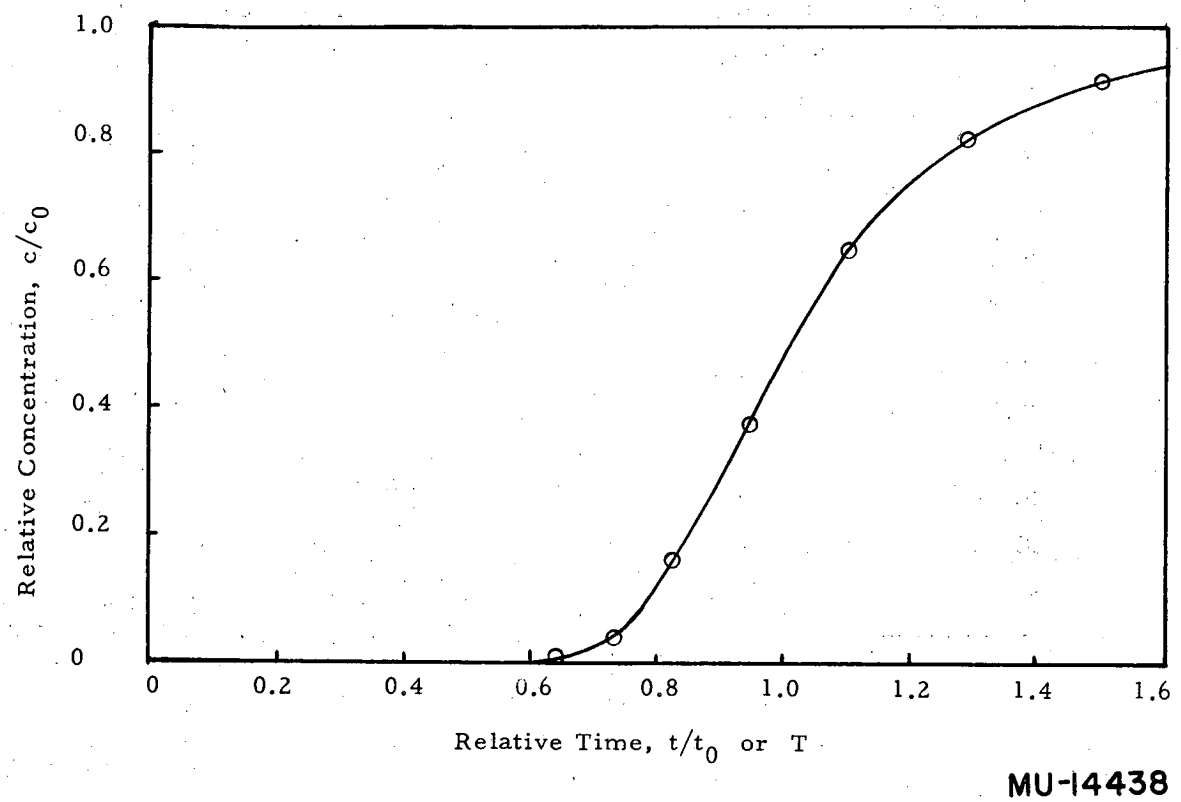

Fig. 33 Dimensionless plot of breakthrough for Run 217-1: Slope, 1.82; N_{Pe} calculated, 1.344.

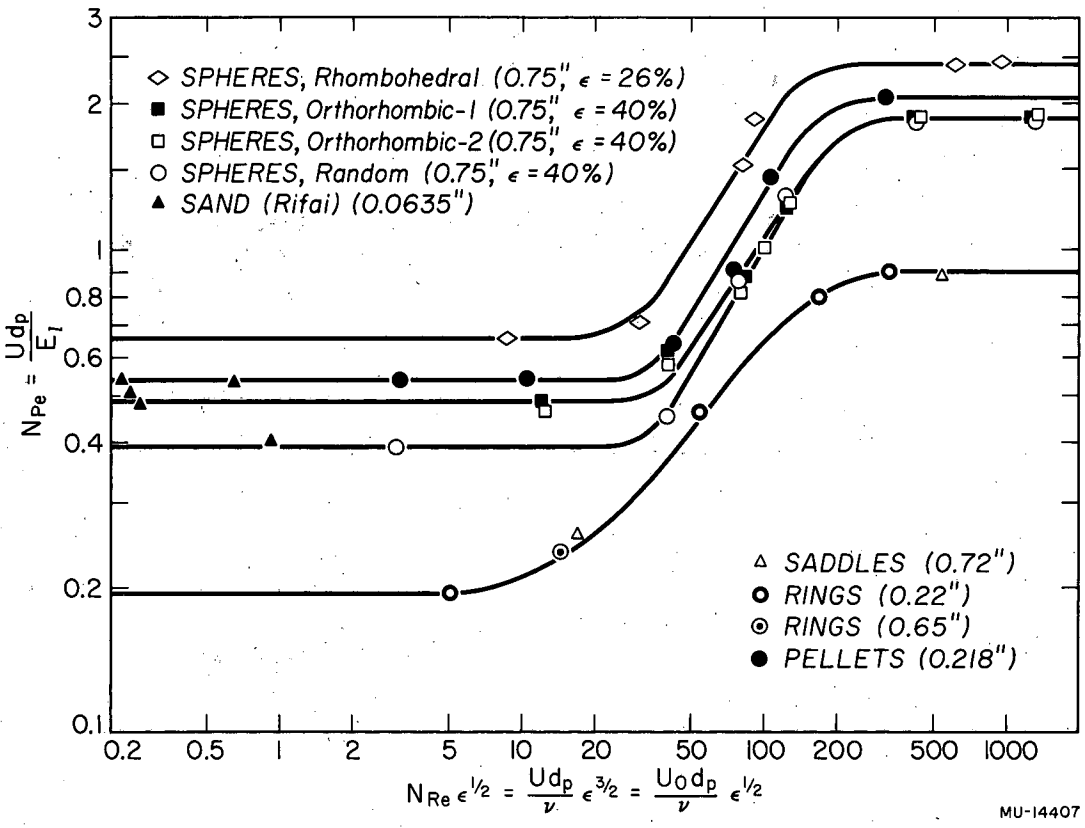

Fig. 34 Longitudinal Peclet number as a function of Reynolds number.

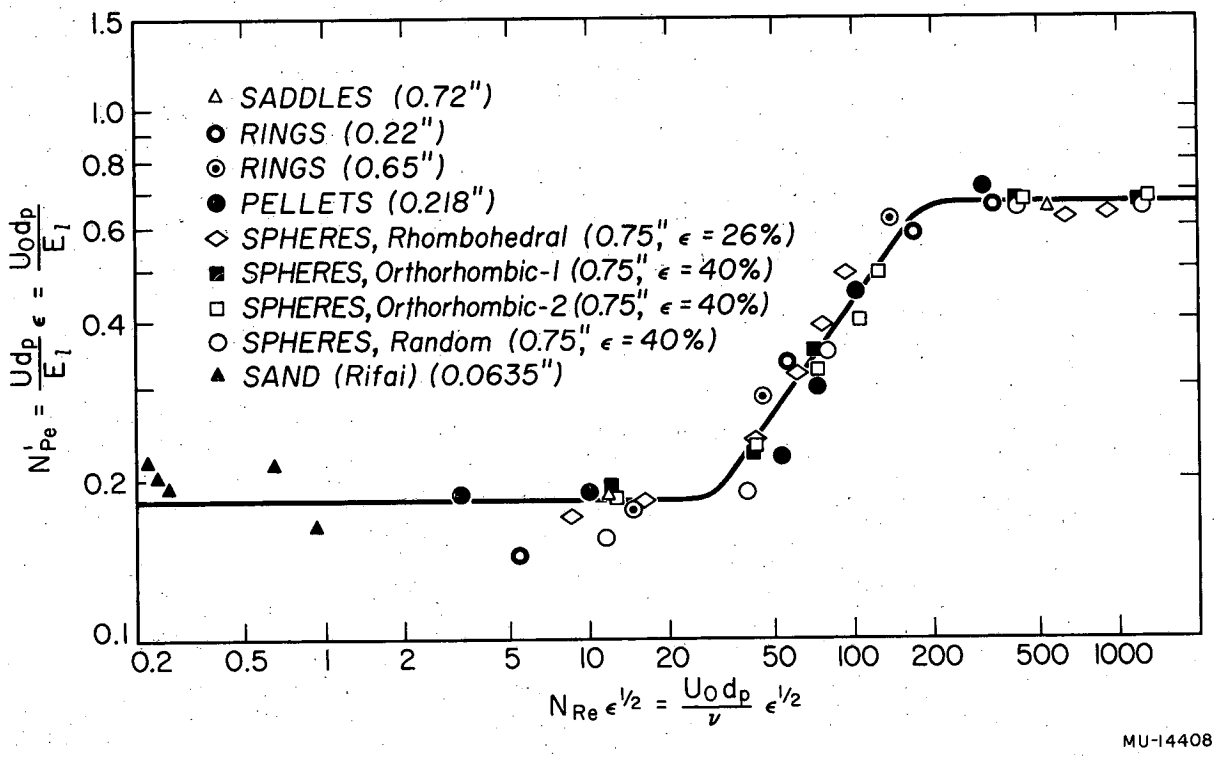

Fig. 35 Modified Peclet number for longitudinal dispersion in single-phase flow, as a function of Reynolds number.

different packings. Figure 35 shows an attempt at a general correlation: a modified Peclet number

$$N_{Pe}' = U d_p \epsilon / E_\ell = U_0 d_p / E_\ell \qquad (57)$$

is plotted against the same Reynolds number product as is used for Figure 34. This correlation fits reasonably well the data for eight different types of packings whose porosity goes from 26% to 73%. Figure 36 confirms that the axial Peclet number is inversely proportional to the porosity.

b. Radial Dispersion

The readings of the steady-state concentration for several values of the distance from the center (ρR) were made at various lengths from the injection plane. From the ratio of the observed values of concentration to the infinite-limit value and the chosen value of ρ, a modified Peclet number is read from Figure 6 and is used to calculate the radial Peclet number. The modified Peclet number is

$$\psi/\zeta = [(N_{Pe})_r R^2] / h d_p \qquad (58)$$

The results obtained are summarized in Appendix I; the arrangement of the tables is similar to that used for longitudinal diffusion. The data included in the tables are the run number, cell position, concentration ratio, modified Peclet number, and radial Peclet number. Generally several runs were made for the same experimental conditions.

The plotted results of the average for each group of experimental results are given by Figures 37 and 38. Figure 37 is a systematic study of the effect of varying Reynolds number on the Peclet number, made for Column 4; Figure 38 indicates the variation of the radial Peclet number with the porosity for turbulent flow. The laminar-flow region has been studied less thoroughly; however, as the results of Table I-15 for a sand-bed (Column 9) seem to indicate, the relationship of Figure 38 probably also applies here.

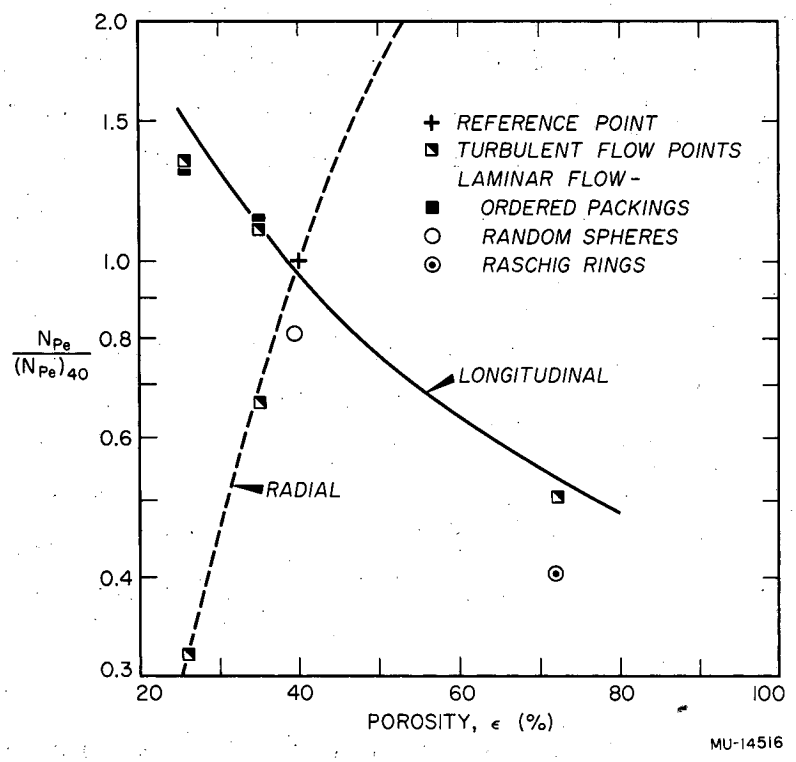

Fig. 36 Relative longitudinal Peclet number as a function of porosity.

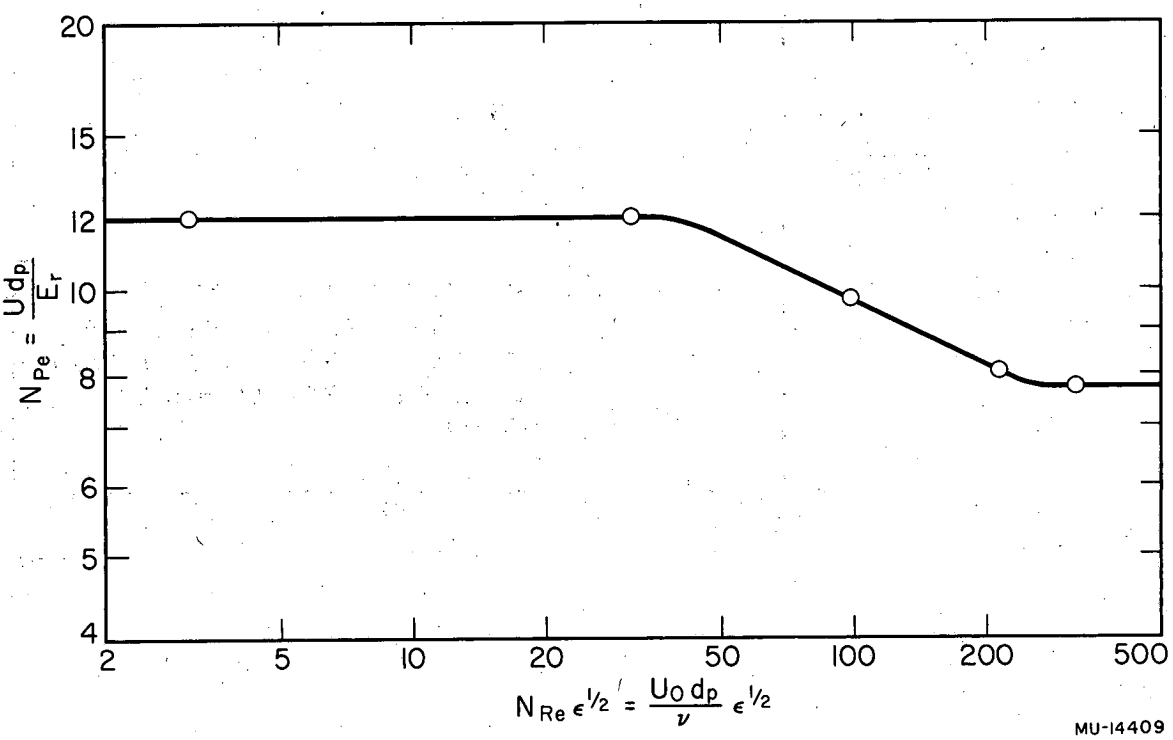

Fig. 37 Radial Peclet number as a function of Reynolds number

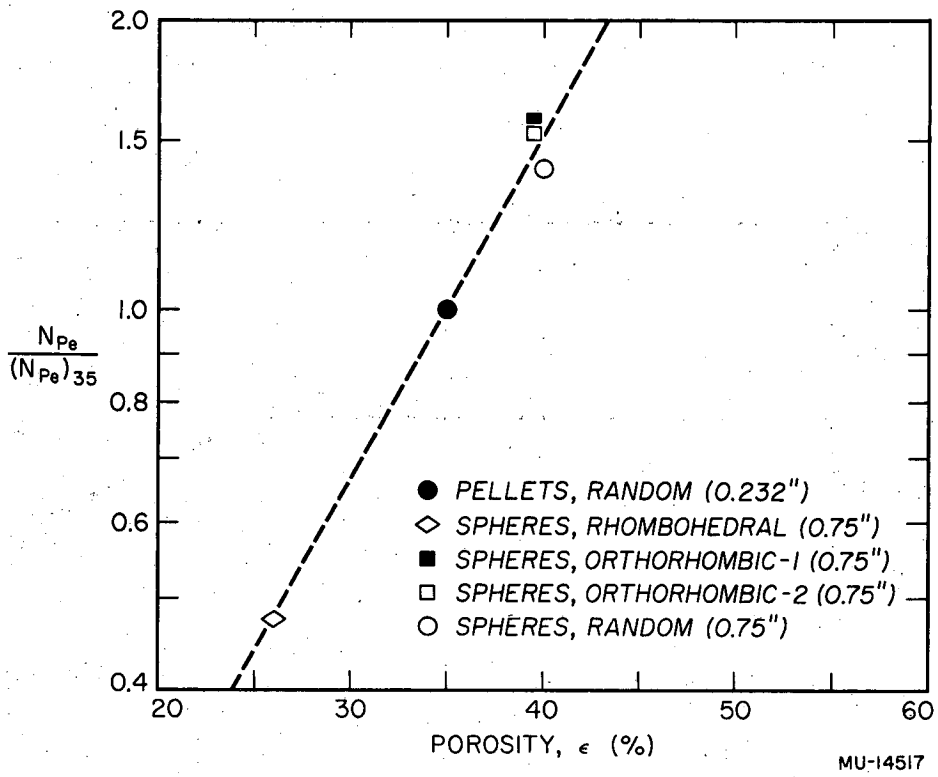

Fig. 38 Relative radial Peclet number in turbulent flow as a function of porosity.

c. Statistical Validity

For each group of runs, calculations were made for the average value and the variance expressed by

$$\sigma^2 = [\ \Sigma\ (x^2) - n\ x_{Av}^{\ 2}\ ] / (n - 1)\ , \qquad (59)$$

where n = number of measurements made,

x = individual value of the Peclet number,

x_{Av} = average value of the n measurements, of x,

σ = variance.

The final results are given for each group of runs in terms of statistical language with a probable error of no more than 5%.

$$N_{Pe} = \bar{x}_{Av} \pm t^{.05}_{n-1} \cdot \frac{\sigma}{\sqrt{n - 1}} \qquad (60)$$

where $t^{.05}_{n-1}$ is Student's t with n-1 degrees of freedom and a 5% probable error.[2] In other words, Equation 60 expresses the fact that an experimental value will fall outside the limits given only 5 times out of 100.

d. Angle of Dispersion

The previously given definitions of the two Peclet numbers are

$$(N_{Pe})_\ell = d_p/H' \cos \alpha$$

and

$$(N_{Pe})_r = d_p/H' \cdot 1/\sin \alpha$$

This may be combined:

$$H'/d_p = \sqrt{1/(N_{Pe})_\ell^2 + 1/(N_{Pe})_r^2}$$

and

$$\tan \alpha = (N_{Pe})_\ell / (N_{Pe})_r \ .$$

The parameters d_p/H' and α may be calculated from our experimental results, as is shown in Table 8.

Table 8

Calculation of total mixing length and angle of dispersion

Packing[a]	Porosity (%)	$(N'_{Pe})_\ell$	$(N_{Pe})_r$	d_p/H'	α
Rhombohedral	25.95	2.444	3.857	2.11	25° 30'
Orthorhombic (Columns 1 and 2	39.54	1.881	12.60	1.865	9° 30'
Random spheres	40.00	1.838	11.67	1.818	9° 54'
Random pellets	35.00	2.082	8.146	2.02	15° 54'
" same, laminar	35.00	0.538	11.9	0.537	2° 54'

[a] Flow turbulent except where shown.

The analysis of these results indicates that:

(1) The mixing length still depends on the packing porosity, to a much lower extent, however, than the Peclet number does.

(2) The angle of dispersion depends considerably on the packing porosity, higher porosity corresponding to smaller angles.

(3) The transition from turbulent to laminar flow is accompanied by an increase in the mixing length and a sharp decrease in the angle of dispersion. The net result of these two effects is that the radial Peclet number is only slightly higher in laminar flow.

The lower angle of dispersion observed for laminar flow may be considered to correspond to a well-defined and unvarying pattern of streamlines in this case. Several layers of packing would be necessary for collapsing of the filaments in laminar flow; this explains the effect on mixing length.

2. Discussion

This investigation has covered a wide range of Reynolds numbers, from 5.3 to 1,940 for axial diffusion, and from 0.38 to 640 for radial diffusion. For this study nine different types of packings were used (three ordered arrangements, and six random packings) covering a range of 26% to 73% for porosity and of 0.011 inch to 0.75 inch for diameter. The packing shapes were spheres, Raschig rings, spheroidal pellets, Intalox saddles, and Ottawa sand. The ordered packings all used spheres 0.75 inch in diameter, and corresponding to rhombohedral, orthorhombic-1, and orthorhombic-2 arrangements.

The examination of the Appendix and the plotted results leads to the following conclusions:

(a) The data show the existence of separate constant values for the Peclet number in the laminar and the turbulent region, and of a fairly sharp transition curve for both radial and axial diffusion.

(b) Both axial and radial Peclet numbers may be correlated as a function of porosity and of the Reynolds number. This remarkable property of the Peclet number makes possible the use of a generalized Peclet number that will correlate as a function of a generalized Reynolds number. Such a correlation, described in Figure 35, applies to the whole range of experimental results.

(c) Constant values of Peclet numbers are calculated, by Equation 13, for axial dispersion, and by Equation 57, for radial dispersion, regardless of the column-height interval taken for measurement.

(d) Regular and random packings give identical results for the same porosity, provided that the ratio of particle diameter to column diameter is not too large. This is illustrated by the nearly identical results for the sand bed and rhombohedral-1 and rhombohedral-2 packings, which have substantially the same porosity of 39.5%. On the other hand the longitudinal Peclet-number results for rhombohedral-1 and rhombohedral-2 packings in laminar flow are higher than the results for the random-packed spheres that correspond to the same ratio (8:1) of column diameter to particle diameter; this is believed due to a wall effect in the random

column. In turbulent flow, this effect appears to be negligible. From this result one can see the need to choose a ratio of column diameter to particle diameter higher than 8 for random packing, although such a ratio has sometimes been assumed to be safe.

(f) In the laminar region, Raschig rings show a lower value than might be expected for the axial Peclet number, and also a wider transition region; this could be explained by availability of two types of orifices in the Raschig rings (between the rings and inside the rings); such a packing may well behave like a mixture of particles of two different diameters.

(g) With water as the flowing liquid, the results obtained with ceramic stoneware, sand, and polyethylene surfaces were similar. Since polyethylene is less readily wetted by water than stoneware is, the wettability of the surface appears to have no marked effect.

LITERATURE CITED

1. T. Baron, Chem. Eng. Progr. 46, 233 (1950).
2. C. A. Bennett and N. L. Franklin, Statistical Analysis in Chemistry and Chemical Industry, Wiley, New York (1954).
3. M. J. Beran, Dispersion of Soluble Matter in Slowly Moving Fluids. Ph.D. dissertation, Harvard Univ., Cambridge, (1955).
4. R. A. Bernard and R. H. Wilhelm, Chem. Eng. Progr. 46, 233 (1950).
5. P. C. Carman, Trans. Inst. Chem. Engrs. (London) 15, 150 (1937).
6. P. V. Danckwerts, Chem. Eng. Sci. 2, 1 (1953).
7. P. Danel, Ankara Symposium on Arid Zone Hydrology, Proceedings, U.N. Educ. Sci. Cult. Org. 2, 99 (1952).
8. P. R. Day, Trans. Am. Geophys. Union. 37, 595 (1956).
9. P. F. Deisler, Jr., and R. H. Wilhelm, Ind. Eng. Chem. 45, 1219 (1953).
10. H. A. Einstein, Der Geschiebetrieb als Wahrscheinlichkeitsproblem. Dissertation, Eidg. techn. Hochschule, Zurich, 1937.
11. L. C. Graton and H. J. Fraser, J. Geo. 43, 785, 910 (1935).
12. A. A. Kalinske and C. L. Pien, Ind. Eng. Chem. 36, 220 (1944).
13. K. Kitagawa, Memoirs, Series A, Kyoto University, College of Science, 17, 37 (1934).
14. K. Kitagawa, ibid., 432 (1935).
15. A. Klinkenberg, H. J. Krajenbrink, and H. A. Lauwerier, Ind. Eng. Chem. 45, 1202 (1953).
16. A. Klinkenberg, Ind. Eng. Chem. 46, 2285 (1954).
17. H. Kramers and G. Alberda, Chem.Eng. Sci. 2, 173 (1953).
18. L. Lapidus and N. R. Amundson, J. Phys. Chem. 56, 984 (1952).
19. G. A. Latinen, Ph.D. dissertation, in Chemical Engineering, Princeton University, 1951.

20. M. Leva, Tower Packing and Packed Tower Design, United States Stoneware Company, Akron, Ohio (1951).

21. J. J. Martin, W. L. McCabe, and C. C. Monrad, Chem. Eng. Progr. 47, 91 (1951).

22. K. W. McHenry, Jr. and R. H. Wilhelm, Am. Inst. Chem. Engrs. J. 3, 83 (1957).

23. T. Miyauchi, "Longitudinal Dispersion in Solvent-Extraction Columns: Mathematical Theory" UCRL-3911, Aug. 1957.

24. Hugh Ogburn, Ph.D. dissertation, Princeton University, 1954.

25. G. Oplatka and E. Cryllus, Acta. Chim. Acad. Sci. Hung., 2, 103 (1952).

26. W. E. Ranz, Chem. Eng. Progr. 48, 247 (1952).

27. N. E. Rifai (with W. J. Kaufman and K. Todd), Dispersion Phenomena in Laminar Flow Through Porous Media (Ph.D. dissertation), University of California, Berkeley, July 1956.

28. R. Aris and N. R. Amundson, Am. Inst. Chem. Engrs. J. 3, 280 (1957).

29. A. E. Scheidegger, Producers'Monthly, 17, 17 (1953).

30. S. Lynn, W. H. Corcoran, and B. H. Sage, Am. Inst. Chem. Engrs. J. 3, 11 (1957).

31. E. Singer and R. H. Wilhelm, Chem. Eng. Progr. 48, 247 (1952).

32. W. O. Smith, Physics, 3, 139 (1932).

33. G. I. Taylor, Proceedings, Roy. Soc. (London) A 219, 186 (1953).

34. G. I. Taylor, Proc. Roy. Soc. (London) A 225, 473 (1954).

35. G. I. Taylor, Proc. Roy. Soc. (London) A 234, 1 (1956).

36. E. W. Thiele, Ind. Eng. Chem. 38, 646 (1946).

37. W. L. Towle and T. K. Sherwood, Ind. Eng. Chem. 31, 462 (1939).

38. J. J. VanDeemter, F. J. Zuiderweg, and A. Klinkenberg, Chem. Eng. Sci. 5, 271 (1956).

39. T. Vermeulen, A. L. Lane, H. R. Lehman, and B. Rubin, Am. Inst. Chem. Engrs. J. (in press).

40. E. Wicke and W. Brötz, Chem. Ing. Tech. 21, 219 (1949).

41. E. Wicke and U. Voight, Angew. Chem. B 19, 94 (1947).

42. H. A. Wilson, Proc. Cambridge Phil. Soc. 12, 406 (1904).

LONGITUDINAL DISPERSION IN SOLVENT-EXTRACTION COLUMNS; PECLET NUMBERS FOR ORDERED AND RANDOM PACKINGS

Part II. TWO-PHASE FLOW

Introduction

Packed columns are frequently selected as an effective and economical means of interphase contacting for liquid-liquid extraction. The usual method for designing an extractor involves computing the NTU required to bring about a given extraction, and multiplying by a height factor (the HTU) determined from previous experience on the subject.

The HTU concept was introduced by Colburn.[3,4] This concept has been applied successfully to adsorption towers; the application to extraction, however, has been less successful. HTU values vary widely with the types of system, the rates of flow, and concentration, making it necessary to have at hand very specific data for the contemplated design.

Numerous experimental studies have been carried out, to measure the effective mass-transfer coefficients and HTU's in such extraction columns, by such workers as Colburn and Welsh,[5] Laddha and Smith,[13] Koffolt, Row, and Withrow,[12] Sherwood, Evans, and Longcor,[19] Hou and Frankel,[9] Knight,[11] Elgin and Browning,[6] Johnson and Bliss,[10] and Allerton, Strom and Treybal.[1] The data obtained have been reviewed by Elgin and Wynkoop,[7] and by Treybal.[20] The HTU's for the individual phases are frequently correlated as some power of the flow-rate ratio, as by Rubin and Lehman;[18] but the result may be regarded as entirely empirical.

Over a twenty-year period it has remained impossible to interpret the experimentally measured performance of packed extraction columns in terms of mass-transfer theory and fluid and packing properties. The great difficulty encountered has suggested that the controlling variables frequently are not those which determine the rate of mass transfer. The investigation reported here was undertaken to determine whether longitudinal diffusion could have a significant adverse effect upon extraction performance. Approximate calculations, based on the Peclet numbers measured in this investigation, are reported below, and show that the HTU's due to mass-transfer resistance may range from 80% to 20% (or even less) of the total apparent HTU.

With knowledge of the dispersion coefficients for the two phases, and of the mass-transfer coefficient, it is possible to write two simultaneous differential equations involving dispersion, following Miyauchi:[16]

$$d^2C_x / dZ^2 - P_x B \, dC_x / dZ - N_{ox} P_x B \, (C_x - mC_y) = 0, \qquad (1)$$

$$d^2C_y / dZ^2 + P_y B \, dC_y / dZ + N_{oy} P_y B \, (C_x - m C_y) = 0, \qquad (2)$$

with the boundary conditions

$$Z = 0, \quad (dC_x / dZ) = P_x B \, (C^o_x - C_{xo}) \qquad (3)$$

$$\text{and} \quad (dC_y / dZ) = 0, \qquad (4)$$

$$\text{at} \quad Z = 1, \quad (dC_x / dZ) = 0 \qquad (5)$$

$$\text{and} \quad (dC_y/dZ) = P_y B \, (C_{yl} - C_y^1), \qquad (6)$$

where P_i is the Peclet number of the i phase,

C_i is the dimensionless point concentration in the i phase,

Z is the dimensionless length variable,

B is the ratio h/d_p, with h the column height and d_p the particle diameter,

m is the slope of the equilibrium curve, and

N_{oi} is the over-all height of transfer unit for the i phase.

Equations 1 and 2 are differential equations of the second order, with constant coefficients. Their solution, obtained by differentiation and subsequent integration of a single fourth-order equation, gives the concentration at any point inside the column. McMullen, Miyauchi, and Vermeulen[15] have tabulated the results given by this solution, for a large number of cases.

Miyauchi has distinguished three kinds of NTU. The first, or true, value is calculated from the mass-transfer coefficient,

$$N_{oi} = K_i a \, h / \epsilon_i U_i , \qquad (7)$$

where K_i is the mass-transfer coefficient, a is the interfacial area per unit volume, U_i is the linear velocity of the i phase in the column, and ϵ_i ks the void fraction of the i phase.

The two other expressions assume that the concentration distribution is known and utilize the integral of definition,

$$N_{oi} = \int_0^h dC_i/(C_i - m\, C_j). \tag{8}$$

There is no choice regarding the upper limit, when the concentration at the exit is C_{xl}. But at the entrance of the bed there is a sudden change of concentration, owing to back-mixing, as expressed by Equation 3. C_xO is the concentration at Z = 0 inside the bed, which usually cannot be measured, and C_x^O is the concentration of the entering stream that is known. Two expressions result:

$$N_{oxM} = \int_{C_{xO}}^{C_{xl}} d\, C_x/(C_x - m\, C_y) \tag{9}$$

(here the concentrations are those actually measured in the column),

and

$$N_{oxP} = \int_{C_x^O}^{C_{xl}} dC_x/(C_x - m\, C_y) \tag{10}$$

(here the concentrations are those computed from the external material balance of the column, without allowance for dispersion.

It is evident that Equations 7, 9, and 10 give different results. The solution of Equations 1 and 2 allows us to calculate the difference between the true NTU given by Equation 7 and the apparent values.

By the principle of addition of resistances, N_{ocP} and N_{oc} (for the continuous phase, in particular) can be related through a number N_{ocD},

$$\frac{1}{N_{ocP}} = \frac{1}{N_{oc}} + \frac{1}{\Lambda\, N_{ocD}}, \tag{11}$$

where N_{ocD} is the number of dispersion units in the two-phase system. But N_{ocD} can be expressed[15] as

$$N_{ocD} = \frac{(N_{Pe})_{oc} B}{\Lambda} + \frac{\ln \Lambda}{(1 - \Lambda)} , \qquad (12)$$

where Λ is the extraction coefficient, $\Lambda = m F_d/F_c$, with F_c and F_d the flows of the continuous phase and the discontinuous phase respectively. If the extraction coefficient Λ is not very different from 1, Equation 12 simplifies to

$$N_{ocD} = 1 + (N_{Pe})_{oc} B ; \qquad (13)$$

here $(N_{Pe})_{oc}$ is an over-all Peclet number, defined as

$$\frac{1}{(N_{Pe})_{oc}} = \frac{1}{(N_{Pe})_c} + \frac{1}{(N_{Pe})_d} , \qquad (14)$$

where $(N_{Pe})_c$ and $(N_{Pe})_d$ correspond to the Peclet numbers of the continuous phase and the discontinuous phase respectively, under the actual flow conditions. These functions are utilized at a later point. (Equations 11-14 provide a good approximation for the situation that is considered here; a still more exact treatment is being developed.)

EXPERIMENTAL OBJECTIVES

The measurement of two-phase systems, in countercurrent flow through packed columns, was undertaken to determine the behavior of the dispersion coefficient that would apply in actual extraction columns. The variables to be considered were: packing-unit shape, arrangement, porosity, fluid properties, and flow rates. Radial dispersion coefficients (for the continuous phase only) were also determined, as a matter of fundamental interest.

APPARATUS AND PROCEDURE

1. Apparatus

a. Columns

Four different columns were used for the investigation, three with different regular packings and one with random packings. The packing characteristics are given by Table 1. Each column was about 6 inches in diameter, and about 26 inches high, as described in Part I.

b. Conductivity

Conductivity was used to determine the breakthrough curve for the continuous phase. The same apparatus and techniques were adopted as for one-phase flow measurements. The cell readings fluctuated owing to interference of droplets of the discontinuous phase in the conductance path. Also, the average cell-constant readings were higher than those for single-phase flow. For this reason calibrations with tap water were made before and after each run, using the conductivity of the laboratory water supply, and maintaining the flow rates for both phases at constant values during both calibrations.

c. Photoelectric Probe

As it was not possible to use conductivity measurements for the discontinuous phase (kerosene), a photoelectric method was adopted. A photoelectric probe was installed at the top of the column. A dye solution in kerosene (DuPont Oil Blue A) was introduced through the injection device, and the breakthrough curve was obtained and analyzed with a procedure similar to that used for the conductivity measurements. The probe used was a modification of the apparatus developed by Langlois, Gullberg, and Vermeulen[14] in their determinations of interfacial areas. A photograph of the probe used is shown in Figure 1. The upper (short) section holds the penlight bulb while the lower (long) section holds the RCA 1P41 (gas-filled) phototube. The gap between these two units could be varied as needed. Figure 2 gives wiring diagrams for the lamp circuit and the photocell circuit.

Table 1

Dimensions and packing of experimental columns

Column number	Packing	Diameter (in.)	Arrangement	Distance between layers(in.)	Porosity	Column height (in.)	Injection height (in.)	Figure number
1	Spheres	0.75	Rhombohedral	0.530	25.95	26.88	2.54	6,10,13
2	Spheres	0.75	Orthorhombic-1	0.649	39.54	25.80	1.725	7,10,13
5	Spheres	0.75	Random	0.705	40.00	26.00	2.00	11,14
6	Spheres	0.75	Orthorhombic-2	0.75	39.54	26.25	1.125	12,15

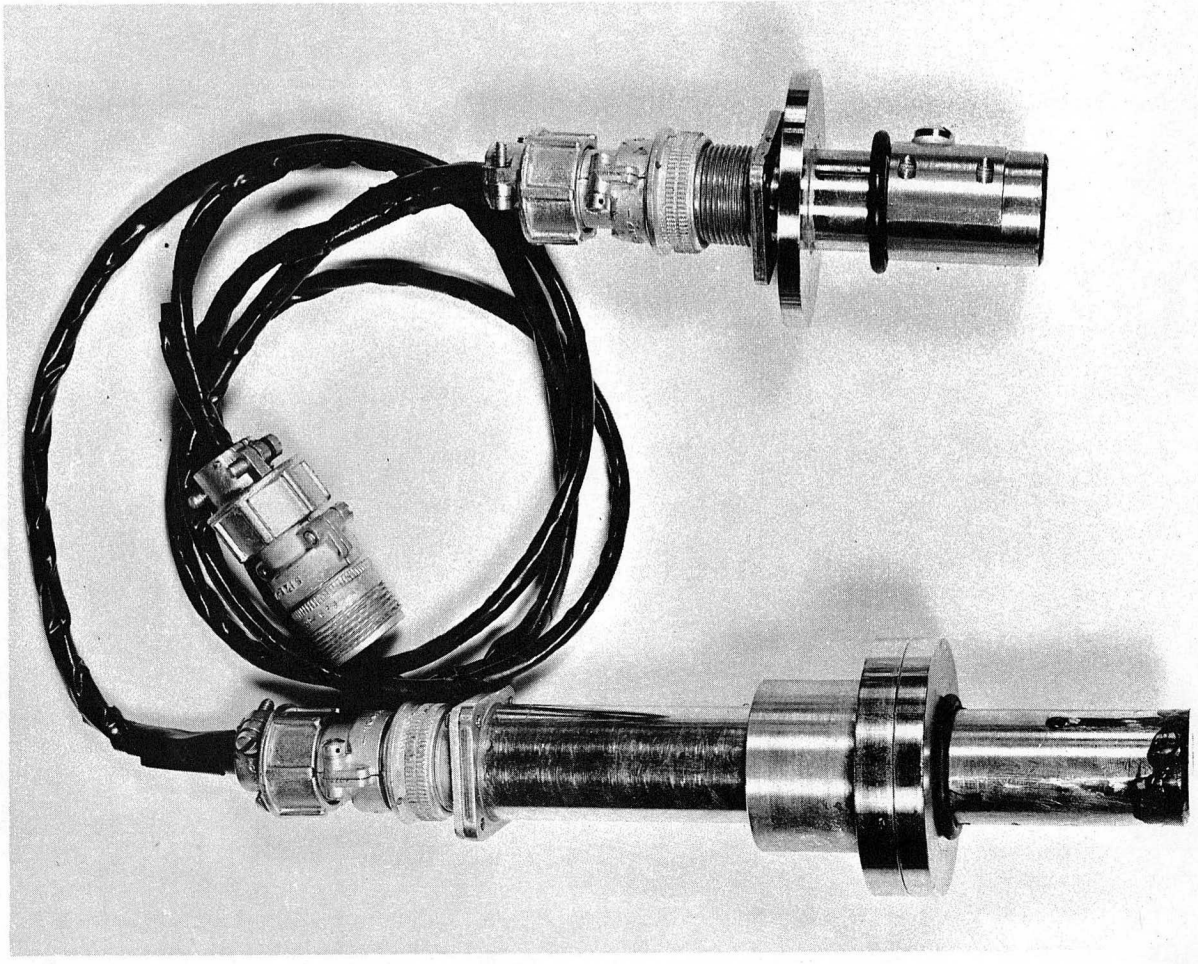

ZN-1815

Fig. 1 Interfacial-area probe.

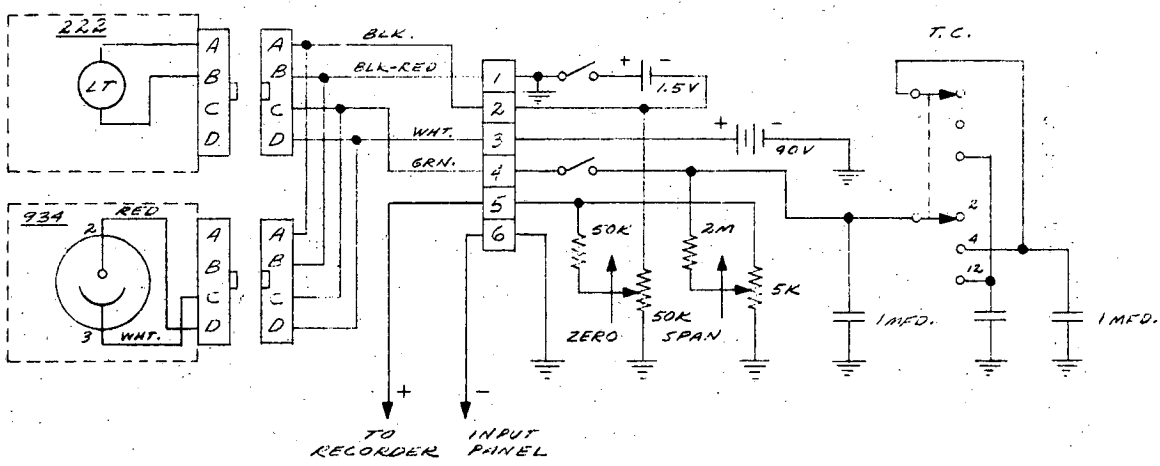

Fig. 2 Lamp and photocell circuit for interfacial area probe.

d. Feed Nozzle

Special consideration was given to the nozzle through which the discontinuous phase is introduced. Uniform drop size was desired, in order to achieve uniform drop rise or fall with a minimum of coalescence of the drops. According to Johnson and Bliss, velocity at the hole has to be maintained between 1000 and 1500 ft/hr, and a hole diameter of 0.10 inch seems to be the optimum.[10] Consequently the distributor nozzle was designed with a set of six removable plates, varying in number of holes, to provide the wide range of flow rates required. Five of these had 0.15-inch diameter holes, while the sixth, for high flow rates, had 0.20-inch holes to avoid too great a drop in pressure.

e. Liquid-Level Control

Conductivity probes were installed in the lower head and the upper head of the column. Each of those probes operated a magnet-controlled take-off valve through relay circuits. Figure 3 gives a wiring diagram of this level-control system. By use of a set of switches it was possible to maintain the interface at either the upper or the lower end of the column. The on-off magnetic valve was bypassed by a globe valve, which could be adjusted so as to assure smooth operation of the liquid-level-control system.

2. Procedure

a. Longitudinal Dispersion in the Continuous Phase

A solution of sodium nitrate was injected through the injection outlets described for one-phase flow. Special precaution was taken to reach steady-state flow conditions in the column before injecting the tracer. A careful setting of the level control was made to avoid any disturbance of the flow of either phase.

b. Longitudinal Dispersion in the Discontinuous Phase

The same steps as above were taken to set the liquid level and to establish steady-state flow in the column. Photoelectric measurements were made instead of conductivity measurements. A water-insoluble blue

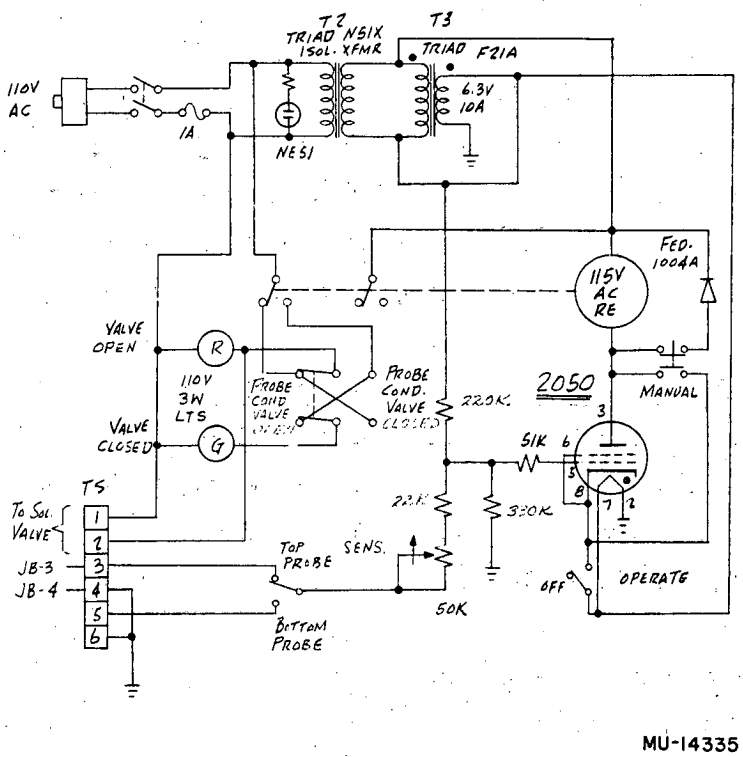

Fig. 3 Conductivity liquid-level controller.

dye (dissolved in kerosene) was injected as a tracer. Measurements were also made using uncolored kerosene, and taking the breakthrough curve for arrival of the discontinuous phase at the top of the column; good agreement was obtained between the two kinds of measurement, as is shown below under "Data".

c. Hold-up

The filling time for either the continuous or the discontinuous phase could be obtained from the preakthrough plot, and corresponds to dimensionless time T = 1. The hold-up volume of the phase is given by the product of volumetric flow rate and filling time. Thus the foregoing procedures also provide a method of measuring the hold-up.

d. Radial Dispersion in the Continuous Phase

Sodium nitrate solution was injected continuously at the center of the injection plane. The measurements and analysis of the data were the same as in Part I. As noted above, cell constants were used that were functions of the flow rates of the two phases.

e. Temperature for the Measurements

All runs were made at an ambient temperature of 68 ± 2°F. At this temperature, the kerosene used had a viscosity of 2.46 cp. and a density of 0.820 gm/liter.

RESULTS

1. Data

a. Longitudinal Dispersion in the Continuous Phase

A plot of the concentration (in percent) versus the ratio of the elapsed time to the time at the 50% concentration point was drawn for each run. The slope was taken at the time corresponding to T = 1, and was utilized for the calculation of the Peclet number by the same procedure as for one-phase measurements. The results are tabulated in Appendix II. Figure 4 shows the ratio of the observed Peclet number to the Peclet number obtained for the same column in single-phase flow versus a Reynolds number based upon the flow rate of discontinuous phase, for various values of the continuous-phase flow rate. Figure 5 gives an approximate correlation for the data as a function of the ratio

$$(U_o)_d/(U_o)_c^2 \quad V_d/V_c^2 .$$

b. Longitudinal Dispersion in the Discontinuous Phase

According to Vermeulen, Williams, and Langlois,[21] the extinction ratio I_o/I (where I_o is the initial intensity and I is the transmitted intensity) can be expressed as

$$I_o/I = b'A + 1,$$

where A is the interfacial area of the discontinuous phase, and b is a function of the ratio of the dispersive indices of both phases. This can be translated in terms of voltage readings from the recorder,

$$v/v_o = bA + 1 ,$$

where v and v_o are the voltage readings for the actual measurement and for the initial time, respectively. Finally, a plot of

$$\frac{v_f}{v}\frac{v - v_o}{v_f - v_o} = \frac{A - A_o}{A_f - A_o}$$

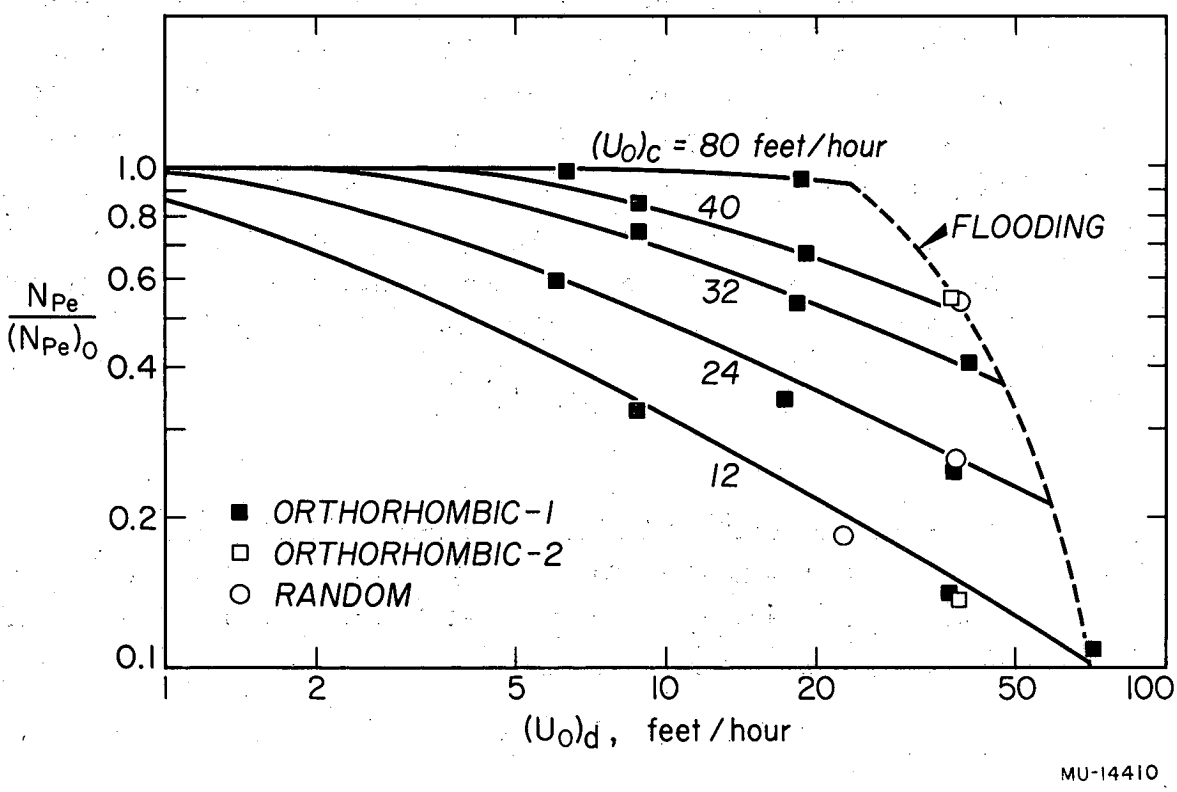

Fig. 4 Longitudinal dispersion in the continuous phase for 0.75-inch-sphere packing.

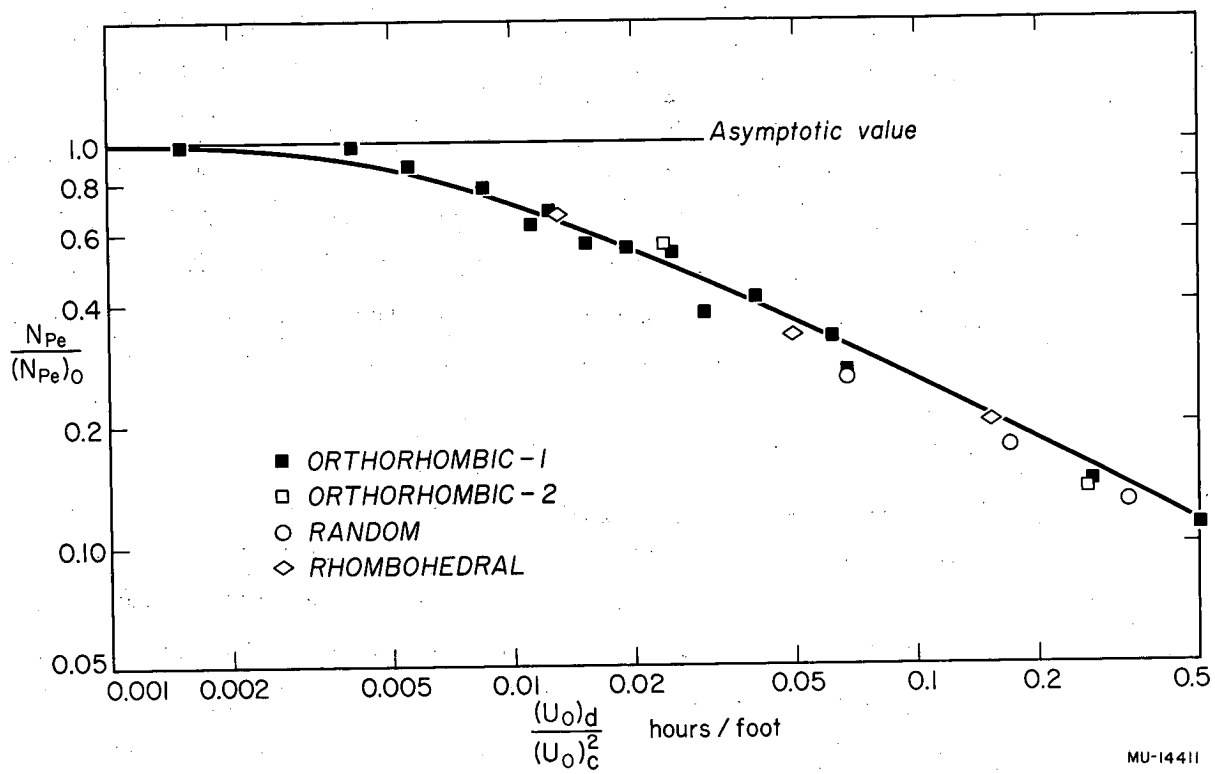

Fig. 5 Correlation plot for continuous-phase longitudinal dispersion.

(where the subscript f indicates the final conditions at the end of the run), gives the breakthrough curve corresponding to the discontinuous phase.

The calculation method can be demonstrated with Run 721-2, made with undyed kerosene, and Run 721-3 with dyed kerosene. Figures 6 and 7 are the respective recorder charts, both corresponding to a recorder-chart speed of 12 inches per minute. Table 2 indicates the results of the calculations for the breakthrough curve. The results are plotted on Figure 8, and give respective slopes of 0.82 and 0.83. The calculations are then conducted in the same way as for one-phase flow measurements. For both $N_D' = 8.44$ and 8.64, Figures 4 and 5 of Part I give $\gamma = 1.015$ and $\delta^2 = 1.15$. The corresponding N_D's are 7.63 and 7.71, and 0.212 and 0.214 were the resulting values of the Peclet numbers. The tables for the two-phase runs are collected in Appendix II. Figures 9 and 10 are plots of the discontinuous-phase results compared to Figures 4 and 5.

c. Radial Dispersion in the Continuous Phase

Radial-dispersion measurements were made for Column 6 as a function of flow conditions. The same procedure as for the one-phase flow was used for analysis of the data. The results are tabulated in Appendix II, and are plotted in Figure 11.

d. Hold-up

Using the breakthrough curves obtained in the measurements of axial dispersion, one finds that the actual time for T = 1 corresponds to the average residence time of the phase under study. The holdup volume is obtained by multiplying the columetric flow rate by the residence time. From the total interior volume of the column between the injection layer and the measuring layer, the fractional porosity for the ith phase is

$$\epsilon_i = \text{Holdup volume/Total column volume.}$$

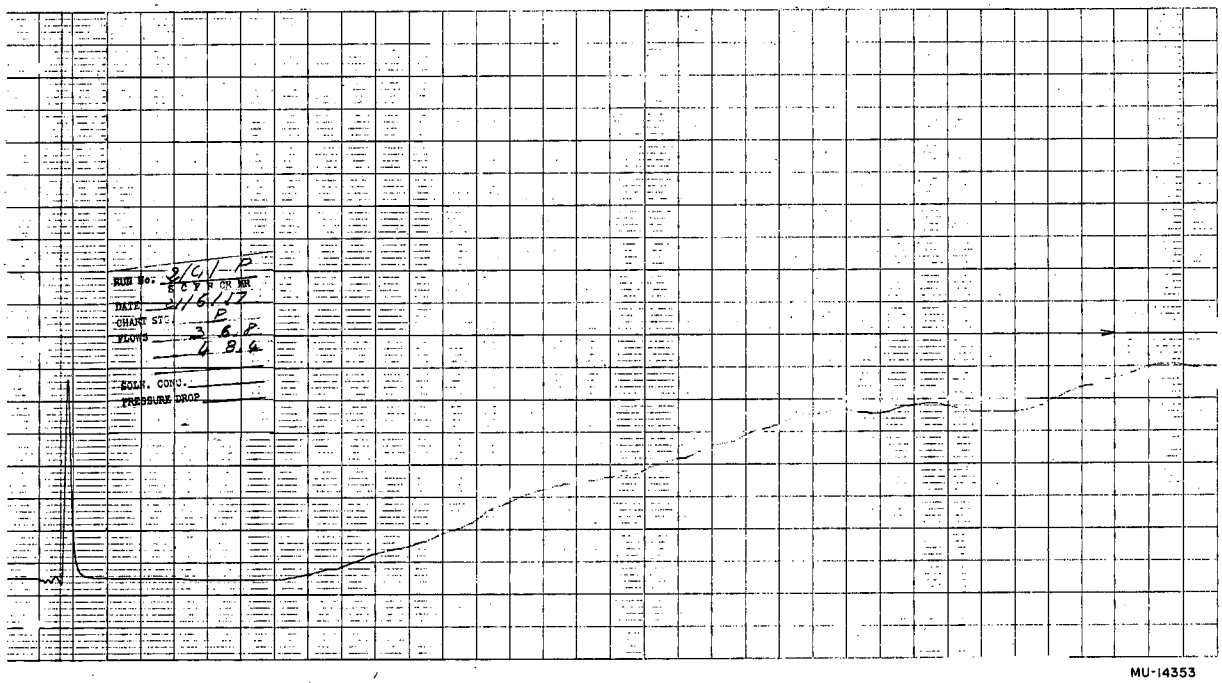

Fig. 6 Recorder chart for Run 721-2 (breakthrough curve of total discontinuous phase).

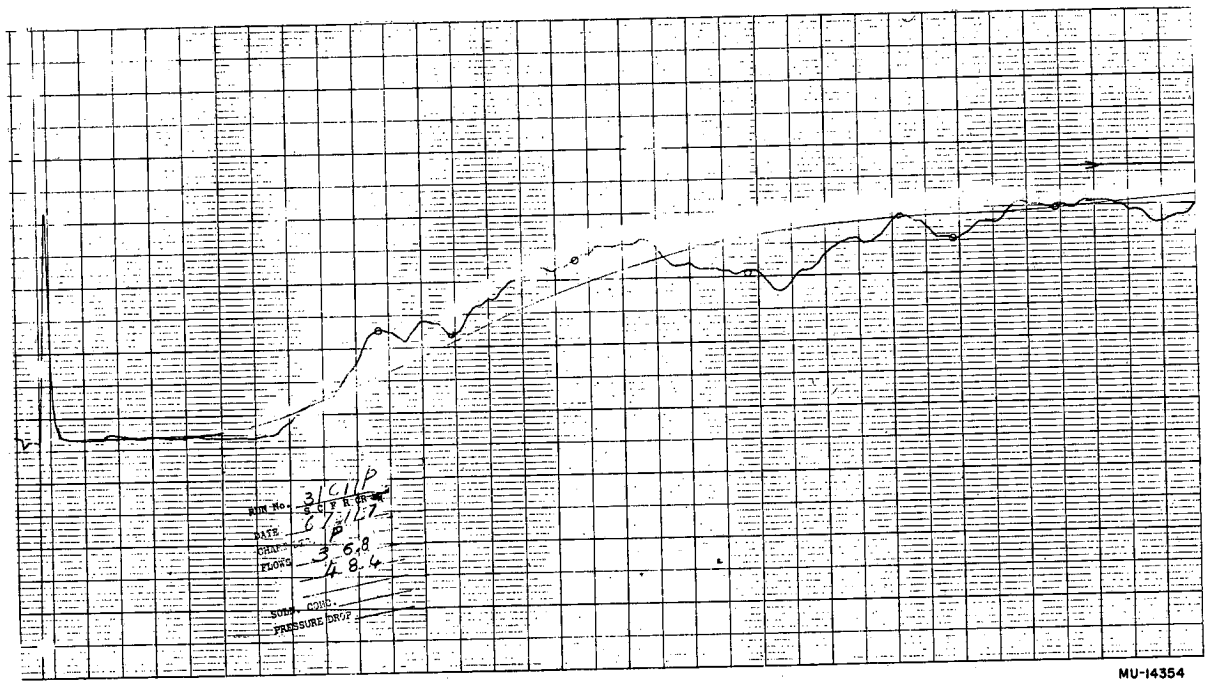

Fig. 7 Recorder chart for Run 721-3 (breakthrough curve of dye injected into the discontinuous phase).

Table 2

Breakthrough-Curve Calculations for the Discontinuous Phase

a. Uncolored Kerosene (Run 721-2)

Recorder-chart readings		Breakthrough curve	
Time (sec.)	Voltage mv	c/c_0, %	$t/t_{50\%}$
0	12.72	0	0
22.50	12.50	4.26	0.409
30.00	12.00	14.47	0.545
45.50	11.00	37.77	0.827
68.00	10.00	65.79	1.24
84.00	9.50	81.90	1.52
∞	9.00	100	∞

b. Colored Kerosene (Run 721-3)

Recorder-chart readings		Breakthrough curve	
Time (sec.)	Voltage mv	c/c_0, %	$t/t_{50\%}$
0	6.30	0	
25.5	4.75	20.04	0.460
31.5	3.70	19.24	0.571
41	3.90	43.15	0.745
54	3.10	37.82	0.981
65.5	3.45	63.71	1.190
69.5	3.30	59.51	1.260
76	3.00	76.96	1.380
∞	2.40	100	∞

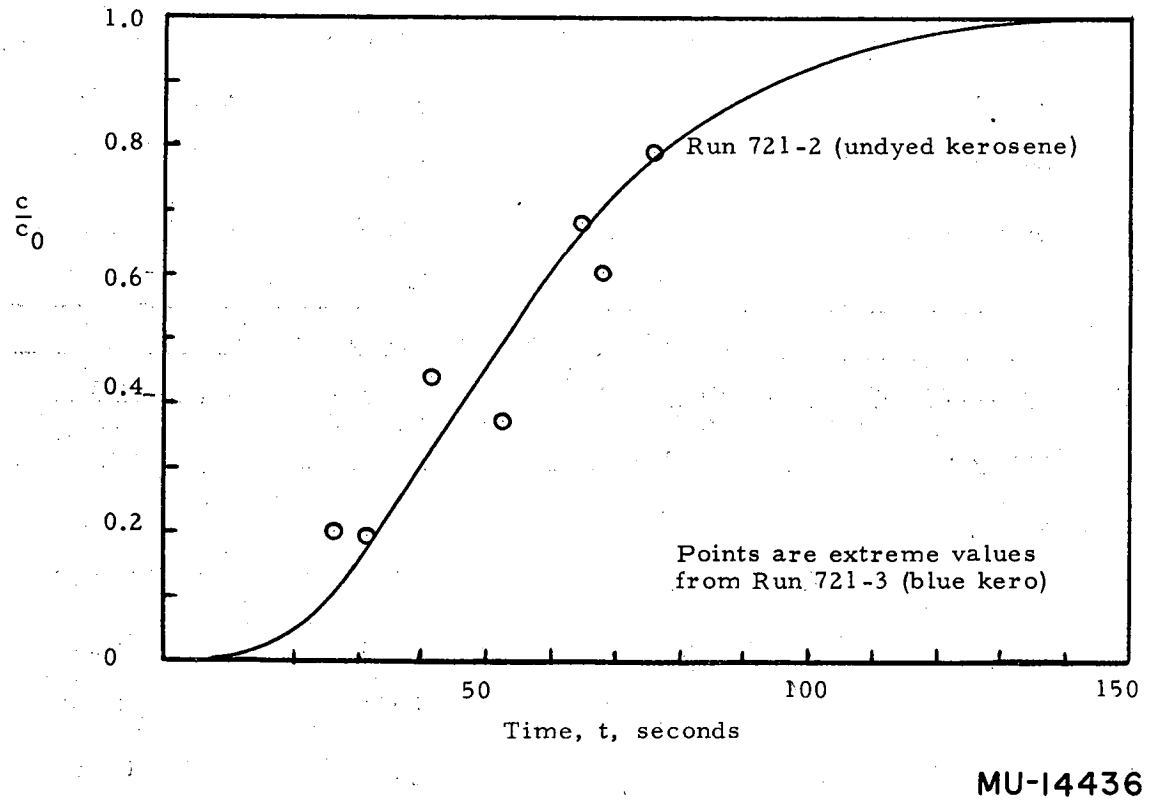

Fig. 8 Crossplot of relative concentration, from Runs 721-2 and 721-3, utilizing points of Table 2.

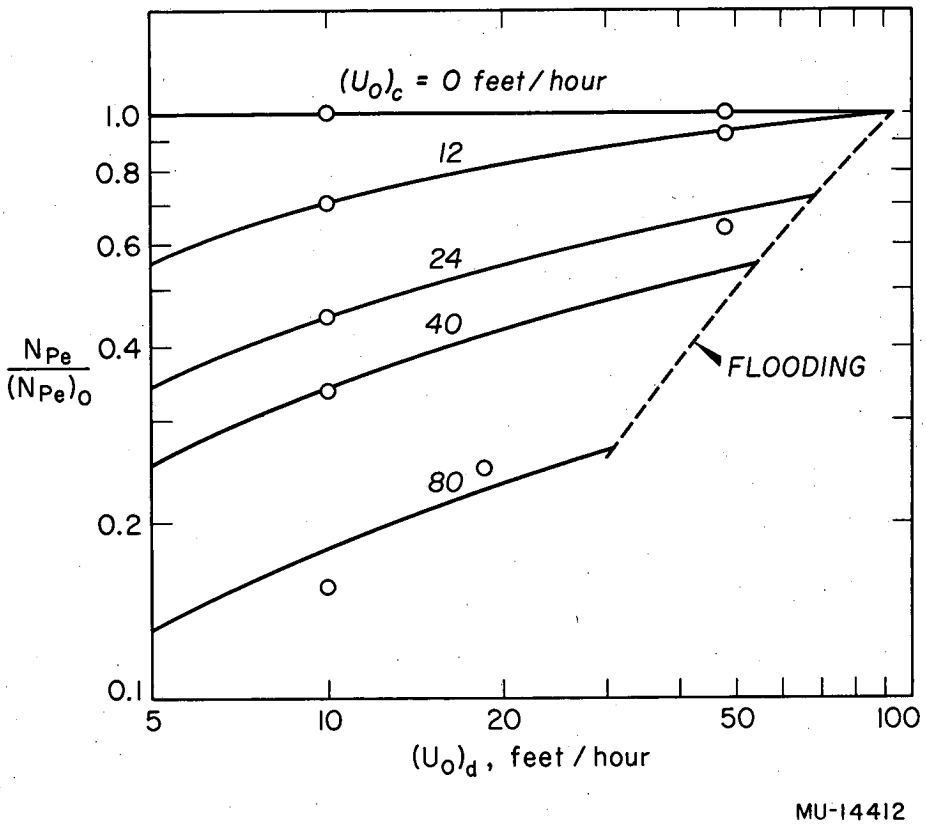

Fig. 9 Longitudinal dispersion in the discontinuous phase for 0.75-inch random packing.

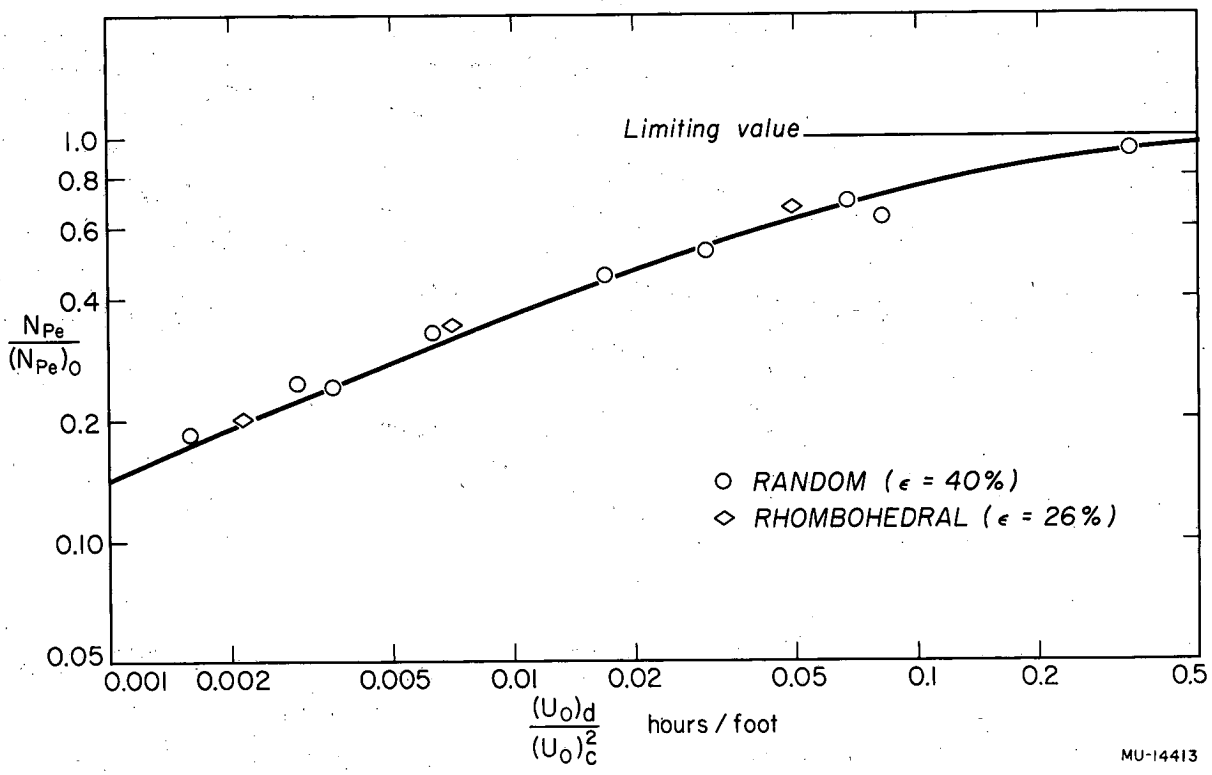

Fig. 10 Correlation plot for discontinuous-phase longitudinal dispersion for 0.75-inch spheres.

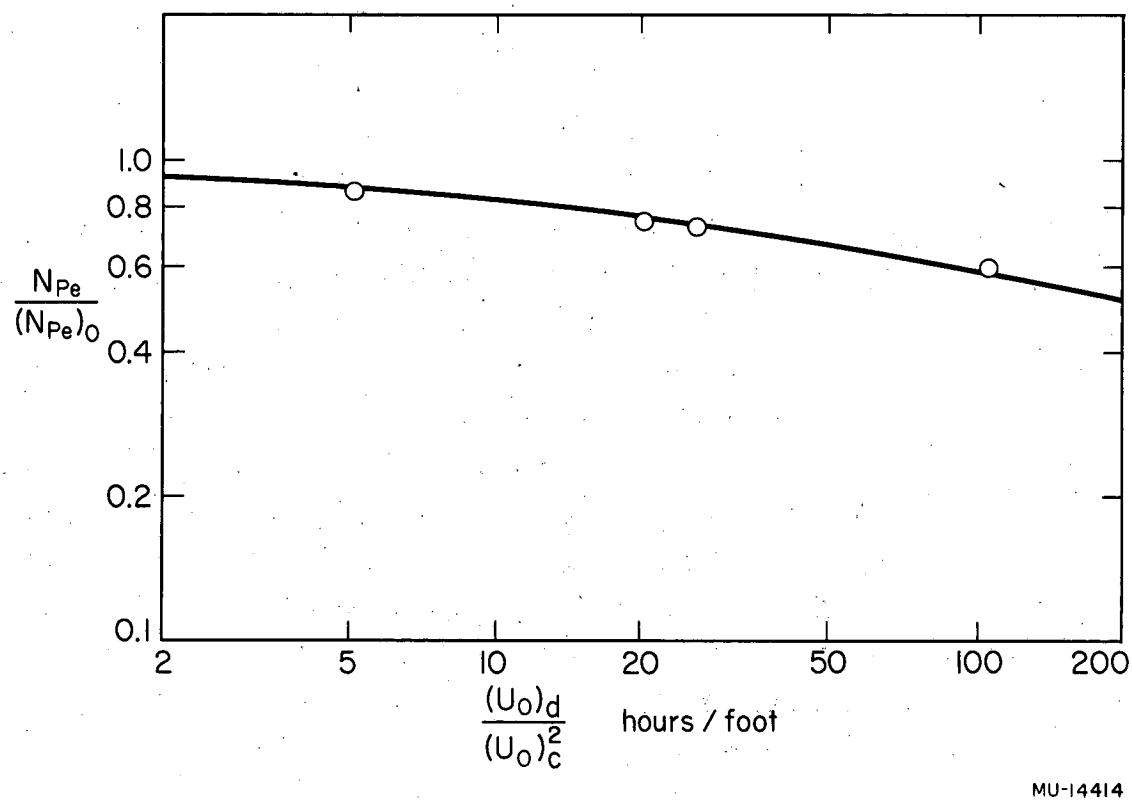

Fig. 11 Radial dispersion in the continuous phase for 0.75-inch sphere packing: Orthorhombic-2 arrangement, 40% porosity.

Further,

$$\epsilon_c + \epsilon_d = \epsilon \ ,$$

where ϵ_c and ϵ_d are the fractional porosity for the continuous phase and the discontinuous phase respectively, and ϵ is the bed porosity. The respective holdups are

$$\chi_c = \epsilon_c / \epsilon \ ,$$

$$\chi_d = \epsilon_d / \epsilon \ ,$$

which may be expressed as percentages (with $\chi_c + \chi_d = 100\%$).

A correlation on "residual saturation" given by Brown[2] indicates that the permanent holdup of the discontinuous phase may reach 2 to 3%. Theoretically, the difference in residence time found for experiments with the undyed and dyed kerosene would correspond to the permanent holdup. The experimental uncertainty in the residence-time values us about 2%, As no definite evidence of permanent holdup was found in the experiments, it was concluded that permanent holdup is less than 2%.

To check the reliability of the experimental determination, holdup values for both phases were obtained. For example, Runs 623-5, 623-1, and 625-1 give an average holdup of 66.73% for the continuous phase (see Table II-9); Runs 708-1, 708-5, 708-2, 708-7, and 709-9 for the same flows (Table II-8) give a holdup of 30.13% for the discontinuous phase. The sum of these results is 96.86%; this would correspond to a permanent holdup of 3.14% which would not disagree with the Brown correlation.

The holdup results are tabulated in Tables II-7, II-8, and II-9, and are plotted in Figures 13 and 14. Figure 12 is a plot of the holdup as function of the continuous-phase flow rate for constant values of the discontinuous-phase flow rate. It is noted that the curve of Figure 12 is flat for the lower values of $(U_{oc})_c$, and starts rising sharply only in the neighborhood of the flooding point.

Extensive studies of holdup were made by Wicks and Beckmann[22] in 1955, following the work of Pratt and coworkers.[8,17] It is planned to utilize the data of these authors in a more general correlation of holdup, as an extension of the present study.

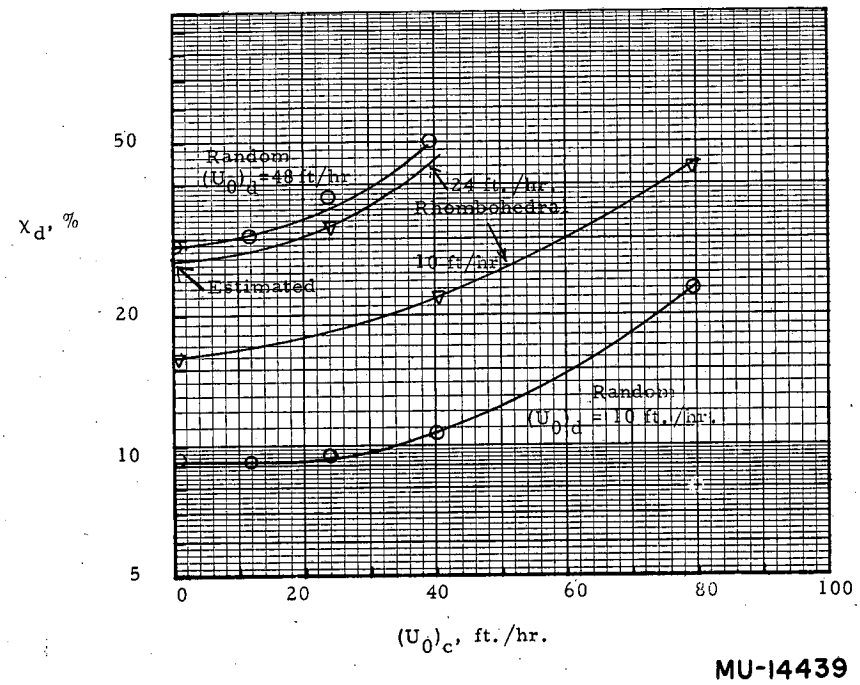

Fig. 12 Holdup of the discontinuous phase for 0.75-inch-diameter spheres.

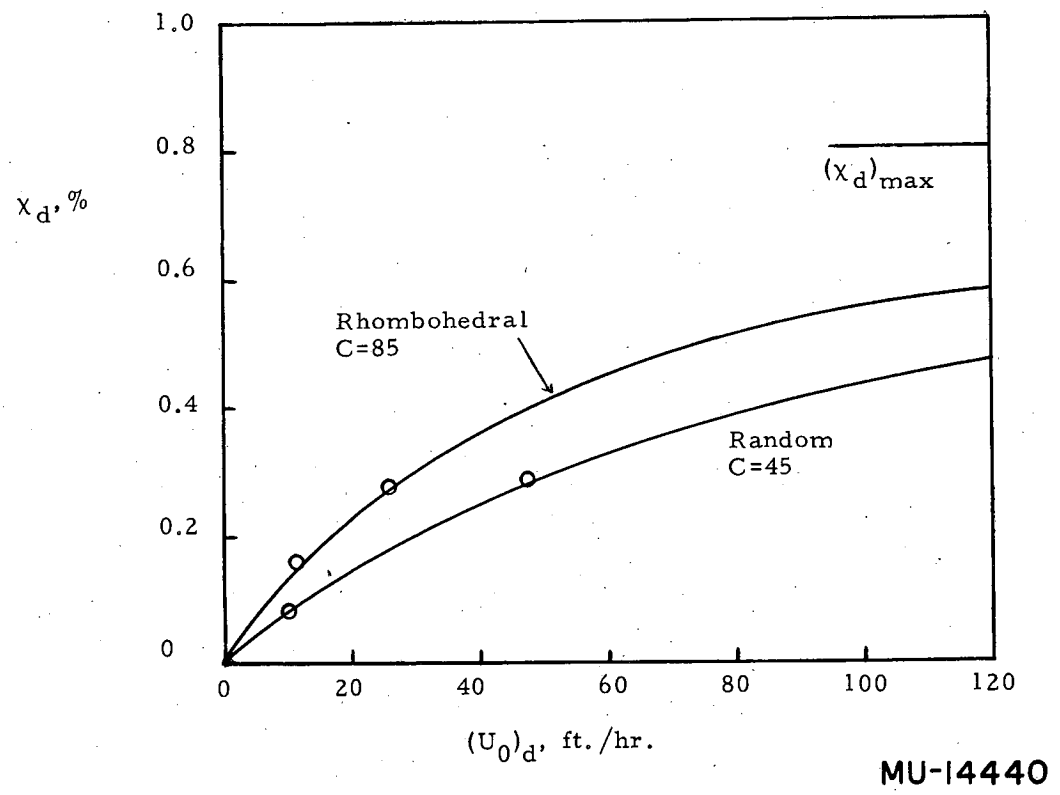

Fig. 13 Holdup of discontinuous phase for stationary continuous phase.

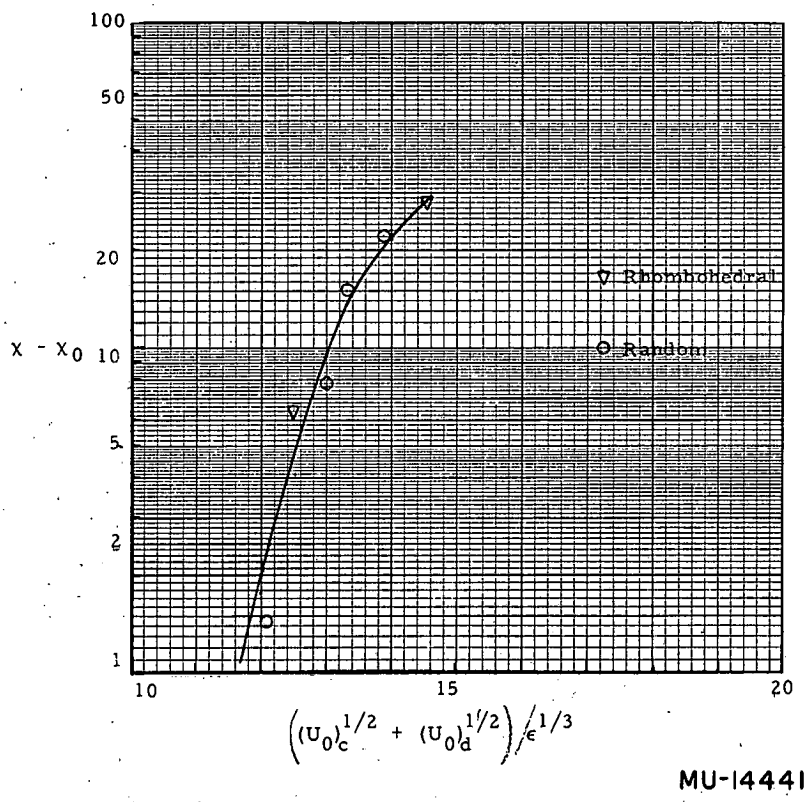

Fig. 14 Correlation plot for holdup, near flooding.

2. Discussion

The analysis of the results obtained leads to the following conclusions:

(a) Flooding occurs at a velocity of the continuous phase that corresponds to the end of the laminar range or the beginning of the transition range.

(b) The longitudinal Peclet numbers obtained are always smaller than, or equal to, the laminar value obtained for one-phase flow. This is found in a continuous-phase velocity corresponding to the single-phase transition range. It appears that the addition of a small amount of discontinuous phase stabilizes the state of laminar flow.

(c) The axial Peclet number of the continuous phase decreases for an increasing flow rate of the discontinuous phase, but also decreases for a decreasing flow rate of the continuous phase (Figure 4).

(d) The axial Peclet number of the discontinuous phase increases for increasing flow rate of the discontinuous phase, but also decreases for decreasing flow rate of the continuous phase (Figure 9).

(e) The radial Peclet number follows qualitatively the same behavior as the axial Peclet number for the continuous phase, but it is somewhat less affected, as shown on Figure 11.

(f) It is possible to correlate all the results expressed as the ratio $N_{Pe} / (N_{Pe})_0$ versus the ratio $(U_0)_d / (U_0)_c^2$, where N_{Pe} is the observed Peclet number, $(N_{Pe})_0$ is the corresponding Peclet number for the laminar region in single-phase flow, and $(U_0)_c$ and $(U_0)_d$ are the flow rates of the continuous phase and the discontinuous phase, respectively. (See Figures 5, 10, and 11.)

(g) The low values obtained - as low as $0.2\ (N_{Pe})_0$ - are an indication that the eddy-diffusion phenomena have far-reaching consequences in extraction.

APPLICATION TO PACKED-COLUMN EXTRACTION

To determine the effect of the diffusion term in Equation 11, this equation was applied to the data of Colburn and Welsh.[5] The results, given in Tables 3 and 4 and plotted on Figure 15, lead to the following conclusions:

1. The over-all Peclet number changes very little, for a given packing type and porosity. For a wide range of flow conditions, in a typical case, N_{Pe} may vary between 0.036 and 0.050 (see Table 3). Consequently the value of N_{ocD} also varies very little; in the same typical case N_{ocD} varies only between 0.5 ft and 0.63 ft.

2. It has been assumed that the flow rates can be varied, while Λ is maintained at unity (where Λ is the extraction coefficient, $\Lambda = m\, F_d/F_c$). Although this would not actually be achieved in any one system, many practical extraction systems do in fact operate with Λ near unity. For a large flow rate of the discontinuous phase and a very small flow of the continuous phase, the dispersion effect may entirely control the HTU. For a small flow rate of the discontinuous phase and a large flow of the continuous phase, however, mass transfer tends to provide the principal resistance (see Figure 15).

3. The ratio of the diffusion term to the HTU can be correlated as an increasing function of

$$G_d \sqrt{G_c}\,, \quad \text{where the G's correspond to mass flow rates.}$$

4. Equation 11 can be written

$$H_{ocP} = H_{oc\infty} + \frac{d_p}{d_p/h + (N_{Pe})_{oc}}\,.$$

Extrapolation of Colburn's and Welsh's results, in the light of this equation, provides the following conclusions:

a. For equal bed heights, the diffusion term in Equation 17 increases for increasing particle diameter as expressed in Figure 16. (The porosity of the bed is assumed to remain constant.)

b. For the same particle diameter and the same porosity, the diffusion term is an increasing function of the length as expressed by Figure 17.

Table 3

Over-all Peclet number calculated for extraction experiments.

Data of Colburn and Walsh.[3]

Continuous phase water, discontinuous phase isobutanol.

G_d (lb/hr/ft^2)	$(N_{Pe})_{oc}$ at G_c = 1,150	$(N_{Pe})_{oc}$ at G_c = 500
270	0.040	0.050
490	0.045	0.045
1010	0.050	0.036

Table 4

Comparison of dispersion resistance with total extraction resistance

(Data of Colburn and Welsh[3])

G_d (lb/hr/ft^2)	G_c = 1,150 lb/hr/ft^2		G_c = 500 lb/hr/ft^2	
	Exptl. H_{ocP} (ft)	$\frac{H_{ocD}}{H_{ocP}}$ (%)	Exptl. H_{ocP} (ft)	$\frac{H_{ocD}}{H_{ocP}}$ (%)
270	4.4	13.7	2.15	23
490	1.7	29	1.05	50
1010	0.75	67	0.50	~100

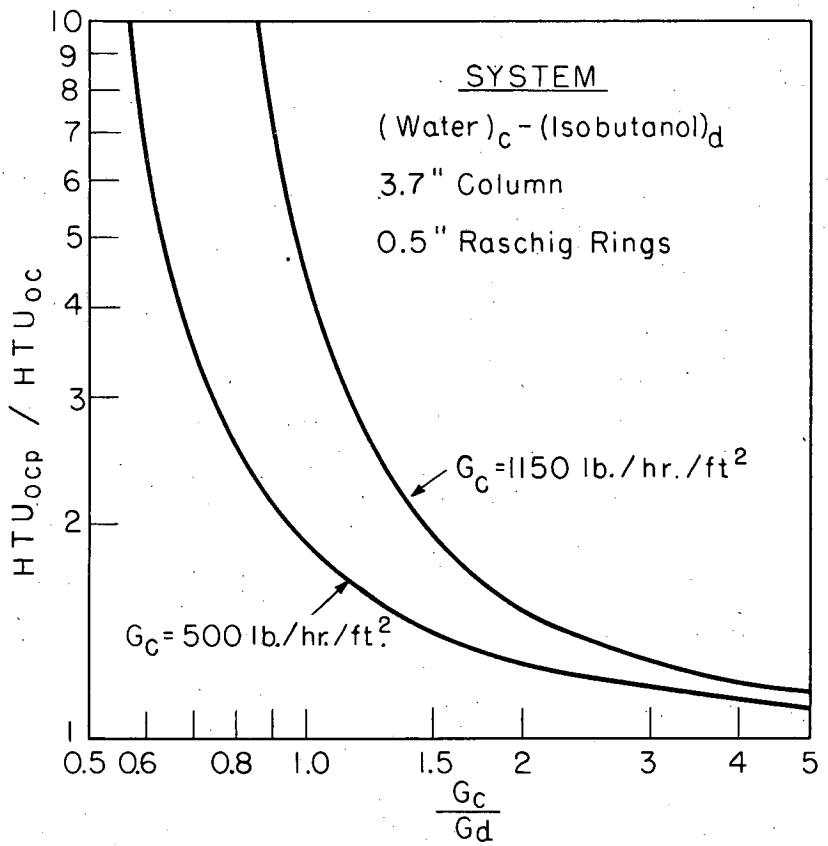

Fig. 15 Effect of longitudinal dispersion on HTU correlation.

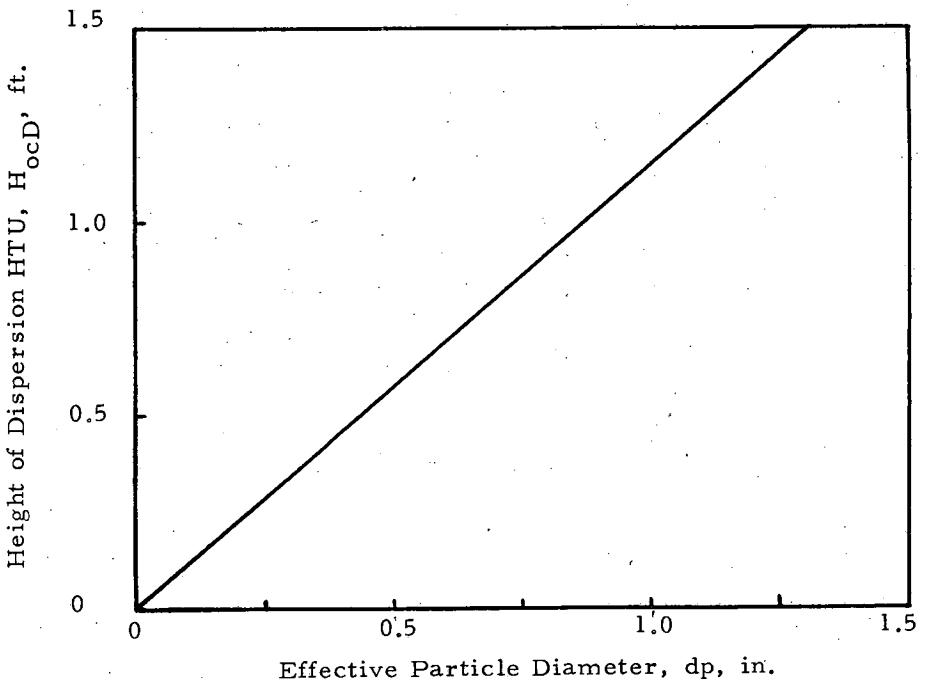

Fig. 16 Effect of particle diameter on H_{ocD} at constant d_p/h ratio.

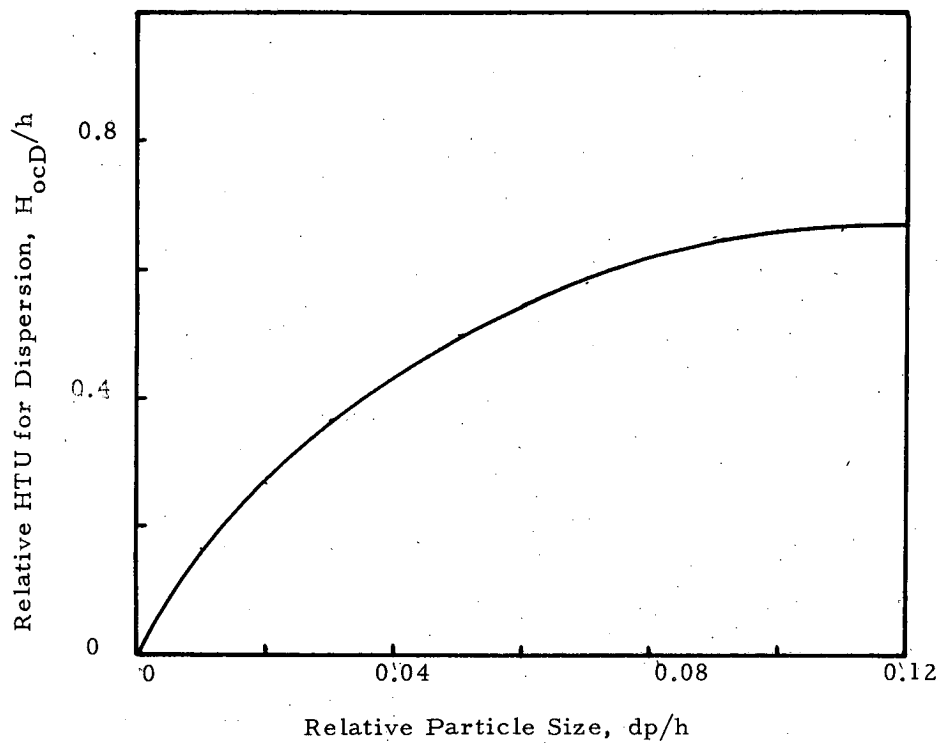

Fig. 17 Effect of particle diameter on H_{ocD} at constant column height.

c. For the same ratio of particle diameter to bed length, and the same porosity, the diffusion term is directly proportional to d_p, (Figure 18).

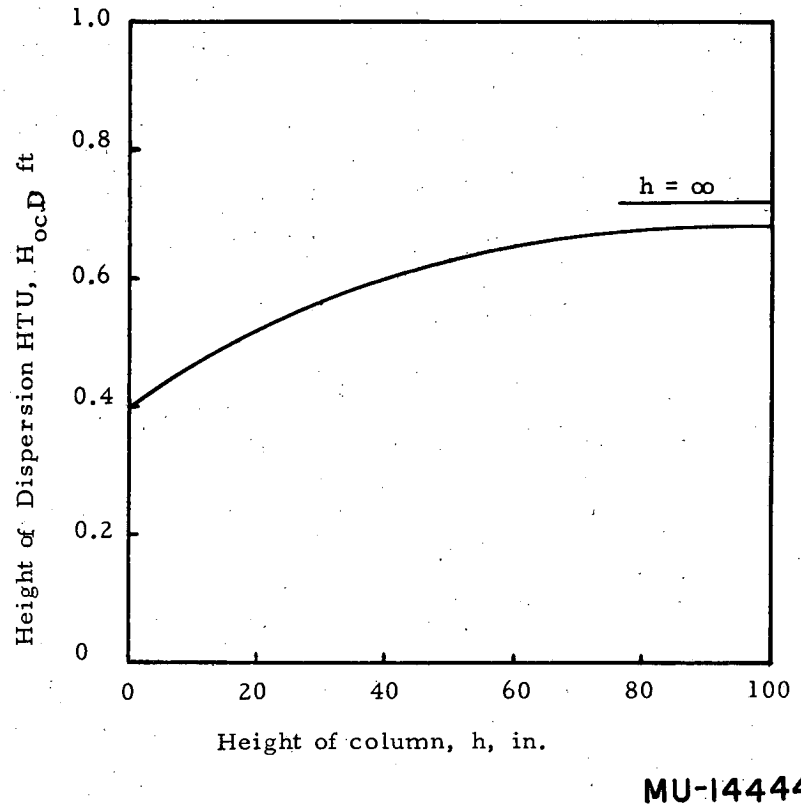

Fig. 18 Effect of column height on H_{ocD} at constant particle diameter (1/2-inch rings).

ACKNOWLEDGMENT

Appreciation is expressed to Professor John Prausnitz and Professor Hans A. Einstein for helpful discussion, to Robert C. Gilmore and Robert B. Waite for their part in the construction of the experimental equipment, to Frederick E. Vogelsberg whose work in the design and installation of the electronic instrumentation was invaluable, and to many fellow students in the Department of Chemical Engineering for their contributions to the author's knowledge of the field.

The work described was performed in the Radiation Laboratory under the auspices of the United States Atomic Energy Commission..

NOTATION

a	Cell constant
A	Interfacial area per unit volume
A_f	Interfacial area at the end of the run
b	Fractional length, h/h_{max}
b'	Light-intensity coefficient
B	Dimensionless height, h/d_p
c	Point concentration inside
c'	Concentration of the entering stream
c''	Concentration of the exit stream
c_o or c_∞	Concentration for perfect mixing
C	Dimensionless concentration
d_p	Particle diameter
D_m	Molecular diffusivity
E	Dispersion coefficient
E_ℓ	Longitudinal dispersion coefficient
E_r	Radial dispersion coefficient
F	Volumetric flow rate
G	Superficial flow rate, weight per unit time per unit area
h	Height of bed
H	Longitudinal mixing length
H'	Mixing-length vector
H_r	Radial mixing length
H_{ox}	Over-all height of transfer unit measured relative to the X phase (mass-transfer component)
H_{oxD}	Over-all height of transfer unit (dispersion component)
H_{oxP}	Over-all height of transfer unit (observed experimentally)
I	Intensity of light
I_o	Initial intensity of light
$\underline{I}_o$	Bessel function of zero order, with imaginary argument
m	Slope of the equilibrium curve
n	Number of runs corresponding to the same experimental conditions

N_D	Number of dispersion units
N_{Pe}	Peclet number
$(N_{Pe})_\ell$	Longitudinal Peclet number
$(N_{Pe})_r$	Radial Peclet number
$(N_{Pe})_{ox}$	Overall Peclet number
(N_{ox})	Number of transfer units (mass-transfer component)
N_{oxD}	Number of transfer units (dispersion component)
N_{oxM}	Number of transfer units (calculated from measured concentrations)
N_{oxP}	Number of transfer units (observed experimentally)
N_{Re}	Reynolds number, $U_o d_p/\nu$
p,P	Probabilities
P	Peclet number (same as N_{Pe})
r	Radial coordinate to a point
R	Radius of the column
s	Slope of the breakthrough curve
$t^{.05}_{n-1}$	Student's t parameter: (n-1) terms, confidence limit
T	Dimensionless time
u	Characteristic velocity
U	Interstitial velocity
U_o	Superficial velocity, equals U_ϵ
v	Voltage
v_o	Voltage at zero time
v_f	Voltage at the end of the run
x	General variable
z	Dimensionless length
α	Angle of dispersion
β	Correction factor, $(\gamma\delta)^{-2}$
γ	Correction factor for breakthrough slope
δ	Correction factor for breakthrough intercept
ϵ	Porosity factor
ζ	Dimensionless length
θ	Characteristic time of mixing
Λ	Extraction factor

μ	Parameter in diffusion equation
ν	Kinematic viscosity
ρ	Radius ratio, r/R
τ	Time
χ	Hold-up of designated phase, in two-phase flow
X	Concentration ratio c/c_∞
ψ	Modified Peclet number
ω	Resistivity
Ω	Resistance

LITERATURE CITED

1. J. Allerton, B. O. Strom, and R. E. Treybal, Trans. Am. Inst. Chem. Engrs. 39, 361 (1943).
2. G. G. Brown and associates, "Unit Operations", New York:Wiley (1950).
3. A. P. Colburn, Trans. Am. Inst. Chem. Engrs. 29, 174 (1939).
4. A. P. Colburn, Ind. Eng. Chem. 33, 459 (1941).
5. A. P. Colburn and D. G. Welsh, Trans. Am. Inst. Chem. Engrs. 38, 179 (1942).
6. J. C. Elgin and F. M. Browning, Trans. Am. Inst. Chem. Engrs. 31, 639 (1935).
7. J. C. Elgin and R. Wynkoop, in J. H. Perry, "Chemical Engineers' Handbook", 3rd ed. New York: McGraw-Hill (1950).
8. R. Gaylor and H. R. C. Pratt, Trans. Inst. Chem. Engrs. (London) 29, 110 (1950).
9. H. L. Hou and N. W. Frankel, Chem. Eng. Prog. 45, 65 (1949).
10. H. F. Johnson and H. Bliss, Trans. Am. Inst. Chem. Engrs. 42, 331 (1946).
11. O. S. Knight, Trans. Am. Inst. Chem. Engrs. 39, 439 (1943).
12. J. H. Koffolt, S. B. Row, and J. R. Withrow, Trans. Am. Inst. Chem. Engrs. 37, 559 (1941).
13. G. S. Laddha and J. M. Smith, Chem. Eng. Progr. 46, 195 (1950).
14. G. E. Langlois, J. E. Gullberg, and T. Vermeulen, Rev. Sci. Instr. 25, 360 (1954).
15. A. K. McMullen, T. Miyauchi, and T. Vermeulen, UCRL Report 3911 - Suppl. (in preparation).
16. T. Miyauchi, UCRL Report 3911 (August 1957).

17. J. B. Lewis, I. Jones, and H. R. C. Pratt, Trans. Inst. Chem. Engrs. (London) 29, 126 (1951).

18. B. Rubin and H. R. Lehman, UCRL Report 718 (1950).

19. T. K. Sherwood, J. E. Evans, and J. V. A. Longcor, Trans. Am. Inst. Chem. Engrs. 35, 597 (1939).

20. R. E. Treybal, "Liquid Extraction" New York:McGraw-Hill (1950).

21. T. Vermeulen, G. M. Williams, and G. E. Langlois, Chem. Eng. Progr. 51, 85 (1955).

22. C. E. Wicks and R. B. Beckmann, Am. Inst. Chem. Engrs. J. 1, 427 (1955).

Part III. APPENDICES

APPENDIX I. SINGLE-PHASE FLOW

Table I-1. Longitudinal Dispersion, 0.75-inch Spheres, Rhombohedral Arrangement (See Fig. 9)

Flow rate, gal./min.	N_{Re} ($d_p U_o/\nu$)	Column height, in.	Run No.	Slope $\frac{d(c/c_o)}{dt}$	N_D	N_{Pe}
0.30	19.4	23.6	301-4	1.33	21.25	0.675
			301-10	1.27	19.36	0.615
			301-11	1.30	20.28	0.644
			302-10	1.32	20.90	0.664
			302-11	1.33	21.25	0.675
			302-12	1.32	20.90	0.664
			Average of 6 runs			0.656±0.039
1.0	64.6	23.6	301-5	1.35	21.87	0.694
			301-6	1.37	22.53	0.715
			301-7	1.33	21.25	0.675
			301-8	1.40	23.54	0.748
			302-8	1.34	21.56	0.684
			302-9	1.38	22.85	0.725
			Average of 6 runs			0.706±0.040
1.40	90.4	23.6	303-1	1.52	28.08	0.892
			303-3	1.53	28.45	0.903
			303-6	1.54	28.82	0.915
			303-7*	1.54	28.82	0.954
			Average of 4 runs			0.916±0.039
2.0	129.2	23.6	302-3	1.78	38.85	1.230
			302-4*	1.73	36.69	1.165
			302-6	1.80	39.73	1.262
			302-7	1.82	40.61	1.290
			Average of 4 runs			1.236±0.105
2.5	161.5	23.6	303-5	2.00	49.30	1.566
			303-10	1.95	46.85	1.488
			303-11	1.93	45.91	1.459
			303-12	1.95	46.85	1.488
			Average of 4 runs			1.500±0.104
3.0	194.0	23.6	301-3	2.15	57.64	1.831
			302-1	2.20	59.83	1.900
			302-5*	2.17	58.20	1.849
			302-6	2.21	60.37	1.917
			Average of 4 runs			1.874±0.079

*Throughout Appendix I, the asterisk will identify runs breakthrough curves were taken both from $c = o$ to $c = c_o$ and from $c = c_o$ to $c = o$.

Table I-1. (cont'd.)

Flow rate, gal./min.	N_{Re} $(d_p U_o/\nu)$	Column height, in.	Run No.	Slope $\frac{d(c/c_o)}{dt}$	N_D	N_{Pe}
10.0	646	23.6	301-2	2.46	75.62	2.402
			302-2*	2.50	77.49	2.462
			304-5	2.53	79.34	2.520
			304-7	2.46	75.02	2.383
			Average of 4 runs			2.442±0.121
30.0	1940	23.6	305-1	2.51	78.18	2.484
			305-2	2.48	76.32	2.424
			305-3	2.45	74.46	2.366
			305-4	2.52	78.80	2.503
			305-5	2.50	77.56	2.464
			Average of 5 runs			2.448±0.100

Table I-2. Longitudinal Dispersion, 0.75-inch Spheres, Orthorhombic-1 Arrangement. (See Fig. 10)

Flow rate, gal./min.	N_{Re} $(d_p U_o/\nu)$	Column height, in.	Run No.	Slope $\frac{d(c/c_0)}{dt}$	N_D	N_{Pe}
0.30	19.4	22.95	426-1	1.12	14.95	0.487
			426-3*	1.15	15.66	0.510
			426.4	1.14	15.39	0.501
			427-1*	1.12	14.85	0.484
			427-2	1.13	14.46	0.471
			Average of 5 runs			0.490±0.027
1.0	64.6	22.95	428-1	1.27	19.25	0.628
			428-2	1.25	18.67	0.608
			Average of 2 runs			0.618±0.040
2.0	129.2	22.95	428-3	1.48	26.57	0.866
			428-7	1.50	27.30	0.889
			Average of 2 runs			0.877±0.037
3.0	194.0	22.95	427-4*	1.75	37.54	1.220
			429-2	1.76	37.98	1.238
			429-4	1.76	37.98	1.220
			Average of 3 runs			1.226±0.030
10.0	646	22.95	426-1	2.16	57.72	1.882
			427-3	2.15	57.19	1.864
			427-6	2.19	59.34	1.934
			Average of 3 runs			1.893±0.050
30.0	1940	22.95	430-1	2.17	58.26	1.899
			430-3	2.15	57.14	1.864
			Average of 2 runs			1.881±0.045

Table I-3. Longitudinal Dispersion, 0.25-inch Raschig Rings(d_p = 0.22 inch).

Flow rate, gal./min.	N_{Re} ($d_p U_o/\nu$)	Column height, in.	Run No.	Slope $\frac{d(c/c_o)}{dt}$	N_D	N_{Pe}
0.30	5.69	26.0	902-1	1.388	23.25	0.196
			902-2	1.350	21.92	0.185
			902-6	1.40	23.66	0.200
			902-8	1.380	22.98	0.194
			Average of 4 runs			0.194±0.063
3.0	56.9	26.0	903-1	2.12	55.47	0.469
			903-5	2.10	54.48	0.460
			Average of 2 runs			0.464±0.020
10.0	189.5	26.0	902-4	2.65	87.32	0.738
			902-5	2.80	97.49	0.824
			903-2	2.76	94.72	0.801
			903-4	2.80	97.49	0.824
			Average of 4 runs			0.796±0.13
20.0	379	26.0	905-1	2.92	106.02	0.896
			905-3	2.94	107.48	0.909
			905-4	2.94	107.48	0.909
			905-6	2.95	108.20	0.913
			905-8	2.92	106.02	0.896
			Average of 5 runs			0.904±0.065

Table I-4. Longitudinal Dispersion, 0.25-inch Polyethylene Pellets (d_p = 0.232 inch).

Flow rate, gal./min.	N_{Re} ($d_p U_0/\nu$)	Column height, in.	Run No.	Slope $\frac{d(c/c_0)}{dt}$	N_D	N_{Pe}
0.3	5.28	2.50	324-1	0.720	5.66	0.525
			324-3	0.710	5.50	0.510
0.3	5.28	5.0	324-2	1.00	11.62	0.539
0.3	5.28	26.0	314-4	2.15	57.19	0.510
			319-6	2.17	58.26	0.519
			320-1*	2.22	60.97	0.543
			320-2*	2.25	62.63	0.558
			320-6	2.26	62.90	0.560
			Average of 5 runs			0.538±0.038
1.0	17.6	26.0	319-7	2.25	62.63	0.558
			319-9	2.27	63.76	0.568
			319-10	2.23	61.54	0.548
			320-7	2.15	57.19	0.510
			Average of 4 runs			0.546±0.069
3.0	52.8	14.0	320-3	1.60	31.09	0.515
			321-1*	1.60	31.09	0.515
			Average of 2 runs			0.515±0.000
4.2	91.5	14.0	320-4*	1.80	39.79	0.632
7.4	130.2	26.0	320-4*	2.84	100.29	0.841
			320-5*	2.88	103.13	0.865
			321-4	2.82	99.84	0.821
			321-5	2.89	103.86	0.863
			Average of 4 runs			0.847±0.018
10.0	176	26.0	319-1*	3.57	160.06	1.364
			319-2*	3.36	136.77	1.544
			319-3*	3.15	124.64	1.380
			319-4	3.24	131.84	1.460
			Average of 4 runs			1.429±0.129
30.0	528	26.0	320-8	4.45	248.68	2.119
			320-9	4.40	243.16	2.072
			320-10	4.39	242.03	2.069
			320-11	4.42	245-37	2.090
			320-12	4.44	247.60	2.109
			321-7	4.36	238.76	2.033
			Average of 6 runs			2.082±0.081

Table I-5. Longitudinal Dispersion, 0.75-inch Spheres, Randomly Packed.

Flow rate, gal./min.	N_{Re} ($d_p U_0/\nu$)	Column height, in.	Run No.	Slope $\frac{d(c/c_0)}{dt}$	N_D	N_{Pe}
0.30	19.4	24.0	205-1*	0.948	10.25	0.361
			215-1	0.945	10.19	0.359
			215-2	1.03	12.10	0.425
			216-1	0.985	11.08	0.390
			217-3	0.990	11.18	0.393
			217-4	1.01	11.64	0.409
			Average of 6 runs			0.389±0.014
0.30	19.4	12.0	209-1	0.710	5.50	0.345
			209-2	0.695	5.27	0.329
			209-3	0.723	5.69	0.355
			210-1*	0.733	5.86	0.365
			Average of 4 runs			0.348±0.152
1.0	64.6	24.0	208-2	1.09	14.076	0.439
			214-4*	1.16	15.930	0.497
			216-2	1.13	15.118	0.472
			Average of 3 runs			0.469±0.124
2.0	129.2	24.0	208-7	1.60	31.21	0.974
			216-1*	1.47	26.33	0.821
			216-2	1.55	24.87	0.776
			216-5*	1.52	28.16	0.880
			216-6	1.54	28.89	0.902
			217-2	1.60	31.21	0.974
			Average of 6 runs			0.887±0.093
3.0	194	24.0	210-1	1.83	41.05	1.280
			210-3*	1.82	40.61	1.260
			210-5*	1.86	42.42	1.325
			211-3	1.78	38.85	1.211
			217-1	1.88	43.34	1.353
			Average of 5 runs			1.285±0.075
10	646	24.0	207-4	2.16	57.72	1.805
			207-5	2.14	56.86	1.772
			208-4	2.15	57.20	1.790
			210-3	2.22	60.97	1.906
			211-2	2.19	58.11	1.816
			211-3	2.20	59.89	1.872
			216-4	2.20	59.89	1.872
			217-8	2.21	60.43	1.889
			217-9	2.17	58.26	1.821
			Average of 9 runs			1.838±0.033

Table I-5. (cont'd.)

Flow rate, gal./min.	N_{Re} $(d_p U_o/\nu)$	Column height, in.	Run No.	Slope $\frac{d(c/c_o)}{dt}$	N_D	N_{Pe}
30.0	1940	24.0	208-6	2.17	58.26	1.821
			210-2	2.20	59.89	1.872
			210-4	2.20	59.89	1.872
			214-3	2.20	59.89	1.872
			Average of 4 runs			1.858±0.099

Table I-6. Longitudinal Dispersion, 0.75-inch Spheres, Orthorhombic-2 Arrangement (See Fig. 15).

Flow rate, gal./min.	N_{Re} $(d_p U_0/\nu)$	Column height, in.	Run No.	Slope $\frac{d(c/c_0)}{dt}$	N_D	N_{Pe}
0.30	19.4	12.75	406-1	0.86	8.21	0.488
		18.75	407-1	1.00	11.62	0.464
		24.00	402-1	1.11	14.45	0.450
			402-3	1.14	15.28	0.476
			406-2	1.15	15.55	0.485
			406-3	1.11	14.45	0.450
			Average of 6 runs			0.469±0.082
1.0	64.6	12.75	409-2	0.920	9.66	0.568
		24.00	406-4	1.25	18.69	0.583
			409-1	1.29	19.88	0.620
			413-9	1.26	18.99	0.592
			Average of 4 runs			0.590±0.092
1.8	116.3	24.00	403-1	1.48	26.63	0.830
			414-2	1.45	25.54	0.796
			Average of 2 runs			0.813±0.180
2.5	161.5	12.75	412-2	1.20	17.14	1.007
		18.75	412-1	1.38	22.22	0.915
		24.00	413-2	1.67	34.10	1.063
			413-3	1.61	31.61	0.986
			413-6	1.67	34.00	1.061
			413-7	1.56	29.67	0.925
			413-8	1.58	30.42	0.949
			414-1	1.66	33.60	1.048
			414-8	1.67	34.00	1.063
			Average of 9 runs			1.001±0.062
3.0	1940	12.75	409-5	1.32	20.83	1.225
			409-11	1.32	20.83	1.225
		18.75	409-4	1.58	30.44	1.217
			409-6	1.61	31.66	1.266
			410-4	1.62	32.00	1.280
		24.00	401-1	1.85	41.97	1.303
			406-7	1.85	41.87	1.303
			409-3	1.83	41.07	1.231
			409-7	1.82	40.62	1.267
			410-5	1.83	41.07	1.281
			Average of 10 runs			1.264±0.033

Table I-6. (cont'd.)

Flow rate, gal./min.	N_{Re} $(d_p U_o/\nu)$	Column height, in.	Run No.	Slope $\frac{d(c/c_o)}{dt}$	N_D	N_{Pe}
10.0	646	12.75	410-9	1.62	31.92	1.876
		18.75	401-2	1.92	45.34	1.813
		24.00	328-1*	2.25	62.64	1.950
			410-3	2.26	63.19	1.971
			410-7	2.16	57.74	1.801
			410-10	2.22	60.98	1.903
			Average of 6 runs			1.885±0.077
30.0	1940	12.75	409-12	1.62	31.92	1.876
		24.00	328-2	2.24	62.07	1.930
			Average of 2 runs			1.903±0.160

Table I-7. Longitudinal Dispersion, 0.75-inch Raschig Rings (d_p = 0.65 inch).

Flow rate, gal./min.	N_{Re} $(d_p U_o/\nu)$	Column height, in.	Run No.	Slope $\frac{d(c/c_o)}{dt}$	N_D	N_{Pe}
0.30	16.8	26.0	828-2	0.90	9.24	0.231
			828-3	0.94	10.08	0.252
			828-4	0.95	10.03	0.258
			828-6	0.88	8.84	0.221
			Average of 4 runs			0.240±0.065
1.0	56.0	26.0	825-4	1.18	16.49	0.412
			825-5	1.15	15.15	0.378
			Average of 2 runs			0.065
3.0	168	26.0	825-1	1.55	29.18	0.729
			825-2	1.52	28.06	0.701
			825-3	1.59	30.71	0.767
			825-6	1.60	31.09	0.777
			Average of 4 runs			0.743±0.087
10.0	560	26.0	823-1	1.68	35.44	0.886
			823-2	1.72	36.24	0.906
			823-3	1.75	37.52	0.938
			823-5	1.72	36.24	0.906
			Average of 4 runs			0.909±0.065

Table I-8. Longitudinal Dispersion, 1.0-inch Intalox Saddles (d_p = 0.72 inch)

Flow rate, gal./min.	N_{Re} ($d_p U_0/\nu$)	Column height, in.	Run No.	Slope $\frac{d(c/c_0)}{dt}$	N_D	N_{Pe}
0.30	18.88	26.0	931-1	0.900	9.25	0.255
			931-2	0.920	10.62	0.293
			931-3	0.890	9.04	0.249
			931-5	0.880	8.84	0.243
			Average of 4 runs			0.260±0.064
10.0	629	26.0	930-1	1.65	33.16	0.915
			930-2	1.62	31.99	0.882
			930-3	1.65	33.16	0.915
			930-4	1.60	31.21	0.861
			Average of 4 runs			0.893±0.066

Table I-9. Radial Dispersion, 0.75-inch Spheres, Rhombohedral Arrangement (See Fig. 9).

Flow rate, gal./min.	N_{Re} ($d_p U_0/\nu$)	Run No.	$\frac{r}{R}$	h, inch	$\frac{c}{c_0}$	$\frac{N_{Pe} R^2}{h d_p}$	$(N_{Pe})_r$
10.0	646	307-2	0.125	3.24	3.50	7.00	3.78
		307-2		5.94	1.90	3.80	3.76
		307-3		3.24	3.20	6.50	3.51
		307-3		5.94	2.00	4.20	4.15
		308-1		3.24	3.70	7.50	4.05
		308-1		5.94	2.10	4.30	4.25
		308-2		3.24	0.900	8.00	4.32
		308-3		3.24	0.980	7.00	3.78
		308-7	0.875	3.24	0.210	7.40	4.00
		308-7		5.94	0.600	3.10	3.07
		308-7		11.88	0.840	1.90	3.76
				Average of 11 values			3.86±0.47

Table I-10. Radial Dispersion, 0.75-inch Spheres, Orthorhombic-1 Arrangement (See Fig. 10).

Flow rate, gal./min.	N_{Re} $(d_p U_0/\nu)$	Run No.	$\frac{r}{R}$	h, inch	$\frac{c}{c_0}$	$\frac{N_{Pe} R^2}{h\ d_p}$	$(N_{Pe})_r$
10.0	646	430-1	0.125	2.65	10.11	25.00	11.06
				5.40	6.21	14.00	12.61
				12.15	3.40	6.80	13.76
				17.55	2.30	4.30	12.61
		430-2	0.125	2.65	10.81	27.00	11.94
				5.40	6.25	14.00	12.61
				12.15	3.28	6.60	13.36
				17.55	2.35	4.40	12.90
				Average of 8 values			12.60±0.76

Table I-11. Radial Dispersion, 0.25-inch Polyethylene Pellets (d_p = 0.232 inch).

Flow rate, gal./min.	N_{Re} ($d_p U_0/\nu$)	Run No.	$\frac{r}{R}$	h, inch	$\frac{c}{c_0}$	$\frac{N_{Pe} R^2}{h\, d_p}$	$(N_{Pe})_r$
0.30	5.28	729-1	0	14.00	9.00	17.00	11.72
		726-5		20.00	5.80	11.20	10.87
		727-1			6.22	12.00	11.65
		727-2			6.42	12.50	12.15
		728-3			6.01	11.50	11.16
		729-1			6.50	12.80	12.42
		801-1			6.58	13.00	12.62
		801-1			5.92	11.40	11.06
		801-2			6.80	13.00	12.62
		803-4			6.51	12.52	12.15
		806-4			6.48	12.51	12.14
		807-3			6.65	13.15	12.76
				Average of 12 values			11.94±0.44
3.0	52.78	730-3	0	14.00	9.10	18.00	12.41
		727-4	0	20.00	6.20	12.00	11.65
		728-1			6.65	13.00	12.62
		728-2			6.32	12.10	11.74
		723-6			5.80	11.00	10.67
		730-2			5.51	10.50	10.19
		730-3			7.01	13.50	13.10
		801-3			5.80	11.00	10.67
		801-7			6.40	12.20	11.84
		803-2			6.91	12.90	12.52
		806-5			6.21	12.00	11.65
		806-6			6.40	12.20	11.84
				Average of 12 values			11.74±0.74
10.0	175.9	726-3	0	20.00	5.65	10.80	10.48
		728-2			4.75	9.00	8.75
		728-4			5.51	10.50	10.19
		730-6			5.01	9.50	9.22
		730-7			5.80	11.00	10.67
		801-5			4.90	9.40	9.12
		803-1			5.50	10.50	10.19
				Average of 7 values			9.80±0.95
20.0	352	324-1	0	2.00	45.00	92.00	8.93
				5.00	17.05	34.00	8.28
				8.00	11.50	22.5	8.75
				14.00	5.90	11.50	7.82
				20.00	4.22	8.00	7.76
		324-3	0	2.00	41.03	80.00	7.77

Table I-11 (cont'd.)

Flow rate, gal./min.	N_{Re} ($d_p U_0/\nu$)	Run No.	$\frac{r}{R}$	h, inch	$\frac{c}{c_0}$	$\frac{N_{Pe} R^2}{h\ d_p}$	$(N_{Pe})_r$
		324-4	0	5.00	19.01	37.50	9.15
				8.00	11.32	22.00	8.56
				14.00	5.81	11.20	7.72
		324-5	0	20.00	4.51	8.30	8.058
		324-10	0.875	20.00	1.71	8.00	7.77
		324-12	0.875	20.00	1.90	7.60	7.37
		324-13	0.875	20.00	1.65	8.20	7.96
				Average of 13 values			8.15±0.35
30.0	527	730-6	0	20.00	4.02	7.60	7.35
		803-2			3.74	7.20	6.99
		803-4			4.25	8.10	7.86
		803-5			4.41	8.40	8.15
		803-6			4.52	8.60	8.35
		803-7			4.15	8.00	7.76
				Average of 6 values			7.74±0.65

Table I-12. Radial Dispersion, 0.75-inch Spheres, Randomly Packed.

Flow rate, gal./min.	N_{Re} ($d_p U_0/\nu$)	Run No.	$\frac{r}{R}$	h, inch	$\frac{c}{c_0}$	$\frac{N_{Pe} R^2}{h\ d_p}$	$(N_{Pe})_r$
10.0	646	224-1	0.216	3.00	7.40	22.50	11.25
				6.00	4.80	11.50	11.50
				12.00	2.50	5.70	11.40
				18.00	1.70	3.7	11.10
		224-3	0.625	3.00	0.20	21.50	10.75
				6.00	0.70	12.00	12.00
				12.00	0.99	6.10	12.20
		224-4	0.875	6.00	0.120	12.25	12.25
				12.00	0.450	6.20	12.40
				18.00	0.710	3.95	11.85
				Average of 10 values			11.67±0.50

Table I-13. Radial Dispersion, 0.75-inch Spheres, Orthorhombic-2 Arrangement (See Fig. 15).

Flow rate, gal./min.	N_{Re} ($d_p U_0/\nu$)	Run No.	$\frac{r}{R}$	h, inch	$\frac{c}{c_0}$	$\frac{N_{Pe} R^2}{h\ d_p}$	$(N_{Pe})_r$
10.0	644	425-1	0.200	3.95	6.60	18.50	12.25
				6.75	4.81	11.50	12.95
				12.75	2.52	5.70	12.11
				18.75	1.60	3.50	10.93
		425-3	0.865	12.75	0.305	5.80	12.34
				18.75	0.551	3.35	10.46
		426-2	0.200	3.95	6.45	17.00	11.25
				6.75	4.90	12.00	13.50
				12.75	2.61	5.90	12.55
				18.75	1.82	4.00	12.50
		426-6	0.200	3.95	6.71	19.00	12.58
				6.75	4.92	12.00	13.51
				12.75	2.62	5.90	12.55
				18.75	1.87	4.20	13.12
				Average of 14 values			12.32±0.65

Table I-14. Radial Dispersion, Ottawa Sand (d_p = 0.0177 inch)

Flow rate, gal./min.	N_{Re} ($d_p U_0/\nu$)	Run No.	$\frac{r}{R}$	h, inch	$\frac{c}{c_0}$	$\frac{N_{Pe} R^2}{h\ d_p}$	$(N_{Pe})_r$
0.30	0.457	809-3	0	20.00	9.10	17.50	16.99
		810-2			8.92	17.20	16.69
		810-4			8.71	17.00	16.50
		810-8			8.50	16.50	16.01
		815-2			9.05	17.48	16.97
				Average of 5 values			16.63±0.68
1.0	1.52	810-4	0	20.00	8.81	17.20	16.69
3.0	4.57	810-6	0	20.00	8.60	16.90	16.40

APPENDIX II. TWO PHASE FLOW

Table II-1. Continuous-Phase Longitudinal Dispersion, 0.75-inch Spheres, Rhombohedral Arrangement.

Continuous flow rate, gal./min.	Discontinuous flow rate, gal./min.	Column height in.	Run No.	Slope $\frac{d(c/c_0)}{dt}$	N_D	N_{Pe}
0.30	0.158	23.6	702-2	0.84	7.91	0.250
			702-3	0.84	7.91	0.250
			703-5	0.80	7.11	0.225
			703-6	0.88	8.84	0.280
			703-9	0.85	7.89	0.250
			Average of 5 runs			0.250±0.015
0.30	0.609	23.6	702-4	0.67	4.78	0.151
			703-6	0.62	3.93	0.124
			704-1	0.65	4.38	0.138
			704-2	0.68	4.90	0.155
			Average of 4 runs			0.142±0.047
0.60	0.158	23.6	628-9	1.09	13.97	0.442
			629-10	1.10	14.22	0.449
			630-1	1.12	14.95	0.473
			630-3	1.10	14.22	0.450
			630-4	1.13	14.46	0.458
			Average of 5 runs			0.454±0.017

Table II-2. Continuous-Phase Longitudinal Dispersion, 0.75-inch Spheres, Orthrhombic-1 Arrangement.

Continuous flow rate, gal./min.	Discontinuous flow rate, gal./min.	Column height in.	Run No.	Slope $\frac{d(c/c_0)}{dt}$	N_D	N_{Pe}
0.30	0.219	22.95	601-2	0.67	4.78	0.153
			608-1	0.69	5.067	0.165
			608-7	0.70	5.215	0.170
			607-8	0.68	4.900	0.160
			607-9	0.70	5.215	0.170
			Average of 5 runs			0.163±0.023
0.30	0.951	22.95	529-4	0.50	2.34	0.076
			530-3	0.47	1.98	0.054
			604-4	0.50	2.34	0.076
			609-5	0.48	2.11	0.069
			Average of 4 runs			0.071±0.02
0.30	1.82	22.95	607-3	0.45	1.77	0.0578
			608-4	0.43	1.55	0.0506
			609-1	0.46	1.89	0.062
			609-2	0.42	1.48	0.0483
			609-4	0.45	1.77	0.0578
			Average of 5 runs			0.055±0.012
0.60	0.158	22.95	602-7	0.92	9.65	0.315
			603-1	0.88	8.84	0.289
			605-2	0.90	9.24	0.302
			605-3	0.87	8.64	0.282
			605-7	0.95	10.30	0.336
			605-9	0.90	9.24	0.302
			Average of 6 runs			0.302±0.064
0.60	0.219	22.95	601-2	0.90	9.24	0.302
			603-2	0.85	7.85	0.258
			603-3	0.87	8.64	0.289
			604-4	0.86	8.077	0.264
			607-1	0.88	8.84	0.289
			607-2	0.86	8.077	0.264
			Average of 6 runs			0.277±0.038
0.60	0.426	22.95	521-1	0.72	5.61	0.183
			521-2	0.69	5.067	0.165
			521-3	0.67	4.78	0.153
			602-4	0.70	5.215	0.170
			602-5	0.73	5.81	0.190
			602-10	0.74	5.95	0.195
			Average of 6 runs			0.176±0.029

Table II-2 (cont'd.)

Continuous flow rate, gal./min.	Discontinuous flow rate, gal./min.	Column height in.	Run No.	Slope $\frac{d(c/c_0)}{dt}$	N_D	N_{Pe}
0.60	0.951	22.95	529-1	0.62	3.93	0.128
			602-6	0.64	4.25	0.138
			604-3	0.62	3.93	0.128
			621-5	0.65	4.38	0.143
			621-7	0.635	4.18	0.137
			Average of 5 runs			0.135±0.028
0.80	0.219	22.95	607-13	0.88	8.84	0.289
			608-8	0.84	7.84	0.256
			608-9	0.86	8.077	0.264
			608-11	0.87	8.64	0.282
			609-10	0.85	7.89	0.258
			Average of 5 runs			0.269±0.0378
0.80	1.00	22.95	607-6	0.75	6.14	0.2008
			607-13	0.78	6.82	0.223
			609-11	0.73	5.81	0.190
			610-1	0.79	6.905	0.225
			610-2	0.72	5.61	0.183
			Average of 5 runs			0.204±0.032
1.00	0.158	22.95	528-1	1.13	14.46	0.471
			528-6	1.15	15.66	0.510
			529-1	1.10	14.22	0.464
			529-7	1.14	15.33	0.501
			Average of 4 runs			0.486±0.088
1.00	0.219	22.95	523-3	1.07	13.43	0.439
			525-1	1.05	12.91	0.422
			525-2	1.06	13.16	0.430
			527-5	1.03	12.33	0.403
			527-6	1.05	12.91	0.422
			528-2	1.02	12.09	0.395
			Average of 6 runs			0.418±0.074
1.00	0.487	22.95	520-1	0.92	9.65	0.315
			521-1	0.95	10.3	0.330
			521-2	0.90	9.24	0.302
			521-3	0.96	10.55	0.344
			523-6	0.95	10.30	0.336
			524-2	0.97	10.78	0.352
			526-5	0.94	10.16	0.332
			526-6	0.92	9.65	0.315

Table II-2 (cont'd.)

Continuous flow rate gal./min.	Discontinuous flow rate gal./min.	Column height in.	Run No.	Slope $\frac{d(c/c_0)}{dt}$	N_D	N_{Pe}
			527-1	0.97	10.78	0.352
			605-1	0.95	10.30	0.336
			Average of 10 runs			0.332±0.013
1.00	0.951	22.95	521-5	0.84	7.91	0.257
			522-5	0.80	7.11	0.232
			523-7	0.86	8.077	0.264
			524-3	0.88	8.84	0.289
			524-4	0.85	7.89	0.258
			525-5	0.88	8.84	0.289
			525-6	0.86	8.077	0.264
			252-7	0.85	7.89	0.258
			526-3	0.87	8.64	0.232
			526-6	0.86	8.077	0.264
			526-7	0.90	9.24	0.302
			527-1	0.85	7.89	0.258
			527-4	0.84	7.84	0.256
			607-2	0.86	8.077	0.264
			Average of 14 runs			0.266±0.064
2.00	0.23	22.95	606-4	1.04	15.33	0.501
			606-7	1.12	14.95	0.487
			606-8	1.15	15.66	0.510
			606-9	1.10	14.22	0.464
			Average of 4 runs			0.491±0.014
2.00	0.46	22.95	606-3	1.09	13.97	0.456
			606-10	1.08	13.82	0.451
			606-11	1.10	14.22	0.464
			606-12	1.12	14.95	0.487
			Average of 4 runs			0.464±0.039

Table II-2A. Experimental Flooding Conditions for 0.75-inch Sphere Packing in Orthorhombic-1 Arrangement

Continuous flow rate, gal./min.	0.30	0.60	0.8	1.0	2.0
Discontinuous flow rate, gal./min.	1.65	1.45	1.20	0.95	0.60

Table II-3. Continuous-Phase Longitudinal Dispersion, 0.75-inch Spheres, Random Arrangement.

Continuous flow rate gal./min.	Discontinuous flow rate, gal./min.	Column height, in.	Run No.	Slope $\frac{d(c/c_0)}{dt}$	N_D	N_{Pe}
0.30	0.609	24.0	622-2	0.50	2.34	0.073
			626-1	0.45	1.77	0.055
			626-2	0.50	2.34	0.076
			626-10	0.48	2.11	0.065
			626-11	0.51	2.43	0.076
			Average of 5 runs			0.069±0.011
0.30	1.21	24.0	623-5	0.42	1.48	0.046
			624-1	0.45	1.77	0.055
			625-1	0.43	1.55	0.048
			Average of 3 runs			0.049±0.020
0.60	0.975	24.0	625-2	0.60	3.64	0.113
			625-3	0.55	2.96	0.0923
			626-1	0.58	3.35	0.104
			626-2	0.61	3.78	0.117
			626-7	0.56	3.10	0.097
			Average of 5 runs			0.105±0.014

Table II-4. Continuous-Phase Longitudinal Dispersion, 0.75-inch Spheres, Orthorhombic-2 Arrangement.

Continuous flow rate gal./min.	Discontinuous flow rate, gal./min.	Column height, in.	Run No.	Slope $\frac{d(c/c_0)}{dt}$	N_D	N_{Pe}
0.30	0.951	24.0	629-1	0.49	2.23	0.069
			629-4	0.50	2.34	0.073
			629-5	0.51	2.43	0.076
			629-9	0.45	1.77	0.055
			Average of 4 runs			0.068±0.025
1.00	0.951	24.0	627-1	0.88	8.84	0.275
			627-2	0.89	8.64	0.269
			627-4	0.90	9.24	0.288
			628-2	0.86	8.08	0.252
			628-5	0.87	8.64	0.269
			Average of 5 runs			0.270±0.030

Table II-5. Discontinuous-Phase Longitudinal Dispersion, 0.75-inch Spheres Rhombohedral Arrangement.

Continuous flow rate, gal./min.	Discontinuous flow rate, gal./min.	Column height, in.	Run No.	Slope $\frac{d(c/c_0)}{dt}$	N_D	N_{Pe}
0.0	0.25	26.88	717-1	1.40	23.60	0.658
			717-2	1.43	24.69	0.688
			717-3	1.37	22.53	0.628
			718-1**	1.41	24.00	0.669
			718-5	1.35	21.92	0.611
			Average of 5 values			0.650±0.041
0.0	0.60	25.88	718-4	1.16	15.93	0.444
			718-6	1.18	16.48	0.460
			720-3	1.20	17.10	0.477
			Average of 3 values			0.460±0.060
1.0	0.25	26.88	718-2	0.84	7.91	0.220
			718-7	0.88	8.84	0.246
			720-1	0.85	7.98	0.224
			721-2	0.82	7.63	0.212
			721-3**	0.83	7.71	0.214
			Average of 5 values			0.223±0.046
2.0	0.25	26.88	721-5	0.67	4.78	0.133
			722-1	0.70	5.215	0.139
			722-3**	0.67	4.78	0.133
			Average of 3 values			0.135±0.010

Table II-6. Discontinuous-Phase Longitudinal Dispersion, 0.75-inch Spheres, Random Arrangement.

Continuous flow rate gal./min.	Discontinuous flow rate, gal./min.	Column height, in.	Run No.	Slope $\frac{d(c/c_0)}{dt}$	N_D	N_{Pe}
0.0	0.25	25.0	707-2	1.01	11.86	0.355
			707-9	1.05	12.88	0.386
			707-10	1.03	12.10	0.363
			707-11**	1.07	12.42	0.402
			Average of 4 values			0.376±0.028
0.0	0.25	25.0	707-1**	1.05	12.88	0.386
			707-8	1.07	13.42	0.402
			Average of 2 values			0.394
0.30	0.25	25.0	710-2**	0.88	8.84	0.265
			710-3	0.90	9.24	0.277
			710-7	0.84	7.91	0.237
			711-5	0.92	9.65	0.289
			Average of 4 values			0.267±0.036
0.30	1.21	25.0	708-1	1.00	11.60	0.348
			708-2	1.02	12.09	0.362
			708-5	0.98	11.08	0.332
			708-7	1.03	12.10	0.363
			709-9	1.05	12.88	0.386
			Average of 5 values			0.358±0.034
0.60	0.25	25.0	713-2	0.72	5.61	0.168
			713-4	0.74	5.95	0.178
			713-5	0.75	6.14	0.184
			Average of 3 values			0.176±0.045
0.60	1.21	25.0	705-2**	0.86	8.08	0.242
			705-3	0.84	7.84	0.235
			705-10	0.87	8.64	0.259
			706-9	0.88	8.84	0.265
			Average of 4 values			0.250±0.032
1.0	0.25	25.0	705-4	0.67	4.78	0.143
			706-5	0.62	3.93	0.118
			706-8**	0.64	4.25	0.127
			706-9	0.65	4.38	0.131
			Average of 4 values			0.129±0.038

**In this and following tables, indicates runs using dyed kerosene.

Table II-6 (cont'd.)

Continuous flow rate gal./min.	Discontinuous flow rate, gal./min.	Column height, in.	Run No.	Slope $\frac{d(c/c_0)}{dt}$	N_D	N_{Pe}
1.0	1.21	25.0	705-5**	0.78	6.82	0.205
			711-2	0.79	6.91	0.207
			715-10	0.81	7.16	0.215
			Average of 3 values			0.209±0.020
2.0	0.25	25.0	705-1	0.46	1.89	0.056
			715-1**	0.50	2.34	0.070
			715-2	0.48	2.11	0.063
			Average of 3 values			0.063±0.025
2.0	0.46	25.0	712-1	0.61	3.78	0.113
			712-3	0.58	3.35	0.100
			715-5**	0.55	2.96	0.088
			Average of 3 values			0.100±0.040

Table II-7. Continuous Phase Radial Dispersion, 0.75-inch Spheres, Orthorhombic-2 Arrangement.

Continuous flow rate, gal./min.	Discontinuous flow rate, gal./min.	Run No.	$\frac{r}{R}$	h inch	$\frac{c}{c_0}$	$\frac{N_{Pe} R^2}{h\, d_p}$	$(N_{Pe})_r$
0.20	0.0	816-2	0.200	6.75	5.81	14.5	16.24
		816-2		12.75	3.42	7.90	16.74
		817-4		6.75	5.90	15.00	16.80
		817-4		12.75	3.20	7.40	15.62
		817-5		12.75	3.51	8.20	17.30
		817-5		18.75	2.65	5.0	15.60
		Average values of 6 runs					16.38±0.88
0.30	0.20	816-6	0.200	12.75	2.49	5.68	12.04
		816-6		18.75	1.91	4.25	13.26
		817-7		12.75	2.54	5.80	12.29
		817-7		18.75	1.82	4.00	12.48
		818-2		12.75	2.61	5.90	12.50
		Average values of 5 runs					12.51±0.86
0.30	1.0	819-2	0.200	12.75	2.10	4.71	9.98
		819-2		18.75	1.50	3.4	10.60
		820-6		6.75	2.82	8.82	9.87
		820-6		12.75	2.22	4.80	10.17
		821-1		12.75	2.31	4.35	9.22
		821-2		12.75	1.99	4.50	9.54
		Average of 6 runs					9.89±0.22
0.60	0.20	821-3	0.200	12.75	3.10	6.8	14.41
		821-4		18.75	1.91	4.5	14.04
		821-5		12.75	3.20	7.40	15.68
		821-5		18.75	1.85	4.20	13.10
		821-6		12.75	3.05	7.00	14.84
		Average of 5 runs					14.41±0.415
0.60	1.00	822-1	0.200	12.75	2.51	5.70	12.08
		822-1		18.75	1.82	4.00	12.48
		822-2		12.75	2.45	5.50	11.66
		822-2		18.75	1.75	3.80	11.85
		Average of 4 runs					12.02±0.54

Table II-8. Discontinuous-Phase Holdup, 0.75-inch Spheres, Rhombohedral Arrangement (Porosity 25.95%).

Continuous flow rate, gal./min.	Discontinuous flow rate, gal./min.	Run No.	$t_{50\%}$	$t_{T=1}$	Holdup volume in^3.	Holdup χ_d, %
0.0	0.25	717-1	36.00	35.10	31.15	15.57
		717-2	37.50	36.56	32.44	16.22
		717-3	36.50	35.58	31.58	15.79
		718-1**	38.00	37.05	32.88	16.44
		718-5	37.00	36.07	32.01	16.00
		Average of 5 runs				16.00±1.90
0.60	0.60	718-4	30.00	28.95	61.83	30.92
		718-6	31.50	30.39	64.94	32.47
		720-3	30.50	29.43	62.86	31.43
		Average of 3 runs				31.60±4.30
1.0	0.25	718-2	53.00	49.29	43.74	21.87
		718-7	55.00	51.15	45.39	22.69
		720-1	55.00	51.15	45.39	22.69
		721-2	54.00	50.14	44.35	22.19
		721-3**	55.00	51.15	45.39	22.69
		Average of 5 runs				22.42±2.77
2.0	0.25	721-5	115	103.5	91.85	45.90
		722-1	105	94.50	83.86	41.93
		722-3	110	99.00	87.86	43.93
		Average of 3 runs				43.92±4.50

Table II-9. Discontinuous-Phase Holdup, 0.75-inch Spheres, Random Arrangement (Porosity 40%).

Continuous flow rate, gal./min.	Discontinuous flow rate, gal./min.	Run No.	$t_{50\%}$	$t_{T=1}$	Holdup volume in^3.	Holdup χ_d, %
0.0	0.25	707-2	33.00	31.74	28.16	9.38
		707-9	30.00	28.86	25.61	8.53
		707-10	35.50	34.15	30.15	10.05
		707-11**	33.50	32.22	28.59	9.53
		Average of 4 runs				9.38±1.42
0.0	1.21	707-1**	22.00	21.12	90.60	30.20
		707-8	20.00	19.20	82.36	27.45
		Average of 2 runs				28.82±4.10
0.30	0.25	710-2**	31.50	29.61	26.278	8.76
		710-3	33.00	31.02	27.53	9.17
		710-7	35.00	32.90	29.20	9.73
		711-5	34.75	32.66	28.98	9.66
		Average of 4 runs				9.33±1.50
0.30	1.21	708-1	20.50	19.68	84.53	28.12
		708-2	21.75	20.88	89.67	29.89
		708-5	23.00	22.08	94.83	31.61
		708-7	22.50	21.60	92.77	30.92
		708-9	22.00	21.12	90.07	30.23
		Average of 5 runs				30.13±2.90
0.60	0.25	713-2**	33.50	31.32	29.57	9.85
		713-4	32.00	29.92	26.55	8.85
		713-5	33.00	30.85	27.38	9.13
		Average of 3 runs				9.28±1.40
0.60	1.21	705-2**	28.00	26.18	112.4	37.46
		705-3	26.00	24.31	104.41	34.80
		705-10	28.50	26.64	114.41	38.13
		706-9	27.00	25.245	108.42	36.41
		Average of 4 runs				36.70±4.49
1.0	0.25	705-4	37.00	33.30	29.55	9.85
		706-5	39.00	35.10	31.15	10.38
		706-8**	37.50	33.75	29.95	9.98
		706-9	38.00	34.20	30.35	10.12
		Average of 4 runs				10.08±2.60
1.0	1.21	705-5**	39.50	36.54	156.93	53.31
		711-2	38.00	35.15	150.96	50.32
		715-10	37.50	34.68	148.95	49.65
		Average of 3 runs				50.76±5.10

Table II-9 (cont'd.)

Continuous flow rate, gal./min.	Discontinuous flow rate, gal./min.	Run No.	$t_{50\%}$	$t_{T=1}$	Holdup volume in^3.	Holdup $X_{\%d}$,
2.0	0.25	705-1	8.500	76.50	67.89	22.63
		715-1**	90.00	81.00	71.88	23.96
		715-2	87.00	78.30	69.49	23.16
		Average of 3 runs				23.35±2.50
2.0	0.46	712-1	100	90.00	146.97	48.90
		715-1	115	103.50	168.19	56.06
		715-5**	120	108.00	176.33	58.77
		Average of 3 runs				54.57±8.10

Table II-10. Continuous-Phase Holdup, 0.75-inch Spheres, Random Arrangement (Porosity 40%).

Continuous flow rate, gal./min.	Discontinuous flow rate, gal./min.	Run No.	$t_{50\%}$	$t_{T=1}$	Holdup volume in^3.	Holdup $X_{\%c}$
0.30	1.21	623-5	183	164	175.0	63.17
		624-1	195	175.5	186.9	67.47
		625-1	201	181	192.7	69.56
		Average of 3 runs				66.73±5.10